

Dissertation zur Erlangung des Doktorgrades
der Fakultät für Chemie und Pharmazie
der Ludwig-Maximilians-Universität München

**Synthetic Strategies and Structural Chemistry
of Novel Nitridogallates, Nitridogermanates,
and Nitridosilicates**

Christine Veronica Pösl

aus

Berlin, Deutschland

2017

Erklärung

Die vorliegende Dissertation wurde im Sinne von § 7 der Promotionsordnung vom 28. November 2011 von Herrn Prof. Dr. Wolfgang Schnick betreut.

Eidesstattliche Versicherung

Diese Dissertation wurde eigenständig und ohne unerlaubte Hilfsmittel erarbeitet.

München, den 28.04.2017

.....

(Christine Pösl)

Dissertation eingereicht am 28. April 2017

1. Gutachter Prof. Dr. Wolfgang Schnick

2. Gutachter Prof. Dr. Oliver Oeckler

Mündliche Prüfung am 06. Juni 2017

Für meine Familie

Acknowledgment

Mein ganz besonderer Dank gilt Herrn Prof. Dr. Wolfgang Schnick für die Möglichkeit, meine Doktorarbeit in seinem Arbeitskreis anfertigen zu können und dass ich mit meinem interessanten und herausfordernden Thema Teil der LED-Gruppe sein durfte. Insbesondere auch dafür, dass er mir die Freiheit gab, mein Thema individuell zu gestalten und ich meine Ideen durch die hervorragenden Arbeitsbedingungen sofort in die Tat umsetzen konnte. Ich danke ihm, dass ich die Ergebnisse meiner Forschung in wissenschaftlichen Fachzeitschriften veröffentlichen durfte und er es mir ermöglichte, wertvolle Erfahrungen auf (inter)nationalen Tagungen sammeln zu können. Die kleinen Ausflüge, z. B. zur Preisverleihung des Deutschen Zukunftspreises 2013 in München, und die großen Ausflüge, insbesondere die Reise zum Phosphor Global Summit 2016 nach Newport Beach, Kalifornien, werden in unvergesslicher Erinnerung bleiben. Der Möglichkeit daran teilnehmen zu dürfen gebührt großer Dank.

Besonderer Dank gilt auch Herrn Prof. Dr. Oliver Oeckler für die Bereitschaft das Koreferat für diese Dissertation zu übernehmen.

Frau Prof. Dr. Lena Daumann, sowie den Herrn Prof. Dr. Konstantin Karaghiosoff, Prof. Dr. Hans-Christian Böttcher und Prof. Dr. Wolfgang Beck, em. danke ich für die Bereitschaft, mir als weitere Prüfer zur Verfügung zu stehen.

Ebenfalls herzlich bedanken möchte ich mich bei allen Kooperationspartnern des Lumileds Development Center Aachen, insbesondere bei Herrn Dr. Peter J. Schmidt und Herrn Volker Weiler. Unsere „Philips-Meetings“ haben mir immer viel Spaß gemacht und waren stets sehr interessant und informativ und gaben mir neue Anregungen für meine Forschung. Ich habe mich sehr gefreut, durch die Besuche in Aachen das LDCA kennenlernen zu dürfen und einen Einblick in die Forschungs- und Fertigungslabore von Lumileds zu erhalten.

Herrn Dr. Constantin Hoch, Herrn Dr. Peter Mayer, Herrn Peter Wagatha, Herrn Thomas Miller und Herrn Philipp Bielec danke ich für die zahlreichen Einkristallmessungen. Großer Dank gilt dabei insbesondere Herrn Dr. Constantin Hoch für sein offenes Ohr und seine ständige Hilfsbereitschaft bei allen kristallographischen Problemen.

Frau Olga Lorenz, Herrn Thomas Miller und Herrn Wolfgang Wünschheim danke ich für das reibungslose „Drumherum“. Für ihre Hilfsbereitschaft bei allerhand organisatorischer und computertechnischer Fragen und auch für die schnelle Beschaffung von Laborutensilien und Chemikalien, die für meine Forschung unerlässlich waren. Mit ihrer Hilfe war es möglich, diverse Umzüge und Sonderaufgaben anlässlich der Abzugssanierungen und der EDV-Sanierung

problemlos zu meistern und trotz der Umstellung des Betriebssystems fast lückenlos weiterarbeiten zu können.

Herrn Christian Minke (Minki) danke ich für die Bereitschaft, unzählige Stunden mit mir und meinen mehr als vollgepackten REM-Trägern am REM zu verbringen. Die durch die vielen Gespräche entstandene Freundschaft wird hoffentlich auch weiterhin mit Grill- und Kegelabenden, Wanderungen in den Bergen und Besuchen auf der Weinmesse bestehen bleiben.

Meinen Praktikanten Maja Hermann, Sabine Auras, Lars Bulthaupt, Patricia Breitenwinkler, Gregor Dahl, Jonathan Kampmann, Eugenia Elzer, Judith Pottbäcker, Vanessa Trauschke und Manuel Scheel danke ich für ihr Interesse an meinem Forschungsgebiet, ihr Vertrauen in mich und ihr außerordentliches Engagement bei allen Synthesen und der zugehörigen Analytik. Sie haben einen großen Teil zu den Ergebnissen meiner Dissertation beigetragen.

Ganz besonders danken möchte ich meinen Laborkollegen Lukas Neudert, Robin Niklaus, Christian Maak, Christina Fraunhofer und Philipp Strobel für die schöne und beinahe zu schnell vergangene Zeit in D2.100. Insbesondere das gemeinsame Nudeln kochen mittags in der Kaffeeküche und die Laborabende werden mir immer in Erinnerung bleiben.

Frau Katrin Horky möchte ich ebenfalls besonders danken, dass sie während meiner gesamten Studienzzeit eine treue Begleiterin war und sie mit mir gemeinsam durch alle Höhen und Tiefen gegangen ist. Sie hatte immer ein offenes Ohr für mich und auch in schwierigen Situationen die richtigen und aufmunternden Worte.

Ich möchte mich auch bei allen weiteren Kollegen der Arbeitskreise Schnick, Johrendt, Hoch, Lotsch und Oeckler für die gute Arbeitsatmosphäre und die tolle Zeit im zweiten Stock bedanken.

Allergrößter Dank gilt aber meiner Familie und ganz besonders meinen Eltern, ohne deren Hilfe das alles nicht möglich gewesen wäre und ich nicht da wäre, wo ich heute bin.

*„Alle Hindernisse und Schwierigkeiten sind Stufen,
auf denen wir in die Höhe steigen.“*

(Friedrich Nietzsche)

Table of Contents

1	Introduction	1
2	Nitridogallates and Nitridogermanates	9
2.1	Introduction.....	9
2.2	Layered Nitridomagnesogallates $\text{CaMg}_2\text{GaN}_3$ and $\text{CaMg}_2\text{Ga}_2\text{N}_4$	11
2.2.1	Introduction.....	12
2.2.2	Results and Discussion	13
2.2.2.1	Syntheses and Chemical Analysis.....	13
2.2.2.2	Structure Determination.....	15
2.2.3	Conclusion.....	25
2.2.4	Experimental Section.....	25
2.2.4.1	General.....	25
2.2.4.2	Synthesis of $\text{CaMg}_2\text{GaN}_3$	26
2.2.4.3	Synthesis of $\text{CaMg}_2\text{Ga}_2\text{N}_4$	26
2.2.4.4	Synthesis of a Mixture of $\text{CaMg}_2\text{GaN}_3$ and $\text{CaMg}_2\text{Ga}_2\text{N}_4$	27
2.2.4.5	Scanning Electron Microscopy	27
2.2.4.6	Transmission Electron Microscopy	27
2.2.4.7	Single-Crystal X-ray Diffraction	27
2.2.4.8	Powder X-ray Diffraction.....	28
2.2.5	References	29
2.3	$\text{Ca}_2\text{Mg}_5\text{GeN}_6$ – A Layered Nitridomagnesogermanate.....	33
2.3.1	Introduction.....	34
2.3.2	Results and Discussion	35
2.3.3	Conclusions	40
2.3.4	Experimental Section.....	41
2.3.4.1	Synthesis of $\text{Ca}_2\text{Mg}_5\text{GeN}_6$	41
2.3.4.2	Single-Crystal X-ray Diffraction	41
2.3.4.3	Scanning Electron Microscopy	42
2.3.4.4	Powder X-ray Diffraction.....	42
2.3.5	References	43
2.4	$\text{Ca}_4\text{Mg}_5\text{Ge}_3\text{N}_{10}$ and $\text{Sr}_2\text{Mg}_3\text{GaN}_{4.33}$ – Two Mg-Containing Nitrides and Their Structural Relation to $(\text{Sr,Ba})_2\text{Si}_5\text{N}_8$	45
2.4.1	Introduction.....	46
2.4.2	Results and Discussion	47
2.4.2.1	Synthesis	47

2.4.2.2	Single-Crystal Structure Analysis	47
2.4.3	Conclusions	54
2.4.4	Experimental Section	55
2.4.4.1	General	55
2.4.4.2	Synthesis of $\text{Ca}_4\text{Mg}_5\text{Ge}_3\text{N}_{10}$	55
2.4.4.3	Synthesis of $\text{Sr}_2\text{Mg}_3\text{GaN}_{4.33}$	56
2.4.4.4	Single-Crystal X-ray Diffraction	56
2.4.5	References	57
2.5	The Crystal Structure of Nitridomagnesogermanate $\text{Ba}[\text{Mg}_3\text{GeN}_4]\text{:Eu}^{2+}$ and Theoretical Calculations of Its Electronic Properties	61
2.5.1	Introduction	62
2.5.2	Results and Discussion	63
2.5.2.1	Synthesis	63
2.5.2.2	Single-Crystal Structure Analysis	63
2.5.2.3	Crystal-Structure Description	65
2.5.2.4	Luminescence	68
2.5.3	Conclusions	72
2.5.4	Experimental Section	73
2.5.4.1	General	73
2.5.4.2	Synthesis	73
2.5.4.3	Single-Crystal X-ray Diffraction	74
2.5.4.4	Powder X-ray Diffraction	74
2.5.4.5	Theoretical Calculations	75
2.5.5	References	76
3	Nitridosilicates	79
3.1	Introduction	79
3.2	Crystal Structure and Nontypical Deep-Red Luminescence of $\text{Ca}_3\text{Mg}[\text{Li}_2\text{Si}_2\text{N}_6]\text{:Eu}^{2+}$	81
3.2.1	Introduction	82
3.2.2	Experimental Section	83
3.2.2.1	Synthesis	83
3.2.2.2	Single-Crystal X-ray Diffraction	84
3.2.2.3	Scanning Electron Microscopy	84
3.2.2.4	Luminescence	84
3.2.3	Results and Discussion	85
3.2.3.1	Synthesis and Chemical Analysis	85
3.2.3.2	Single-Crystal Structure Analysis	85
3.2.3.3	Luminescence	90
3.2.4	Conclusions	93

3.2.5	References	95
4	Conclusion and Outlook.....	99
5	Summary.....	105
5.1	Layered Nitridomagnesogallates $\text{CaMg}_2\text{GaN}_3$ and $\text{CaMg}_2\text{Ga}_2\text{N}_4$	105
5.2	$\text{Ca}_2\text{Mg}_5\text{GeN}_6$ – A Layered Nitridomagnesogermanate.....	107
5.3	$\text{Ca}_4\text{Mg}_5\text{Ge}_3\text{N}_{10}$ and $\text{Sr}_2\text{Mg}_3\text{GaN}_{4.33}$ – Two Mg-Containing Nitrides and Their Structural Relation to $(\text{Sr,Ba})_2\text{Si}_5\text{N}_8$	109
5.4	The Crystal Structure of Nitridomagnesogermanate $\text{Ba}[\text{Mg}_3\text{GeN}_4]\text{:Eu}^{2+}$ and Theoretical Calculations of Its Electronic Properties	111
5.5	Crystal Structure and Nontypical Deep-Red Luminescence of $\text{Ca}_3\text{Mg}[\text{Li}_2\text{Si}_2\text{N}_6]\text{:Eu}^{2+}$	113
6	Appendix.....	115
6.1	Supporting Information for Chapter 2.2	115
6.2	Supporting Information for Chapter 2.3	119
6.3	Supporting Information for Chapter 2.4	121
6.4	Supporting Information for Chapter 2.5	125
6.5	Supporting Information for Chapter 3.2	127
7	Publications.....	129
7.1	List of Publications	129
7.2	Conference Contributions	133
7.3	Deposited Crystallographic Data	133
8	Curriculum Vitae	135

1 Introduction

Faster, higher, further – continuous improvement is the guiding principle of all technologies. Since the beginning of mankind, new technologies are meant to facilitate human's life. As technological advances grow worldwide, so does the demand for scarce and exhaustible raw materials. Sustainability is therefore a term of rising importance. Besides the thrust toward renewable energies, development and use of energy-efficient technologies help to protect the environment. This represents a major challenge for all scientists due to considerably increased requirements for novel and already existing technologies.

Both the automobile and electric light are revolutionary inventions of the 19th century. Since they represent large energy consumers, it is necessary to improve their ecological footprints. In the automotive sector, carbon emission as well as the use of fossil fuels shall be reduced by switching from internal combustion engines to electric vehicles, which will be charged with renewable energies. At the end of 2015, 1.26 million electric cars had already been registered worldwide. This is about twice as much as in 2014, and according to government officials this number should further be increased to 20 million electric cars by 2020.^[1] In case of electric light, high potential for savings is seen for the replacement of inefficient incandescent light bulbs. In this light source, approximately 90% of the energy is lost in the form of heat and only remaining 10% is converted into visible light.^[2] Compact fluorescent lamps and light-emitting diodes (LEDs) represent energy-efficient alternatives and are commercially available since several years. Although LEDs have previously been of no importance for general illumination purposes, compact fluorescent lamps are currently more and more displaced by them. Due to their efficient conversion of electric energy into visible light, their exceptional durability and environmental friendliness, LEDs are meanwhile seen as the light sources of the future. According to an energy savings forecast given by the United States Department of Energy, a 75% reduction in energy consumption in the lighting sector by 2035 is predicted by using LEDs instead of incandescent light bulbs. This corresponds to the current energy consumption of approximately 45 million U.S. households.^[3]

Solid-state materials play an important role in many novel technologies, including innovations for electric vehicles and lighting.^[4,5] Materials scientists and solid-state chemists deal with syntheses, comprehensive structural characterizations and materials property investigations of

novel compounds. Especially, the compound class of nitrides has gained significant importance over the last decade. Li-containing nitrides may find application as solid-state electrolytes in Li-ion-batteries^[6-8] with a possible use in electric vehicles. Thoroughly investigated Li_2SiN_2 is one example of a lithium nitridosilicate exhibiting Li-ion conductivity.^[8-10] Regarding lighting industry, several nitrides show luminescence properties upon doping with rare earth ions like Eu^{2+} or Ce^{3+} , and are applicable as luminescent materials in phosphor-converted light-emitting diodes (pc-LEDs).^[11-18] However, syntheses and handling of nitrides are fairly challenging. When exposed to air or moisture, most nitrides are easily hydrolyzed and oxidized. As a consequence, all manipulations have to be done under strict exclusion of oxygen. This behavior can be explained by the stability of chemical bonds and the differences in dissociation energies of O_2 ($498 \text{ kJ}\cdot\text{mol}^{-1}$) and N_2 ($945 \text{ kJ}\cdot\text{mol}^{-1}$).^[19] Because chemical bonds to oxygen are typically more stable than chemical bonds to nitrogen, most solid oxides are more stable than solid nitrides. Furthermore, because of the higher dissociation energy of N_2 compared to O_2 , and unless a high degree of condensation within the nitride kinetically prevents dissociation, nitrides decompose more rapidly with the loss of N_2 upon heating than oxides.

Two classes of nitrides turned out to have a huge impact on technological developments, namely nitridosilicates and nitridoaluminates.^[20,21] The crystal structures of both compound classes are usually described as nitridometallate anions, charge balanced by electropositive ions, for example, alkaline earth metal ions. In almost all cases, nitridometallate anions consist of SiN_4 or AlN_4 tetrahedra, which may be connected through common vertices or edges, by forming more- or less-condensed anionic frameworks. This leads to diverse structural possibilities, considerably more than for oxosilicates, which exhibit, except fibrous SiO_2 ,^[22] only corner sharing SiO_4 tetrahedra. Nevertheless, the existence of fibrous SiO_2 has not yet been confirmed unequivocally. Structural motifs similar to nitridosilicates and nitridoaluminates can be found in closely related compound classes of nitridogallates and nitridogermanates.

Nitridogallates derive from the binary nitride GaN and their crystal structures are made up of GaN_4 tetrahedra with Ga in oxidation state +III. These may be linked through common corners and edges resulting in anionic substructures of infinite chains (e.g. $\text{Ba}_3\text{Ga}_3\text{N}_5$),^[23] layers (e.g. $\text{Ca}_3\text{Ga}_2\text{N}_4$)^[24] or three-periodic networks (e.g. $\text{Sr}_3\text{Ga}_3\text{N}_5$).^[24] Moreover, nitridogallates containing isolated GaN_3 units are known (e.g. Ca_6GaN_5).^[25] Alkaline earth metal ions thereby act as counter ions and are distributed among the voids of the anionic networks. Deviating from oxidation state +III, Ga may also occur in metallic CaGaN ^[26] with layers made up of Ga atoms,

the subnitride $(\text{Ca}_7\text{N}_4)[\text{Ga}_x]$ ^[27] with linear chains of Ga atoms, in the Zintl phase $\text{Ca}_5\text{Ga}_2\text{N}_4$,^[28] and in clusters like $(\text{Ba}_6\text{N})\text{Ga}_5$.^[29]

The importance of Ga-containing compounds has increased significantly since the investigations of InGaP, GaAsP, or AlGaAs, which represent solid-solutions of III-V-semiconductor materials that are technologically important for LEDs.^[30] Based on the findings about electroluminescence by Henry J. Round in 1907^[31] and Oleg Losev in the mid 1920s,^[32,33] the first LEDs in the visible using GaAsP as semiconducting red emitting material have been developed by Holonyak et al. in 1962.^[34] Nowadays, GaN, especially its ternary alloys InGaN and AlGaIn, find application as blue emitting semiconductor materials in high-performance pc-LEDs.^[30,35-38] Prerequisite for this invention was the synthesis of high-quality GaN single crystals, which represented a major challenge for many years and has not been possible until the development of new crystal growth techniques like Metal Organic Vapor Phase Epitaxy (MOVPE) in the 1970s.^[39-42] Besides, there are some nitridogallates known from literature that show luminescence in the visible region upon doping with Eu^{2+} , even though the band gaps for nitridogallates are generally expected to be too small. The reason why these nitridogallates, namely, $\text{Mg}_3\text{Ga}_3\text{N}_5:\text{Eu}^{2+}$ ($\lambda_{\text{max}} = 578 \text{ nm}$),^[43] $\text{Ba}_3\text{Ga}_3\text{N}_5:\text{Eu}^{2+}$ ($\lambda_{\text{max}} = 639 \text{ nm}$),^[23] and $\text{Ba}[\text{Mg}_2\text{Ga}_2\text{N}_4]:\text{Eu}^{2+}$ ($\lambda_{\text{max}} = 649 \text{ nm}$)^[44] do not find application as LED phosphors yet is the fact that they were obtained only as side phases during synthesis. Because of their promising luminescence properties, succeeding in optimizing synthesis would open up prospects for their application in pc-LEDs.

Analogous structural motifs of nitridogallates can also be found in the class of nitridogermanates. They are made up of either isolated GeN_3 triangles or GeN_4 tetrahedra with Ge in oxidation state +IV. GeN_4 tetrahedra may be linked through common vertices and edges, by resulting in more- or less-condensed anionic substructures, which are charge balanced by alkaline earth metal ions. In contrast to nitridosilicates, the field of nitridogermanates is quite unexplored so far. To the best of our knowledge, only six ternary compounds are known to date, namely, CaGeN_2 ,^[45] Ca_4GeN_4 ,^[46] Ca_7GeN_6 ,^[47] Sr_7GeN_6 ,^[47] $\text{Sr}_5\text{Ge}_2\text{N}_6$,^[48] and $\text{Ba}_9\text{Ge}_3\text{N}_{10}$.^[49] All of these, except for CaGeN_2 , exhibit non-condensed anionic substructures containing isolated $[\text{GeN}_3]^{5-}$ triangles ($\text{Ba}_9\text{Ge}_3\text{N}_{10}$), isolated $[\text{GeN}_4]^{8-}$ tetrahedra (Ca_4GeN_4 and M_7GeN_6) or $[\text{Ge}_2\text{N}_6]^{10-}$ double tetrahedra ($\text{Sr}_5\text{Ge}_2\text{N}_6$). A higher degree of condensation can be found in CaGeN_2 , and in quaternary nitridogermanates, of which only five are known. $\text{Sr}_3\text{MgGeN}_4$ ^[50] and $\text{Ba}_3\text{MgGeN}_4$ ^[51] exhibit infinite chains of alternating MgN_4 and GeN_4 tetrahedra; $\text{Sr}[\text{Mg}_3\text{GeN}_4]$ ^[52] exhibits a three-periodic anionic network made up of $(\text{Mg,Ge})\text{N}_4$ tetrahedra with mixed occupancy Mg/Ge. The Li-containing quaternary nitridogermanate $\text{Ca}_{13}\text{Li}_4\text{Ge}_6\text{N}_{18}$ ^[53] is made up of infinite chains of

corner-sharing GeN_4 tetrahedra, interconnected by chains of corner-sharing $[\text{Li}_2\text{N}_6]$ ‘bow tie’ units. Furthermore, $\text{Sr}_3\text{Li}_4\text{Ge}_2\text{N}_6$ ^[54] as the fifth example of quaternary nitridogermanates, exhibits non-condensed $[\text{Ge}_2\text{N}_6]^{10-}$ double tetrahedra, and corner- and edge-sharing $[\text{Li}_2\text{N}_6]$ ‘bow tie’ units. Layered nitridogermanates are not known to date.

Further structural motifs beside GeN_4 tetrahedra can be found, for example, in the ternary compounds $M_3\text{Ge}_2\text{N}_2$ ^[55,56] and $M_6\text{Ge}_5\text{N}_2$ ^[57] ($M = \text{Sr}, \text{Ba}$). Thereby, Ge occurs in oxidation states $-II$ and $+II$, by forming infinite zigzag chains of Zintl anions Ge^{2-} , and dumbbell-shaped anions $[\text{Ge}^{\text{II}}\text{N}_2]^{4-}$. As illustrated by the example of $\text{Sr}_{11}\text{Ge}_4\text{N}_6$,^[58] which is composed of $[\text{Ge}^{-\text{IV}}\text{N}_2\text{Sr}_7]^{4+}$ antiperovskite-type slabs and $[\text{Sr}_4\text{Ge}^{-\text{IV}}]^{4+}$ layers, separated by sheets of $[\text{Ge}^{\text{II}}\text{N}_2]^{4-}$ ions, Ge may also occur in oxidation state $-IV$ and is thereby solely coordinated by metal ions.

Elemental Ge is a semiconductor and finds application in transistors, optical devices, and in special alloys. The germanate Mg_2GeO_4 shows red emission upon doping with Mn^{2+} , or Eu^{3+} .^[59,60] Luminescence of rare earth-doped nitridogermanates has not yet been observed. Due to the close structural relations to nitridogallates, -aluminates, and -silicates, basic research on novel nitridogermanates and accompanying structure elucidation is of great interest regarding their transferability to other compound classes, which may exhibit promising luminescence properties upon doping, for example, with Eu^{2+} . Especially, quaternary compounds are in the focus of research, because they are expected to be more stable due to their hitherto observed higher degree of condensation.

Syntheses of both classes of nitrides, nitridogallates and nitridogermanates, were typically performed using the NaN_3 route. Therefore, pure elements as well as NaN_3 and Na were sealed under inert conditions in Ta or Nb ampules. The reaction mixture was heated up to approximately $760\text{ }^\circ\text{C}$, held for a few hours and subsequently cooled down with slow cooling rates. During heating, NaN_3 decomposes, by generating an increased nitrogen pressure within the reaction vessel. Na acts as flux (melting point $97.8\text{ }^\circ\text{C}$; boiling point $881.3\text{ }^\circ\text{C}$)^[61] and helps to enhance diffusion rates of the solid-state reaction.^[62] Moreover, the formation of nitrides is facilitated by addition of alkaline earth metal ions, which are able to increase solubility of nitrogen in liquid sodium.^[63] Slow cooling rates encourage crystal growth of the products.

The NaN_3 route has become established because solid-state reactions generally show low diffusion coefficients and would require long reaction periods. This could be accelerated by increasing the reaction temperature, which is limited by decomposition of nitrides through the loss of N_2 , or by using a flux. Important factors for the choice of the flux agent are a low melting

point, ideally accompanied by a high boiling point, inertness to starting materials and products as well as removability after synthesis. Especially Na can easily be separated by evaporation at 320 °C under vacuum.

Unlike nitridogallates and nitridogermanates, there are plenty of synthesis routes that have been established for nitridosilicates.^[20] Classical reactions were high-temperature reactions of binary nitrides at approximately 1700 °C, which are essential regarding high chemical and thermal stability of Si₃N₄. Because high-temperature reactions will mostly lead to thermodynamic products, the number of possible novel nitridosilicates using this method is limited, and new synthetic approaches had to be developed. These include precursor routes, by using, for example, alkaline earth metal amides and silicon diimide Si(NH)₂^[21,64] as reactive starting materials, flux methods, by using liquid Na or Li in combination with respective alkaline metal azides (NaN₃ or LiN₃),^[18,65] solid-state metathesis reactions, by using a reactive flux and coproducing a metathesis salt as driving force of the reaction,^[66] and also ammonothermal syntheses in supercritical ammonia at elevated temperatures.^[67] Nowadays, high-quality bulk GaN crystals, which represent the basis for several current technologies, are accessible by the ammonothermal technique.^[68]

The objectives of this thesis were synthesis, identification and structural characterization of novel nitridogallates, nitridogermanates and nitridosilicates. In order to investigate luminescence properties of resulting materials, 1-3 mol% Eu²⁺ were added as dopant to each synthesis approach. For nitridogallates, the emphasis lied on the development of new synthetic strategies in order to obtain novel quaternary compounds with high yields of the reaction product. For nitridogermanates and nitridosilicates, the main focus was on synthesis of novel Mg-containing compounds and their luminescence properties upon doping with Eu²⁺. Syntheses were performed either in weld shut Ta ampules in tube furnaces, or also in W crucibles, which were placed in a radio-frequency furnace and heated under N₂ atmosphere. Different analytical methods helped to identify and characterize the reaction products. Therefore, energy-dispersive X-ray (EDX) spectroscopy was employed for quantitative and qualitative analyses. X-ray diffraction on powders and on single crystals was applied for structural elucidation. Calculations of bond-valence sums and of the Madelung part of the lattice energy, as well as electron microscopy was applied to confirm the structural models obtained from X-ray diffraction analysis. A luminescence microscope was applied to determine the remarkable luminescence properties of the presented nitridosilicate, which indicates its possible application as optical material in specialized fields.

References

- [1] Organisation for Economic Co-operation and Development / International Energy Agency, *Global Electric Vehicle Outlook 2016 - Beyond One Million Electric Cars*, **2016**. (https://www.iea.org/publications/freepublications/publication/Global_EV_Outlook_2016.pdf)
- [2] W. Schnick, *Phys. Status Solidi RRL* **2009**, 3, A113.
- [3] U.S. Department of Energy, *Energy Savings Forecast of Solid-State Lighting in General Illumination Applications*, **2016**. (https://energy.gov/sites/prod/files/2016/09/f33/energysavingsforecast16_2.pdf)
- [4] Y. Zhu, X. He, Y. Mo, *J. Mater. Chem. A* **2016**, 4, 3253.
- [5] J. M. Phillips, M. E. Coltrin, M. H. Crawford, A. J. Fischer, M. R. Krames, R. Mueller-Mach, G. O. Mueller, Y. Ohno, L. E. S. Rohwer, J. A. Simmons, J. Y. Tsao, *Laser Photonics Rev.* **2007**, 1, 307.
- [6] A. D. Robertson, A. R. West, A. G. Ritchie, *Solid State Ionics* **1997**, 104, 1.
- [7] M. S. Whittingham, *Chem. Rev.* **2004**, 104, 4271.
- [8] H. Yamane, S. Kikkawa, M. Koizumi, *Solid State Ionics* **1987**, 25, 183.
- [9] S. Pagano, M. Zeuner, S. Hug, W. Schnick, *Eur. J. Inorg. Chem.* **2009**, 1579.
- [10] M. S. Bhambra, D. J. Fray, *J. Mater. Sci.* **1995**, 30, 5381.
- [11] X.-H. He, N. Lian, J.-H. Sun, M.-Y. Guan, *J. Mater. Sci.* **2009**, 44, 4763.
- [12] K. Uheda, N. Hirosaki, H. Yamamoto, *Phys. Status Solidi A* **2006**, 203, 2712.
- [13] P. Pust, V. Weiler, C. Hecht, A. Tücks, A. S. Wochnik, A.-K. Henß, D. Wiechert, C. Scheu, P. J. Schmidt, W. Schnick, *Nat. Mater.* **2014**, 13, 891.
- [14] H. Watanabe, N. Kijima, *J. Alloys Compd.* **2009**, 475, 434.
- [15] R.-J. Xie, N. Hirosaki, Y. Li, T. Takeda, *Materials* **2010**, 3, 3777.
- [16] H. A. Höpfe, H. Lutz, P. Morys, W. Schnick, A. Seilmeier, *J. Phys. Chem. Solids* **2000**, 61, 2001.
- [17] M. Zeuner, P. J. Schmidt, W. Schnick, *Chem. Mater.* **2009**, 21, 2467.
- [18] S. Schmiechen, H. Schneider, P. Wagatha, C. Hecht, P. J. Schmidt, W. Schnick, *Chem. Mater.* **2014**, 26, 2712.
- [19] E. Riedel, *Anorganische Chemie*, de Gruyter, Berlin, New York, **2011**.
- [20] M. Zeuner, S. Pagano, W. Schnick, *Angew. Chem.* **2011**, 123, 7898; *Angew. Chem. Int. Ed.* **2011**, 50, 7754.
- [21] W. Schnick, H. Huppertz, *Chem. Eur. J.* **1997**, 3, 679.

- [22] A. Weiss, A. Weiss, *Z. Anorg. Allg. Chem.* **1954**, 276, 95.
- [23] F. Hintze, F. Hummel, P. J. Schmidt, D. Wiechert, W. Schnick, *Chem. Mater.* **2012**, 24, 402.
- [24] S. J. Clarke, F. J. DiSalvo, *Inorg. Chem.* **1997**, 36, 1143.
- [25] G. Cordier, P. Höhn, R. Kniep, A. Rabenau, *Z. Anorg. Allg. Chem.* **1990**, 591, 58.
- [26] P. Verdier, P. L'Haridon, M. Maunaye, R. Marchand, *Acta Crystallogr., Sect. A: Found. Crystallogr.* **1974**, 30, 226.
- [27] P. Höhn, G. Auffermann, R. Ramlau, H. Rosner, W. Schnelle, R. Kniep, *Angew. Chem.* **2006**, 118, 6833; *Angew. Chem. Int. Ed.* **2006**, 45, 6681.
- [28] G. Cordier, *Z. Naturforsch., B: Chem. Sci.* **1988**, 43, 1253.
- [29] G. Cordier, M. Ludwig, D. Stahl, P. C. Schmidt, R. Kniep, *Angew. Chem.* **1995**, 107, 1879; *Angew. Chem. Int. Ed. Engl.* **1995**, 34, 1761.
- [30] C. Ronda, *Luminescence - From Theory to Applications*, WILEY-VCH, Weinheim, **2008**.
- [31] H. J. Round, *Electr. World* **1907**, 49, 308.
- [32] N. Zheludev, *Nat. Photonics* **2007**, 1, 189.
- [33] O. V. Losev, *Phil. Mag.* **1928**, 6, 1024.
- [34] N. Holonyak, S. F. Bevacqua, *Appl. Phys. Lett.* **1962**, 1, 82.
- [35] S. Nakamura, *MRS Bull.* **2011**, 22, 29.
- [36] S. Nakamura, S. Pearton, G. Fasol, *The Blue Laser Diode: The Complete Story*, Springer-Verlag Berlin Heidelberg, **1997**, **2000**.
- [37] S. Nakamura, M. Senoh, T. Mukai, *Appl. Phys. Lett.* **1993**, 62, 2390.
- [38] S. Nakamura, T. Mukai, M. Senoh, *Appl. Phys. Lett.* **1994**, 64, 1687.
- [39] H. M. Manasevit, F. M. Erdmann, W. I. Simpson, *J. Electrochem. Soc.* **1971**, 118, 1864.
- [40] H. Amano, N. Sawaki, I. Akasaki, Y. Toyoda, *Appl. Phys. Lett.* **1986**, 48, 353.
- [41] Y. Koide, H. Itob, M. R. H. Khan, K. Hiramatsu, N. Sawaki, I. Akasaki, *J. Appl. Phys.* **1987**, 61, 4540.
- [42] I. Akasaki, H. Amano, Y. Koide, K. Hiramatsu, N. Sawaki, *J. Crystal Growth* **1989**, 98, 209.
- [43] F. Hintze, N. W. Johnson, M. Seibald, D. Muir, A. Moewes, W. Schnick, *Chem. Mater.* **2013**, 24, 4044.
- [44] P. Pust, F. Hintze, C. Hecht, V. Weiler, A. Locher, D. Zitnanska, S. Harm, D. Wiechert, P. J. Schmidt, W. Schnick, *Chem. Mater.* **2014**, 26, 6113.
- [45] M. Maunaye, J. Guyader, Y. Laurent, J. Lang, *Bull. Soc. Fr. Minéral. Crist.* **1971**, 94, 347.
- [46] S. J. Clarke, F. J. DiSalvo, *Inorg. Chem.* **2000**, 39, 2631.

- [47] S. C. Junggeburth, O. Oeckler, D. Johrendt, W. Schnick, *Inorg. Chem.* **2008**, 47, 12018.
- [48] S. C. Junggeburth, O. Oeckler, W. Schnick, *Z. Anorg. Allg. Chem.* **2008**, 634, 1309.
- [49] D. G. Park, F. J. DiSalvo, *Bull. Korean Chem. Soc.* **2008**, 29, 2413.
- [50] D. G. Park, Z. A. Gál, F. J. DiSalvo, *J. Alloys Compd.* **2003**, 360, 85.
- [51] D. G. Park, F. J. DiSalvo, *Bull. Korean Chem. Soc.* **2011**, 32, 353.
- [52] D. G. Park, Y. Dong, F. J. DiSalvo, *Solid State Sci.* **2008**, 10, 1846.
- [53] D. G. Park, F. J. DiSalvo, *Bull. Korean Chem. Soc.* **2012**, 33, 1759.
- [54] D. G. Park, Z. A. Gál, F. J. DiSalvo, *J. Solid State Chem.* **2003**, 172, 166.
- [55] S. J. Clarke, G. R. Kowach, F. J. DiSalvo, *Inorg. Chem.* **1996**, 35, 7009.
- [56] H. Yamane, F. J. DiSalvo, *J. Alloys Compd.* **1996**, 241, 69.
- [57] D. G. Park, Z. A. Gál, F. J. DiSalvo, *Bull. Korean Chem. Soc.* **2005**, 26, 1543.
- [58] Z. A. Gál, S. J. Clarke, *Chem. Commun.* **2005**, 728.
- [59] M. Iwasaki, D. N. Kim, K. Tanaka, T. Murata, K. Morinaga, *Sci. Technol. Adv. Mater.* **2003**, 4, 137.
- [60] H.-M. Yang, J.-X. Shi, H.-B. Liang, M.-L. Gong, *Mater. Sci. Eng., B* **2006**, 127, 276.
- [61] A. F. Holleman, N. Wiberg, *Lehrbuch der Anorganischen Chemie*, de Gruyter, Berlin, New York, **2007**.
- [62] M. G. Kanatzidis, R. Pöttgen, W. Jeitschko, *Angew. Chem.* **2005**, 117, 7156; *Angew. Chem. Int. Ed.* **2005**, 44, 6996.
- [63] H. Yamane, *J. Ceram. Soc. Japan* **2009**, 117, 1021.
- [64] W. Schnick, H. Huppertz, R. Lauterbach, *J. Mater. Chem.* **1999**, 9, 289.
- [65] Z. A. Gál, P. M. Mallinson, H. J. Orchard, S. J. Clarke, *Inorg. Chem.* **2004**, 43, 3998.
- [66] H.-J. Meyer, *Dalton Trans.* **2010**, 39, 5973.
- [67] T. M. M. Richter, R. Niewa, *Inorganics* **2014**, 2, 29.
- [68] B. Wang, M. J. Callahan, *Cryst. Growth Des.* **2006**, 6, 1227.

2 Nitridogallates and Nitridogermanates

2.1 Introduction

The chemistry of Mg-containing nitridogallates and nitridogermanates is quite unexplored and only a small number of compounds have yet been reported in literature. These include the homeotypic compounds $\text{Sr}[\text{Mg}_2\text{Ga}_2\text{N}_4]$,^[1] $\text{Ba}[\text{Mg}_2\text{Ga}_2\text{N}_4]$ ^[2] and $\text{Sr}[\text{Mg}_3\text{GeN}_4]$ ^[1] as well as the isotypic nitridogermanates $\text{Sr}_3\text{MgGeN}_4$ ^[3] and $\text{Ba}_3\text{MgGeN}_4$.^[4] Because Mg and Ga, or Mg and Ge are part of the anionic tetrahedral network, the compounds can be more appropriately classified as nitridomagnesogallates and nitridomagnesogermanates. Whereas the latter two, $\text{Sr}_3\text{MgGeN}_4$ and $\text{Ba}_3\text{MgGeN}_4$, exhibit chains of edge-sharing MgN_4 and GeN_4 tetrahedra in an alternating manner, the other compounds show disordering of tetrahedrally coordinated ions $\text{Mg}^{2+}/\text{Ga}^{3+}$ or $\text{Mg}^{2+}/\text{Ge}^{4+}$ within its three-periodic anionic substructures. Mixed occupation of network-building ions is also known from other compound classes, e.g. nitridoalumosilicates (CaAlSiN_3) ^[5,6] or nitridomagnesosilicates $(\text{Sr}[\text{Mg}_3\text{SiN}_4])$.^[7] One further Mg-containing compound is the ternary nitride Mg_3GaN_3 .^[8] It contains both, MgN_4 and GaN_4 tetrahedra, which are connected via common corners and vertices. Due to the resulting uncharged tetrahedral network and its strong relationship to the binary nitrides Mg_3N_2 and GaN , Mg_3GaN_3 has to be designated as a double nitride of Mg and Ga instead of a nitridomagnesogallate.

In the following, numerous novel Mg-containing nitridogallates and –germanates are presented. The first part of this chapter deals with the layered nitridomagnesogallates $\text{CaMg}_2\text{GaN}_3$ and $\text{CaMg}_2\text{Ga}_2\text{N}_4$. Both compounds were synthesized by solid-state metathesis reactions, which represent a new synthetic approach for nitridogallates. The crystal structure of $\text{CaMg}_2\text{GaN}_3$ is isotypic with previously reported nitridomagnesosoaluminate $\text{CaMg}_2\text{AlN}_3$ ^[9] and homeotypic with $\text{Ca}_2\text{Mg}_5\text{GeN}_6$, a novel nitridomagnesogermanate, which is thoroughly described in the second part of this chapter. The crystal structure of $\text{CaMg}_2\text{Ga}_2\text{N}_4$ resembles that of $\text{CaMg}_2\text{GaN}_3$, with a slightly modified composition of layers. TEM investigations also provide indications of formation of composite crystals. The third part of this chapter includes a detailed description of the structurally related compounds $\text{Ca}_4\text{Mg}_5\text{Ge}_3\text{N}_{10}$ and $\text{Sr}_2\text{Mg}_3\text{GaN}_{4.33}$. Its crystal structures are homeotypic with $\text{Ca}_2\text{MgGa}_3\text{N}_5$ and represent higher condensed variants of the widely known $M^{\text{II}}_2\text{Si}_5\text{N}_8$ ($M^{\text{II}} = \text{Sr}, \text{Ba}$)^[10] type of structure. Because several nitridosilicates as well as nitridogallates show interesting luminescence properties when doped with rare earth ions, the

Eu²⁺-doped nitridomagnesogermanate Ba[Mg₃GeN₄]:Eu²⁺ has been synthesized for luminescence investigations. Its crystal structure as well as theoretical calculations of electronic properties allow for comparison of Ba[Mg₃GeN₄]:Eu²⁺ with other compounds isostructural to UCr₄C₄. Results are summarized in the last part of this chapter.

References

- [1] D. G. Park, Y. Dong, F. J. DiSalvo, *Solid State Sci.* **2008**, 10, 1846.
- [2] P. Pust, F. Hintze, C. Hecht, V. Weiler, A. Locher, D. Zitnanska, S. Harm, D. Wiechert, P. J. Schmidt, W. Schnick, *Chem. Mater.* **2014**, 26, 6113.
- [3] D. G. Park, Z. A. Gál, F. J. DiSalvo, *J. Alloys Compd.* **2003**, 360, 85.
- [4] D. G. Park, F. J. DiSalvo, *Bull. Korean Chem. Soc.* **2011**, 32, 353.
- [5] K. Uheda, N. Hirotsaki, H. Yamamoto, *Phys. Status Solidi A* **2006**, 203, 2712.
- [6] M. Kubus, H.-J. Meyer, *Z. Anorg. Allg. Chem.* **2013**, 639, 669.
- [7] S. Schmiechen, H. Schneider, P. Wagatha, C. Hecht, P. J. Schmidt, W. Schnick, *Chem. Mater.* **2014**, 26, 2712.
- [8] F. Hintze, N. W. Johnson, M. Seibald, D. Muir, A. Moewes, W. Schnick, *Chem. Mater.* **2013**, 25, 4044.
- [9] M. Kubus, K. Levin, S. Kroeker, D. Ensling, T. Jüstel, H.-J. Meyer, *Dalton Trans.* **2015**, 44, 2819.
- [10] T. Schlieper, W. Milius, W. Schnick, *Z. Anorg. Allg. Chem.* **1995**, 621, 1380.

2.2 Layered Nitridomagnesogallates $\text{CaMg}_2\text{GaN}_3$ and $\text{CaMg}_2\text{Ga}_2\text{N}_4$

published in: *Eur. J. Inorg. Chem.* **2017**, 1067-1074

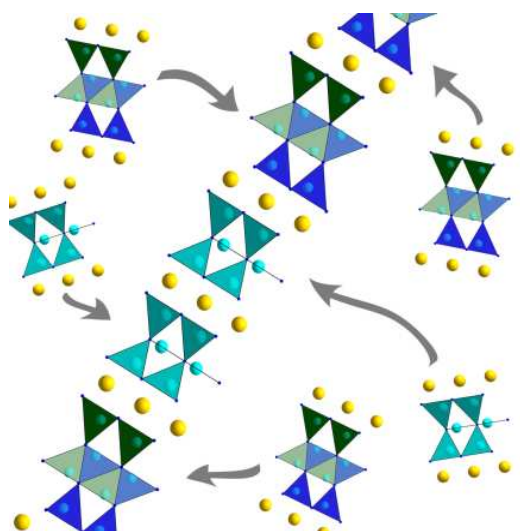
authors: Christine Poesl, Lukas Neudert, and Wolfgang Schnick

DOI: 10.1002/ejic.201601381

Copyright © 2017 Wiley-VCH Verlag GmbH & Co. KGaA, Weinheim

<http://onlinelibrary.wiley.com/doi/10.1002/ejic.201601381/abstract>

Abstract: The quaternary nitrides $\text{CaMg}_2\text{GaN}_3$ and $\text{CaMg}_2\text{Ga}_2\text{N}_4$ were synthesized by means of solid-state metathesis reactions. The crystal structures of both nitridomagnesogallates contain layers made up of either tetrahedral MN_4 units ($\text{CaMg}_2\text{Ga}_2\text{N}_4$) or both tetrahedral MN_4 units and planar MN_3 triangles ($\text{CaMg}_2\text{GaN}_3$) with mixed occupation of central atoms Mg and Ga. $\text{CaMg}_2\text{GaN}_3$ was obtained as a gray powder. Its crystal structure was determined on the basis of X-ray powder diffraction data [$P6_3/mmc$ (no. 194), $a = 3.43093(8)$ and $c = 17.3989(5)$ Å,



$V = 177.368(9)$ Å³, $Z = 2$]. The compound is isotypic with $\text{CaMg}_2\text{AlN}_3$ and homeotypic with $\text{Ca}_2\text{Mg}_5\text{GeN}_6$, ScAl_3C_3 and UAl_3C_3 . The crystal structure of $\text{CaMg}_2\text{Ga}_2\text{N}_4$ [$P\bar{3}m1$ (no. 164), $a = 3.3859(3)$, $c = 11.2378(11)$ Å, $V = 111.57(2)$ Å³, $Z = 1$] was determined from single-crystal X-ray diffraction data and corroborated by Rietveld refinement. TEM investigations confirmed the metrics of both crystal structures and indicate the presence of both compounds as side products within one reaction batch. Structural similarities between $\text{CaMg}_2\text{GaN}_3$ and $\text{CaMg}_2\text{Ga}_2\text{N}_4$ are discussed.

2.2.1 Introduction

The binary nitride GaN is an important direct wide-band-gap semiconductor and thus technologically useful. When doped by electropositive metals like Mg^{2+} or Zn^{2+} (p-doping), GaN shows electroluminescence resulting from the recombination of electrons and holes in a p-n-junction. The p-doping of its ternary alloys InGaN as well as AlGaN is of fundamental importance for highly efficient blue light-emitting diodes (LED), and is key for LED-based lighting technologies.^[1-5]

In general, the structures of nitridogallates are derived from GaN and contain GaN_4 tetrahedra as structural motifs. These tetrahedra may be linked through common corners and/or edges to form anionic substructures of infinite chains, layers, or three-dimensional networks. In addition, trigonal-planar GaN_3 units occur in nitridogallates.^[6-9]

There is a close structural relationship between nitridogallates, nitridoaluminates, and nitridosilicates as illustrated by the structurally related compounds $\text{MMg}_2\text{Ga}_2\text{N}_4$ ($M = \text{Sr}, \text{Ba}$),^[10,11] MLiAl_3N_4 ($M = \text{Ca}, \text{Sr}$),^[12,13] or MMg_3SiN_4 ($M = \text{Ca}, \text{Sr}, \text{Ba}$).^[14,15] Unlike nitridogallates, the number of known quaternary or higher nitridoaluminates and nitridosilicates has increased significantly in the past few years. A possible reason for this may be the broad spectrum of synthetic approaches in the cases of nitridosilicates and nitridoaluminates (see below) that have been developed.^[16-25] The classical reactions using binary nitrides (e.g. Si_3N_4 or AlN) as starting materials require high temperatures of 1550-1750 °C because of the high chemical and thermal stability of both nitrides and the low diffusion coefficients in solid-state reactions.^[22,23] To reduce the reaction temperature, new synthetic approaches leading to ternary or quaternary nitridoaluminates and nitridosilicates had to be developed. These include precursor routes (unreactive starting materials are replaced by reactive ones), flux methods (employment of liquid metals like sodium or lithium, which are able to dissolve a variety of metals), and solid-state metathesis reactions (reduction of the ignition temperature by using a reactive flux). None of the aforementioned synthetic approaches have been reported for nitridogallates so far. Syntheses of ternary or quaternary nitridogallates have been exclusively described by employing the NaN_3 route.^[10,26-29] For this purpose, a mixture of NaN_3 , the respective elements, and Na metal was sealed under the exclusion of oxygen and moisture in Ta or Nb ampules and heated to approximately 760 °C. Sodium azide decomposes while heating, thereby inducing an increased nitrogen pressure within the ampule. Solubility of nitrogen in sodium can be improved by the addition of electropositive metals like alkaline earth metals.^[30] Reaction products of

nitridogallates often contain an inhomogeneous mixture of several compounds. Owing to inhomogeneity, and in some cases small crystal sizes or bad crystallinity, the combination of X-ray powder diffraction with electron microscopy, especially selected-area electron diffraction (SAED), and energy-dispersive X-ray spectroscopy (EDX), is a reasonable approach for structure determination. However, the number of described quaternary or higher nitridogallates is relatively small. Only three quaternary compounds containing Mg within the anionic tetrahedral network are known to date, namely, $\text{Ca}_2\text{MgGa}_3\text{N}_5$,^[27] $\text{SrMg}_2\text{Ga}_2\text{N}_4$,^[10] and $\text{BaMg}_2\text{Ga}_2\text{N}_4$.^[11] All of these compounds were synthesized by using the NaN_3 route.

In this contribution, we report on $\text{CaMg}_2\text{GaN}_3$ and $\text{CaMg}_2\text{Ga}_2\text{N}_4$, two new nitridomagnesogallates with layered anionic substructures. Both compounds were synthesized by using solid-state metathesis reactions,^[31-34] which represent a promising synthetic approach for nitridogallates. The crystal structures will be discussed in detail.

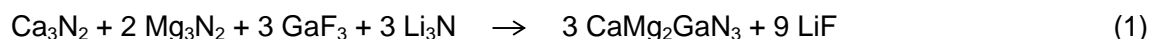
2.2.2 Results and Discussion

2.2.2.1 Syntheses and Chemical Analysis

$\text{CaMg}_2\text{GaN}_3$ and $\text{CaMg}_2\text{Ga}_2\text{N}_4$ were obtained from three different reaction batches after solid-state metathesis reactions. The key feature of this reaction method is the employment of reactive starting materials by coproduction of a metathesis salt.

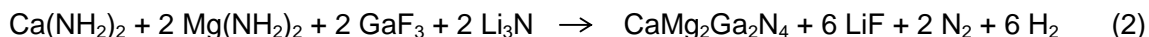
$\text{CaMg}_2\text{GaN}_3$

The nitridomagnesogallate was obtained as a gray powder from a mixture of Ca_3N_2 , Mg_3N_2 , GaF_3 , and Li_3N . The starting materials were placed in a tungsten crucible, which was heated in a radiofrequency furnace under an N_2 atmosphere to 850 °C. Equation (1) illustrates an idealized stoichiometric metathesis reaction.



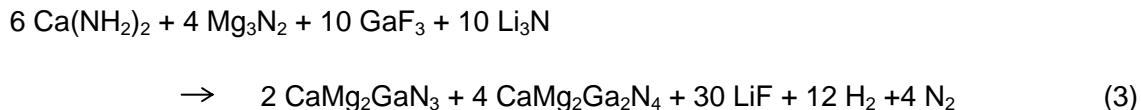
$\text{CaMg}_2\text{Ga}_2\text{N}_4$

A heterogeneous product with colorless blocklike single crystals of $\text{CaMg}_2\text{Ga}_2\text{N}_4$ was obtained by reaction of $\text{Ca}(\text{NH}_2)_2$, $\text{Mg}(\text{NH}_2)_2$, GaF_3 , and Li_3N in sealed Ta ampules in a tube furnace at 1000 °C. CsCl was added as flux. A possible stoichiometric reaction is given in Equation (2).



$\text{CaMg}_2\text{GaN}_3$ and $\text{CaMg}_2\text{Ga}_2\text{N}_4$

The synthesis of both compounds as side products within one reaction batch was performed in an open tungsten crucible in a radiofrequency furnace under a N_2 atmosphere at 850 °C with $\text{Ca}(\text{NH}_2)_2$, Mg_3N_2 , GaF_3 and Li_3N as starting materials. Equation (3) illustrates a possible stoichiometric metathesis reaction.



The thermodynamic driving force of all three reactions is the formation of LiF. Both nitridomagnesogallates are sensitive towards air and moisture. Elemental analyses were performed with the aid of EDX spectroscopy. It gave an atomic ratio of Ca/Mg/Ga/N of 1.0:2.3:1.0:2.8 for powder samples of $\text{CaMg}_2\text{GaN}_3$ and 1.0:1.9:2.0:4.0 for single crystals of $\text{CaMg}_2\text{Ga}_2\text{N}_4$. Besides small amounts of oxygen that can be ascribed to the high sensitivity to moisture, no further elements were detected.

2.2.2.2 Structure Determination

$\text{CaMg}_2\text{GaN}_3$

The crystal structure of $\text{CaMg}_2\text{GaN}_3$ was determined with the charge-flipping algorithm based on X-ray powder diffraction data. The compound crystallizes in the hexagonal space group $P6_3/mmc$ with lattice parameters $a = 3.43093(8)$ and $c = 17.3989(5)$ Å. It is isotypic with $\text{CaMg}_2\text{AlN}_3$ and homeotypic with $\text{Ca}_2\text{Mg}_5\text{GeN}_6$, ScAl_3C_3 , and UAl_3C_3 .^[31,35,36] In contrast to $\text{CaMg}_2\text{GaN}_3$ and $\text{Ca}_2\text{Mg}_5\text{GeN}_6$, the crystal structures of $\text{CaMg}_2\text{AlN}_3$ and the carbides can be described by two different space groups ($P6_3mc$ (no. 186) and $P6_3/mmc$ (no. 194)). Generally, owing to identical systematic absence conditions, it is not possible to distinguish between the five space groups $P31c$ (no. 159), $P\bar{3}1c$ (no. 163), $P6_3mc$ (no. 186), $P6_2c$ (no. 190), and $P6_3/mmc$ (no. 194). For $\text{CaMg}_2\text{GaN}_3$, minimal R values and the most reasonable structural parameters were found for refinement in space group $P6_3/mmc$. Relevant crystallographic data as well as atomic coordinates are given in Tables 1 and 2. Rietveld refinement showed the presence of the secondary phases LiF, MgO, and CaO as well as small amounts of an unidentified side phase (Figure 1).^[37-39] The assignment of the reflections for hexagonal metrics of $\text{CaMg}_2\text{GaN}_3$ was validated by electron diffraction (Figure 2). Formation of LiF is due to the reaction mechanism; formation of MgO and CaO can be attributed to the sensitivity of the starting materials as well as the product towards air and moisture.

Table 1. Crystallographic data for $\text{CaMg}_2\text{GaN}_3$.

Formula	$\text{CaMg}_2\text{GaN}_3$
Space group	$P6_3/mmc$ (no. 194)
Lattice parameters /Å,	$a = 3.43093(8)$ $c = 17.3989(5)$
Cell volume /Å ³	177.368(9)
Formula units per unit cell Z	2
Density /g·cm ⁻³	3.652
μ /mm ⁻¹	24.436
T /K	298(2)
Diffractometer	Stoe StadiP
2θ range /°	$5.00 \leq 2\theta \leq 98.75$
Data points	6251
Number of parameters / background parameters	46 / 12
Constraints	5
Weight percent of the content /%	76
Background function	Shifted Chebychev
R_{wp}	0.080
R_{exp}	0.073
R_{p}	0.059
R_{Bragg}	0.033
GoF	1.101

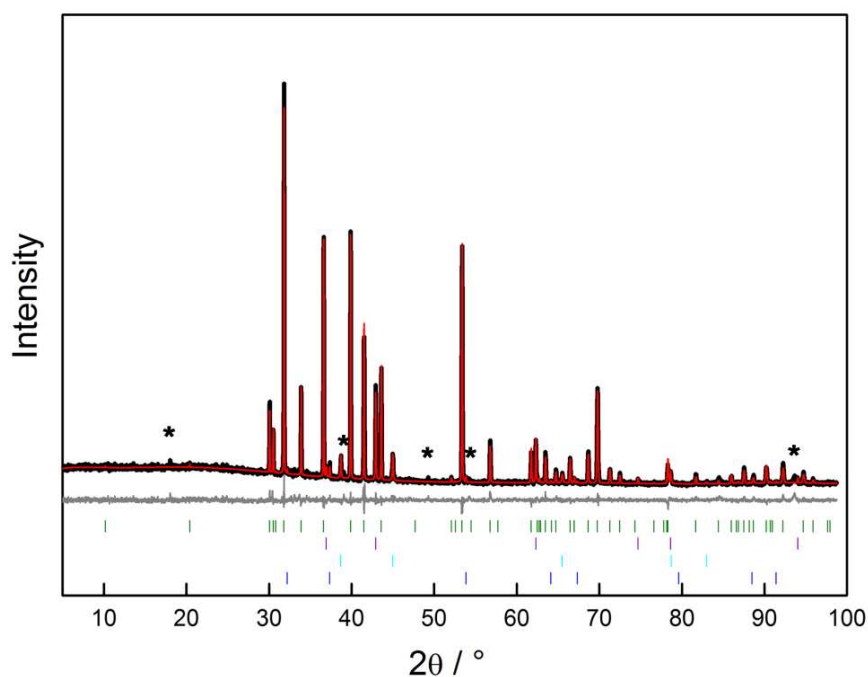


Figure 1. Observed (black line) and calculated (red line) powder diffraction pattern of $\text{CaMg}_2\text{Ga}_2\text{N}_3$ as well as secondary phases LiF, MgO, and CaO. The difference profile (gray line) and Bragg reflections of $\text{CaMg}_2\text{Ga}_2\text{N}_3$ (green bars), MgO (violet bars), LiF (light blue bars), and CaO (dark blue bars) are displayed below the refinement. Unidentified reflections are marked with asterisks.

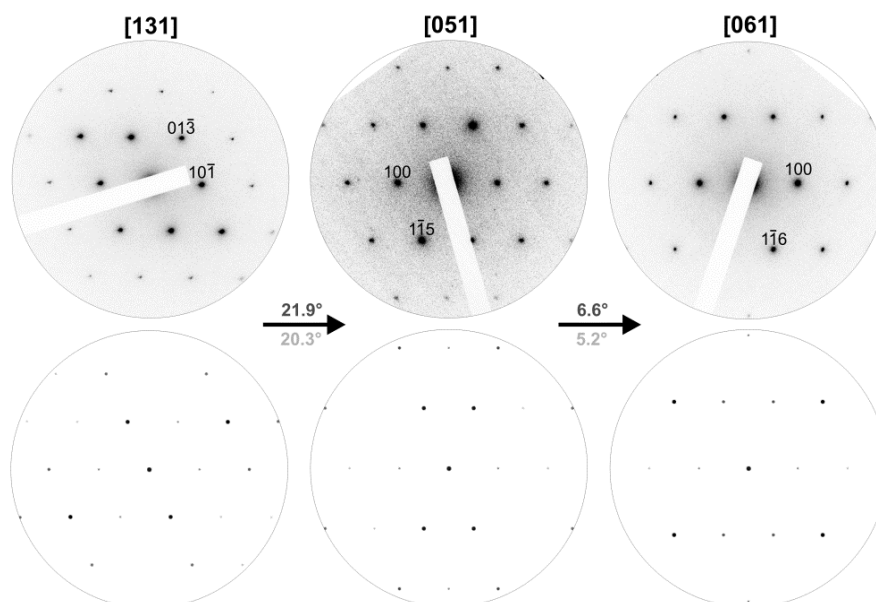


Figure 2. Tilt series of thick microcrystals of $\text{CaMg}_2\text{Ga}_2\text{N}_3$. Experimental pattern and tilt angles (top); simulated data based on the structure model from X-ray data (bottom).

Figure 3 shows the crystal structure of $\text{CaMg}_2\text{GaN}_3$. It is characterized by a layered anionic network with mixed occupation Mg/Ga in the centers of tetrahedral MN_4 units and planar MN_3 triangles. Each layer within $\text{CaMg}_2\text{GaN}_3$ can be described as a highly condensed planar double layer of corner-sharing $(\text{Mg}/\text{Ga})\text{N}_4$ tetrahedra (Mg1/Ga1), forming condensed *dreier* rings^[40] in the *ab* plane. These $(\text{Mg}/\text{Ga})\text{N}_4$ tetrahedra are linked by N atoms in the middle of the double layer, which in turn form highly condensed *dreier* rings, centered by another Mg/Ga site (Mg2/Ga2). In general, the arrangement of Mg/Ga atoms within double layers can be described as hexagonal close packing with an A–B–A–B stacking order (Figure 3b).

Table 2. Atomic coordinates and equivalent isotropic displacement parameters $/\text{\AA}^2$ of $\text{CaMg}_2\text{GaN}_3$.

Atom	Wyckoff-site	x	y	z	B_{eq}	s.o.f.
Ca1	2a	0	0	0	0.0067(10)	1
Mg1/Ga1	4f	1/3	2/3	0.63242(12)	0.0126(9)	0.66(4)/0.34(4)
Mg2/Ga2	2c	1/3	2/3	1/4	0.022(2)	0.79(8)/0.20(8)
N1	4f	1/3	2/3	0.0932(4)	0.013(2)	1
N2	2d	1/3	2/3	3/4	0.013(2)	1

The structural motif of the trigonal planar coordination of Mg^{2+} or Ga^{3+} ions by N also occur in Ca_6GaN_5 , Sr_6GaN_5 , Sr_3GaN_3 , $\text{Sr}_4\text{GaN}_3\text{O}$, $\text{LiBa}_5\text{GaN}_3\text{F}_5$, and Mg_3BN_3 , for example.^[6-9,41] The bond lengths of these compounds range from 1.88 to 1.96 Å for Ga–N and 2.05 Å for Mg–N. The averaged (Mg/Ga)–N bond length of 1.98 Å found in $\text{CaMg}_2\text{GaN}_3$ agrees well with these typical distances and also with the sum of the ionic radii.^[42] Distances to N found for tetrahedrally coordinated Mg/Ga ions range from 2.05 to 2.10 Å, also in good agreement with the sum of the ionic radii as well as with typical Mg/Ga–N bond lengths (e.g., $\text{Ca}_2\text{MgGa}_3\text{N}_5$ 1.95–2.12 Å or $\text{SrMg}_2\text{Ga}_2\text{N}_4$ 1.97–2.10 Å).^[10,27,42] Detailed data of selected bond lengths and angles in $\text{CaMg}_2\text{GaN}_3$ are listed in Table 5. The site occupation factor was refined by assuming full occupancy of Mg/Ga sites. Refinements lead to 66% Mg and 34% Ga on Mg1/Ga1 site and 80% Mg and 20% Ga on the Mg2/Ga2 site. Bond valence sum (BVS) calculations^[43] also show a predominant occupation of Mg on both sites. Ca^{2+} is surrounded by six N, which results in an octahedral coordination. Ca–N bond lengths of 2.56 Å are in good agreement with typical values of other nitridogallates and the calculated sum of the ionic radii.^[26,27,42,44,45]

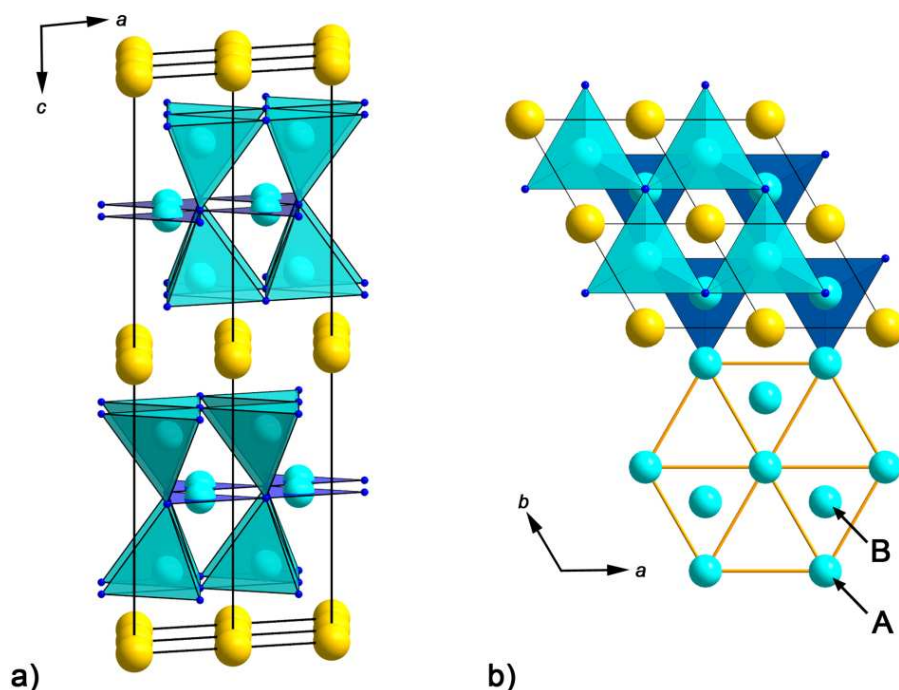


Figure 3. Crystal structure of $\text{CaMg}_2\text{GaN}_3$ with $(\text{Mg}/\text{Ga})\text{N}_4$ tetrahedra of the $\text{Mg1}/\text{Ga1}$ site (turquoise), $(\text{Mg}/\text{Ga})\text{N}_3$ units of the $\text{Mg2}/\text{Ga2}$ site (blue). Atom types: Ca (yellow), Mg/Ga (turquoise), N (dark blue). a) Perspective view of a quadruple cell; b) viewing direction along $[001]$.

$\text{CaMg}_2\text{Ga}_2\text{N}_4$

Structure solution and refinement of $\text{CaMg}_2\text{Ga}_2\text{N}_4$ were performed in the trigonal space group $P\bar{3}m1$ from single-crystal X-ray diffraction data. Crystallographic data is summarized in Table 3. Atomic coordinates and equivalent isotropic displacement parameters are listed in Table 4.

The crystal structure of $\text{CaMg}_2\text{Ga}_2\text{N}_4$ is related to that of $\text{CaMg}_2\text{GaN}_3$. It consists of a layered anionic network with mixed-occupation Mg/Ga of tetrahedral centers. The point symbol $\{3^8.4^{24}.5^3\}\{3^{30}.4^{45}.5^3\}$ of this new layered structure was determined by using TOPOS software.^[46] Figure 4a shows the crystal structure of $\text{CaMg}_2\text{Ga}_2\text{N}_4$ with planar layers, which can be divided into four sublayers A, A', B, and B'. $(\text{Mg}/\text{Ga})\text{N}_4$ tetrahedra of each sublayer are connected through three edges forming highly condensed *dreier* rings (illustrated in Figure 4b with the example of sublayer A). By reflection at a mirror plane m_A (m_B), sublayer A (B) can be converted to sublayer A' (B'). $(\text{Mg}/\text{Ga})\text{N}_4$ tetrahedra of sublayers A' and B' are linked through three edges to one another, forming *sechser* ring channels along $[001]$ (Figure 4c). Ca ions are positioned in the center of *sechser* ring channels (Figure 4d) and octahedrally coordinated by six N atoms.

Figure 5 displays $(\text{Mg}/\text{Ga})\text{N}_4$ polyhedra of both crystallographic Mg/Ga sites (sublayers A and B: Mg1/Ga1; sublayers A' and B': Mg2/Ga2). Whereas Mg1/Ga1 exhibits tetrahedral coordination by four N in a regular manner; $(\text{Mg2}/\text{Ga2})\text{N}_4$ tetrahedra show one elongated bond length $(\text{Mg2}/\text{Ga2})\text{--N1}$. Its coordination can alternatively be described as nonplanar, pyramidal $(\text{Mg}/\text{Ga})\text{N}_3$ units. A similar transition between nonplanar, pyramidal, and tetrahedral coordination was reported for the borates $M_6\text{B}_{22}\text{O}_{39}\cdot\text{H}_2\text{O}$ ($M = \text{Fe}, \text{Co}$)^[47] as well as for $\text{Al}_5\text{C}_3\text{N}$.^[48] Similar to distorted BO_3 units in $M_6\text{B}_{22}\text{O}_{39}\cdot\text{H}_2\text{O}$ ($M = \text{Fe}, \text{Co}$), thermal ellipsoids of Mg2/Ga2 and adjacent N atoms in $\text{CaMg}_2\text{Ga}_2\text{N}_4$ show displacements of Mg2/Ga2 and N1 nearly parallel to their connecting line. Nonplanar, pyramidal $(\text{Mg}/\text{Ga})\text{N}_3$ units can thus also be considered as an intermediate state between a trigonal planar $(\text{Mg}/\text{Ga})\text{N}_3$ group and a $(\text{Mg}/\text{Ga})\text{N}_4$ tetrahedron. Distances $(\text{Mg}/\text{Ga})\text{--N}$ (2.02–2.09 Å) of the crystallographic Mg1/Ga1 site as well as bond lengths Ca--N within CaN_6 octahedra (2.53 Å) are in good agreement with the calculated sum of ionic radii as well as with typical distances in comparable nitrides.^[26,27,42,44,45,49–51] $(\text{Mg2}/\text{Ga2})\text{N}_4$ tetrahedra show a rather long distance $(\text{Mg}/\text{Ga})\text{--N}$ of 2.20 Å. Precise details of selected bond lengths and angles are given in Table 5.

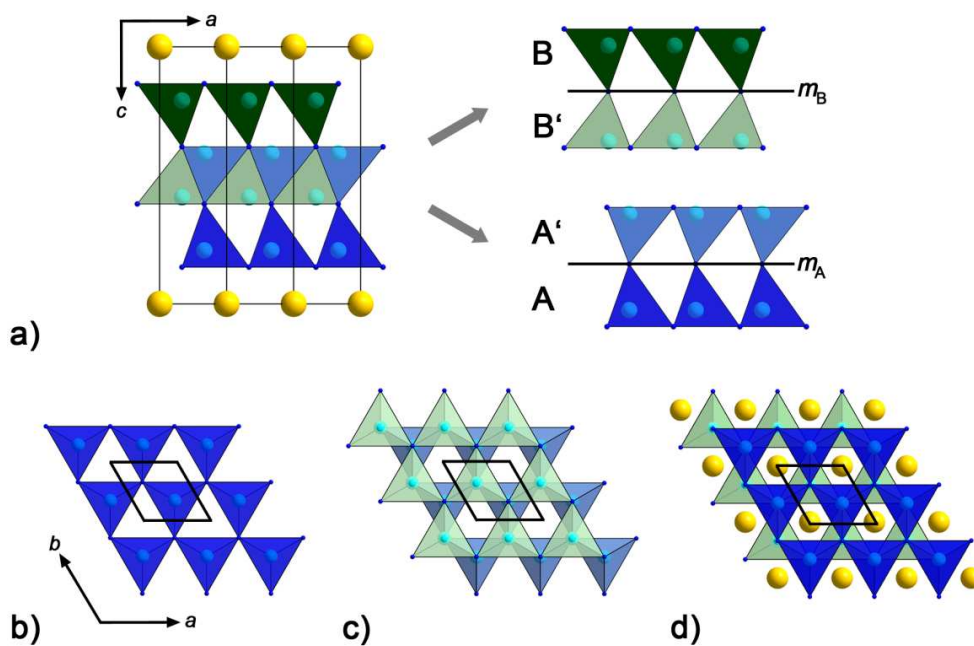


Figure 4. Crystal structure of $\text{CaMg}_2\text{Ga}_2\text{N}_4$ with Ca (yellow), Mg/Ga (turquoise), and N (dark blue). a) Viewing direction along [010] with a detailed description of planar layers, which can be divided into four sublayers A, A', B and B'. Sublayer A (B) can be mirrored at m_A (m_B) resulting in sublayer A' (B'); b) corner-sharing $(\text{Mg}/\text{Ga})\text{N}_4$ tetrahedra of sublayer A forming highly condensed *dreier* rings; c) $(\text{Mg}/\text{Ga})\text{N}_4$ tetrahedra of sublayers A' and B', linked via three edges to one another forming *sechser* ring channels along [001]; d) crystal structure of $\text{CaMg}_2\text{Ga}_2\text{N}_4$ with viewing direction along c.

Table 3. Crystallographic data for $\text{CaMg}_2\text{Ga}_2\text{N}_4$.

Formula	$\text{CaMg}_2\text{Ga}_2\text{N}_4$
Space group	$P\bar{3}m1$ (no. 164)
Lattice parameters /Å	$a = 3.3859(3)$ $c = 11.2378(11)$
Cell volume /Å ³	111.57(2)
Formula units per unit cell Z	1
Density /g·cm ⁻³	4.229
μ /mm ⁻¹	13.353
T /K	293(2)
Diffractometer	D8 Venture
Radiation	Mo-K α ($\lambda = 0.71073$ Å)
$F(000)$	134
2θ range /°	$10.88 \leq 2\theta \leq 60.95$
Total no. of reflections	3383
Independent reflections	172
Refined parameters	15
Goodness of fit	1.203
R_1 (all data) / $R_1 [F^2 > 2\sigma(F^2)]$	0.0614 / 0.0545
wR_2 (all data) / $wR_2 [F^2 > 2\sigma(F^2)]$	0.1014 / 0.0968
$\Delta\rho_{\min}, \Delta\rho_{\max}$ / e·Å ⁻³	-2.716, 3.310

Table 4. Atomic coordinates and equivalent isotropic displacement parameters /Å² of $\text{CaMg}_2\text{Ga}_2\text{N}_4$.

Atom	Wyckoff-site	x	y	z	U_{eq}	s.o.f.
Ca1	1a	0	0	0	0.0028(6)	1
Mg1/Ga1	2d	1/3	2/3	0.2084(2)	0.0051(5)	½ / ½
Mg2/Ga2	2d	1/3	2/3	0.5851(2)	0.0166(6)	½ / ½
N1	2d	1/3	2/3	0.3890(10)	0.009(2)	1
N2	2d	1/3	2/3	0.8568(10)	0.010(2)	1

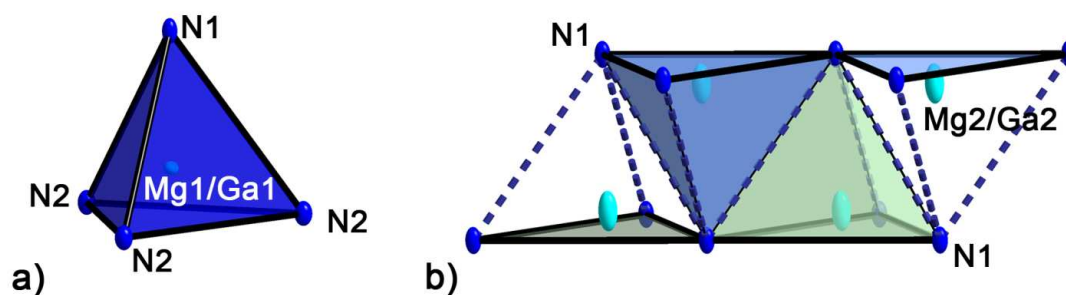


Figure 5. Coordination polyhedra of mixed Mg/Ga sites. a) Tetrahedral coordination of Mg1/Ga1 of sublayers A and B; b) tetrahedral or nonplanar, pyramidal coordination of Mg2/Ga2 of sublayers A' and B', drawn with 50% thermal ellipsoids.

Table 5. Selected bond lengths and angles in the crystal structures of $\text{CaMg}_2\text{GaN}_3$ and $\text{CaMg}_2\text{Ga}_2\text{N}_4$.^[a]

	Bond length /Å		Bond angle /°	
$\text{CaMg}_2\text{GaN}_3$	Ca1–N1	2.560(4)	N1–Ca1–N1	180.0(1) (3x)
	Mg1/Ga1–N1	2.095(2)		84.2(1) (6x)
	Mg1/Ga1–N2	2.046(2) (3x)		95.8(1) (6x)
	Mg2/Ga2–N2	1.9809(1) (3x)	N1–Mg1/Ga1–N1	109.9(1) (3x)
			N1–Mg1/Ga1–N2	109.0(2) (3x)
$\text{CaMg}_2\text{Ga}_2\text{N}_4$			N2–Mg2/Ga2–N2	120.0 (3x)
	Ca1–N2	2.532(7) (6x)	N2–Ca1–N2	180.0(4) (3x)
	Mg1/Ga1–N1	2.029(11)		83.9(3) (6x)
	Mg1/Ga1–N2	2.088(4) (3x)		96.1(3) (6x)
	Mg2/Ga2–N1	1.976(2) (3x)	N1–Mg1/Ga1–N2	110.6(3) (3x)
		2.204(11)	N2–Mg1/Ga1–N2	108.4(3) (3x)
			N1–Mg2/Ga2–N1	117.9(2) (3x)
				98.5(3) (3x)

[a] Standard deviations are given in parentheses.

As seen from Table 3, there is a high residual electron density within the crystal structure of $\text{CaMg}_2\text{Ga}_2\text{N}_4$. In general, possible reasons for the remaining electron density after structure refinement may be due to incorrect assignments of atom types or space groups as well as twinning problems. For $\text{CaMg}_2\text{Ga}_2\text{N}_4$, elemental analyses confirmed the respective metals. Twinning problems could be excluded since no splitting of reflections within reciprocal lattice sections ($nk\bar{l}$, hnl , hkn with $n = 0-3$), reconstructed from single-crystal X-ray data, can be observed. We also found no typical indications for a merohedric twin. To check for overlooked lower symmetry, the structure solution and refinement were also performed in $P1$ (no. 1) as well as $P\bar{3}$ (no.147). Subsequent examination with PLATON^[52,53] confirmed symmetry $P\bar{3}m1$ (no. 164). Refinement of the site occupation factor of Mg/Ga sites was performed based on the assumption of full occupancy and led to $\text{Mg1/Ga1} = 0.54(2)/0.46(2)$ and $\text{Mg2/Ga2} = 0.64(2)/0.36(2)$, which means an increased Mg content for $\text{CaMg}_2\text{Ga}_2\text{N}_4$. As these experimental data do not lead to electroneutrality of the sum formula, the occupancy Mg/Ga of both crystallographic sites was fixed at $\frac{1}{2} / \frac{1}{2}$. In addition, bond valence sum (BVS) calculations were performed and show a mixed occupancy with ratio 1:1 for Mg and Ga, thereby resulting in electroneutrality. Visualization of the residual electron density was performed by using the program package Jana.^[54] As shown in Figure 6 as red spheres, it is located at $(\frac{1}{3}, \frac{2}{3}, z)$ and $(0, 0, z)$, which correspond to atomic coordinates of the metal atoms Ca and Mg/Ga in the structurally closely related compounds $\text{CaMg}_2\text{GaN}_3$ and $\text{CaMg}_2\text{Ga}_2\text{N}_4$ (Tables 2 and 4). TEM investigations and simultaneous EDX analyses corroborate the presence of both nitridomagnesogallates within one reaction batch and show the additional presence of a further nitridomagnesogallate as a minor side phase (trigonal metrics with $a = 3.51$ and $c = 18.17$ Å). Since the lattice parameters as well as chemical composition of this phase show similarities to $\text{CaMg}_2\text{GaN}_3$ and $\text{CaMg}_2\text{Ga}_2\text{N}_4$, the existence of a further phase with slightly different layer sequences could be possible. Figure 7 shows an example of the formation of a possible composite crystal. Combination of layers out of $\text{CaMg}_2\text{Ga}_2\text{N}_4$ with layers of $\text{CaMg}_2\text{GaN}_3$ would lead to a new unit cell with an elongated c axis. The residual electron density observed for $\text{CaMg}_2\text{Ga}_2\text{N}_4$ therefore could originate from a composite crystal consisting of layers out of both nitridomagnesogallates described here.

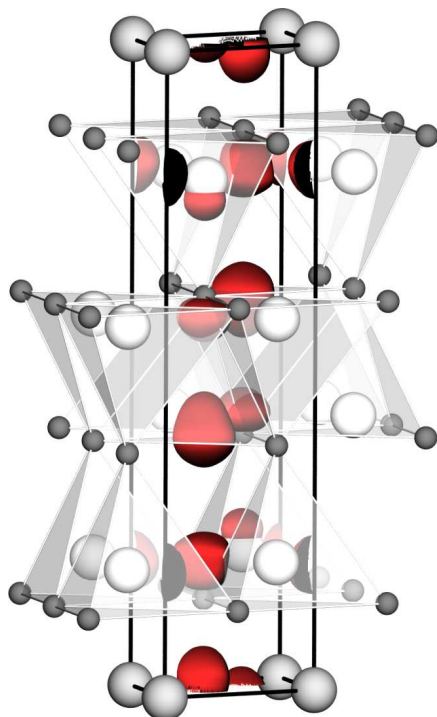


Figure 6. Unit cell of $\text{CaMg}_2\text{Ga}_2\text{N}_4$ with residual electron density marked as red spheres with contour level $1.5 \text{ e} \cdot \text{\AA}^{-3}$.

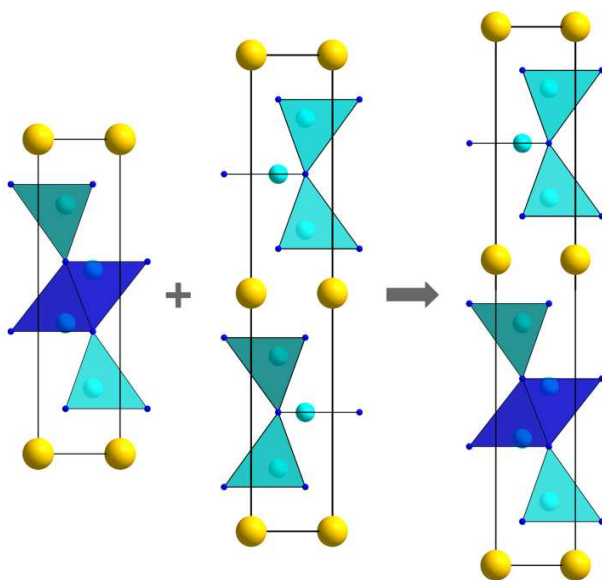


Figure 7. Combination of unit cells of $\text{CaMg}_2\text{Ga}_2\text{N}_4$ (left) and $\text{CaMg}_2\text{GaN}_3$ (center) and a possible composite crystal (right) with an elongated c axis.

2.2.3 Conclusion

In this contribution, we report on $\text{CaMg}_2\text{GaN}_3$ and $\text{CaMg}_2\text{Ga}_2\text{N}_4$, two new nitridomagnesogallates with layered crystal structures. Syntheses of both compounds were performed on the basis of solid-state metathesis reactions, thereby representing a new synthetic approach for nitridogallates. The crystal structure of $\text{CaMg}_2\text{GaN}_3$ was determined by using powder X-ray diffraction data combined with TEM investigations. Structure solution and refinement of $\text{CaMg}_2\text{Ga}_2\text{N}_4$ was carried out by using single-crystal X-ray diffraction data. The metrics of both nitridomagnesogallates were confirmed by using TEM investigations. $\text{CaMg}_2\text{GaN}_3$ is isotypic with $\text{CaMg}_2\text{AlN}_3$ and homeotypic with $\text{Ca}_2\text{Mg}_5\text{GeN}_6$ with a layered anionic network, which emphasizes structural relations between the compound classes of nitridoaluminates, -germanates, and -gallates. The crystal structure of $\text{CaMg}_2\text{Ga}_2\text{N}_4$ is closely related to that of $\text{CaMg}_2\text{GaN}_3$. The respective lattice parameters a and b are quite similar; the structures differ only in the composition of anionic layers and their stacking along c . In addition, TEM studies show the presence of another nitridomagnesogallate with trigonal metrics as a minor side phase. The nitridomagnesogallates discussed here have a marked degree of similarity within the ab plane but other dimensions along $[001]$, therefore the formation of composite crystals seems likely.

In summary, solid-state metathesis reactions seem to be a good alternative to the common NaN_3 route for an explorative search of new structures within the class of quaternary nitridogallates. Besides small amounts of single crystals, powder samples containing nitridogallates in high percentages could also be obtained.

2.2.4 Experimental Section

2.2.4.1 General

Because of the sensitivity against air and moisture of some starting materials as well as the products, all manipulations were performed under inert-gas conditions using argon-filled glove boxes (Unilab, MBraun, Garching, $\text{O}_2 < 1$ ppm, $\text{H}_2\text{O} < 1$ ppm) and combined Schlenk/vacuum lines (10^{-3} mbar). Argon was dried with silica gel (Merck), KOH (Merck, $\geq 85\%$), molecular sieves (Fluka, 4 Å), P_4O_{10} (Roth, $\geq 99\%$), and titanium sponge (Johnsen Matthey, 99.5%) at 700 °C before use. The starting materials were ground in an agate mortar and placed in a crucible. Ta

ampules (length 30 mm, inner diameter 9.5 mm, wall thickness 0.5 mm) as well as W crucibles were used as reaction containers. The Ta ampules were arc-welded under Ar while cooling the crucible holder with water to avoid chemical reactions. The sealed ampules were heated within an evacuated glass ampule up to 1000 °C in a tube furnace. Further syntheses were performed in W crucibles in a water-cooled silica glass reactor of a radio-frequency furnace (Type AXIO 10/450, max. electrical output 10 kW, Hüttinger Elektronik, Freiburg) at 850 °C.

2.2.4.2 Synthesis of $\text{CaMg}_2\text{GaN}_3$

A powder sample containing $\text{CaMg}_2\text{GaN}_3$ was obtained after the reaction of Li_3N (0.42 mmol, 14.7 mg, Sigma-Aldrich, 99.99%), Ca_3N_2 (0.10 mmol, 18.8 mg, synthesized according to literature procedures),^[55] Mg_3N_2 (0.20 mmol, 20.2 mg, Sigma-Aldrich, 99.5%) and GaF_3 (0.30 mmol, 38.0 mg, Alfa Aesar, 99.999%) in a radio-frequency furnace under nitrogen atmosphere. EuF_3 ($5.3 \cdot 10^{-3}$ mmol, 1.1 mg, Sigma-Aldrich, 99.99%) was added for doping experiments. The finely ground powder was placed in a tungsten crucible and heated to 850 °C over 1.5 h. The temperature was maintained for 17.5 hours. Subsequently, the reaction mixture was quenched to room temperature by switching off the furnace.

2.2.4.3 Synthesis of $\text{CaMg}_2\text{Ga}_2\text{N}_4$

Single crystals of $\text{CaMg}_2\text{Ga}_2\text{N}_4$ were isolated after reaction of Li_3N (0.43 mmol, 15.0 mg, Sigma-Aldrich, 99.99%), $\text{Ca}(\text{NH}_2)_2$ (0.20 mmol, 14.4 mg, synthesized according to literature procedures),^[55] $\text{Mg}(\text{NH}_2)_2$ (0.24 mmol, 13.5 mg, synthesized according to literature procedures),^[55] and GaF_3 (0.22 mmol, 28.0 mg, Alfa Aesar, 99.999%) in a Ta ampule at 1000 °C. CsCl (0.48 mmol, 80.0 mg, Sigma-Aldrich, 99.9%) was added as flux; EuF_3 ($4 \cdot 10^{-3}$ mmol, 0.84 mg, Sigma-Aldrich, 99.99%) was added for doping experiments. The sample mixture was heated within a tube furnace up to 950 °C, held for 24 h, and then fired to 1000 °C. This temperature was maintained for another 24 h and subsequently cooled down to 500 °C with a rate of $3.4 \text{ °C} \cdot \text{h}^{-1}$. Subsequently, the reaction mixture was quenched to room temperature by switching off the furnace.

2.2.4.4 Synthesis of a Mixture of $\text{CaMg}_2\text{GaN}_3$ and $\text{CaMg}_2\text{Ga}_2\text{N}_4$

A powder sample containing $\text{CaMg}_2\text{GaN}_3$ and $\text{CaMg}_2\text{Ga}_2\text{N}_4$ was synthesized by heating a mixture of Li_3N (0.42 mmol, 14.7 mg, Sigma-Aldrich, 99.99%), $\text{Ca}(\text{NH}_2)_2$ (0.30 mmol, 21.6 mg, synthesized according to literature procedures),^[55] Mg_3N_2 (0.20 mmol, 20.2 mg, Sigma-Aldrich, 99.5%), and GaF_3 (0.30 mmol, 38.0 mg, Alfa Aesar, 99.999%) in a radio-frequency furnace under a nitrogen atmosphere. EuF_3 ($6 \cdot 10^{-3}$ mmol, 1.25 mg, Sigma-Aldrich, 99.99%) was added for doping experiments. The finely ground powder was filled in a tungsten crucible and heated to 850 °C. The temperature was maintained for 48 hours and subsequently cooled down to 600 °C in 16 h. The reaction mixture was quenched to room temperature by switching off the furnace.

2.2.4.5 Scanning Electron Microscopy

Elemental analyses were performed by using energy dispersive X-ray spectroscopy. Therefore, samples of the products were placed on an adhesive conductive carbon pad and coated with a conductive carbon film (BAL-TEC MED 020, Bal Tec AG). The chemical composition of the reported products was determined by using a FEI Helios G3 UC scanning electron microscope equipped with an EDX detector, scanning transmission detector, and focused ion beam.

2.2.4.6 Transmission Electron Microscopy

Solvent-free samples for TEM were prepared on a copper grid (Plano) under an argon atmosphere and transferred on a double-tilt holder into the microscope. For TEM investigations, a Jeol 2010 operated at 200 kV and equipped with a LaB_6 emitter, TemCam F216 with 2048 x 2048 pixels (TVIPS), and an Apollo XLT EDX-detector (EDAX) was used. The data was evaluated with the following software: Digital Micrograph,^[56] Process Diffraction,^[57] JEMS^[58] (all SAED), and TEAM^[59] (EDX spectra).

2.2.4.7 Single-Crystal X-ray Diffraction

Single crystals of $\text{CaMg}_2\text{Ga}_2\text{N}_4$ were isolated from the product by using a microscope, washed in dried paraffin oil, and sealed within glass capillaries. Data collection was performed with a D8

Venture diffractometer (Bruker, Billerica MA, USA). Absorption corrections were done by using the multi-scan method (SADABS).^[60] Structure solution was performed by using direct methods (SHELXS), and structure refinement by full-matrix least-squares methods (SHELXL-97).^[61]

Further details of the crystal structure investigations of $\text{CaMg}_2\text{Ga}_2\text{N}_4$ may be obtained from the Fachinformationszentrum Karlsruhe, 76344 Eggenstein-Leopoldshafen, Germany (Fax: +49-7247-808-666; E-Mail: crysdata@fiz-karlsruhe.de) on quoting the depository number CSD-432099)

2.2.4.8 Powder X-ray Diffraction

The powder samples were investigated by using powder X-ray diffraction. The samples were finely ground with an agate mortar, filled into glass capillaries (inner diameter 0.18 mm), and sealed under Ar. Powder X-ray diffraction data were recorded with a STOE STADI P diffractometer ($\text{Cu-K}\alpha_1$ radiation, Ge(111) monochromator, MYTHEN 1 K detector) in Debye-Scherrer geometry. Secondary phases were identified by using the program package WinXPOW.^[62] Simulation of the powder diffraction pattern, calculated on the basis of single-crystal structure data, was carried out with WinXPOW. Structure solution and structure refinement was performed by using the TOPAS Academic 4.1 package.^[63] The reflections of the powder pattern were indexed by using the SVD-algorithm,^[64] and their intensities were extracted with the Pawley-method. The structural model of $\text{CaMg}_2\text{GaN}_3$ was obtained by using the charge-flipping algorithm^[65-67] and the final refinement was carried out by using the Rietveld method, by employing the fundamental parameters approach with direct convolution of source emission profiles, axial instrument contributions, crystallite size, and microstrain effects.^[68,69] The preferred orientation of the crystallites within the capillary was corrected by using the spherical harmonics model of the fourth order.^[70] The capillary absorption correction was performed with regard to the calculated absorption coefficient and the diameter of the capillary. The background function was handled by using a shifted Chebychev function.

Further details of the crystal structure of $\text{CaMg}_2\text{GaN}_3$ may be obtained from the Fachinformationszentrum Karlsruhe, 76344 Eggenstein-Leopoldshafen, Germany (Fax: +49-7247-808-666; E-Mail: crysdata@fiz-karlsruhe.de) on quoting the depository number CSD-432100)

2.2.5 References

- [1] S. Nakamura, T. Mukai, M. Senoh, *Appl. Phys. Lett.* **1994**, 64, 1687.
- [2] E. Kauer, A. Rabenau, *Z. Naturforsch.* **1958**, 13a, 531.
- [3] H. G. Grimmeiss, H. Koelmans, *Z. Naturforsch.* **1959**, 14a, 264.
- [4] T. Mukai, S. Nagahama, N. Iwasa, M. Senoh, T. Yamada, *J. Phys. Condens. Matter* **2001**, 13, 7089.
- [5] P. Pust, P. J. Schmidt, W. Schnick, *Nat. Mater.* **2015**, 14, 454.
- [6] G. Cordier, P. Höhn, R. Kniep, A. Rabenau, *Z. Anorg. Allg. Chem.* **1990**, 591, 58.
- [7] D. G. Park, Z. A. Gál, F. J. DiSalvo, *Inorg. Chem.* **2003**, 42, 1779.
- [8] P. M. Mallinson, Z. A. Gál, S. J. Clarke, *Inorg. Chem.* **2006**, 45, 419.
- [9] F. Hintze, W. Schnick, *Solid State Sci.* **2010**, 12, 1368.
- [10] D. G. Park, Y. Dong, F. J. DiSalvo, *Solid State Sci.* **2008**, 10, 1846.
- [11] P. Pust, F. Hintze, C. Hecht, V. Weiler, A. Locher, D. Zitnanska, S. Harm, D. Wiechert, P. J. Schmidt, W. Schnick, *Chem. Mater.* **2014**, 26, 6113.
- [12] P. Pust, V. Weiler, C. Hecht, A. Tücks, A. S. Wochnik, A.-H. Henß, D. Wiechert, C. Scheu, P. J. Schmidt, W. Schnick, *Nat. Mater.* **2014**, 13, 891.
- [13] P. Pust, A. S. Wochnik, E. Baumann, P. J. Schmidt, D. Wiechert, C. Scheu, W. Schnick, *Chem. Mater.* **2014**, 26, 3544.
- [14] S. Schmiechen, H. Schneider, P. Wagatha, C. Hecht, P. J. Schmidt, W. Schnick, *Chem. Mater.* **2014**, 26, 2712.
- [15] S. Schmiechen, P. Strobel, C. Hecht, T. Reith, M. Siegert, P. J. Schmidt, P. Huppertz, D. Wiechert, W. Schnick, *Chem. Mater.* **2015**, 27, 1780.
- [16] J. C. Fitzmaurice, A. L. Hector, I. P. Parkin, *J. Chem. Soc. Dalton Trans.* **1993**, 2435.
- [17] J. C. Fitzmaurice, A. Hector, A. T. Rowley, I. P. Parkin, *Polyhedron* **1994**, 13, 235.
- [18] E. G. Gillan, R. B. Kaner, *Inorg. Chem.* **1994**, 33, 5693.
- [19] A. L. Hector, I. P. Parkin, *Chem. Mater.* **1995**, 7, 1728.
- [20] W. Schnick, H. Huppertz, *Chem. Eur. J.* **1997**, 3, 679.
- [21] I. P. Parkin, A. M. Nartowski, *Polyhedron* **1998**, 17, 2617.
- [22] W. Schnick, H. Huppertz, R. Lauterbach, *J. Mater. Chem.* **1999**, 9, 289.
- [23] M. Levinshtein, S. Ruymantsev, M. Shur, *Properties of Advanced Semiconductor Materials, GaN, AlN, InN, BN, SiC, SiGe*, Wiley, New York, **2001**.
- [24] H.-J. Meyer, *Dalton Trans.* **2010**, 39, 5973.

- [25] M. Zeuner, S. Pagano, W. Schnick, *Angew. Chem. Int. Ed.* **2011**, 50, 7754; *Angew. Chem.* **2011**, 123, 7898.
- [26] S. J. Clarke, F. J. DiSalvo, *Inorg. Chem.* **1997**, 36, 1143.
- [27] F. Hintze, W. Schnick, *Z. Anorg. Allg. Chem.* **2012**, 638, 2243.
- [28] F. Hintze, F. Hummel, P. J. Schmidt, D. Wiechert, W. Schnick, *Chem. Mater.* **2012**, 24, 402.
- [29] H. Yamane, F. J. DiSalvo, *Acta Crystallogr., Sect. C: Cryst. Struct. Commun.* **1996**, 52, 760.
- [30] P. E. Rauch, A. Simon, *Angew. Chem. Int. Ed. Engl.* **1992**, 31, 1519; *Angew. Chem.* **1992**, 104, 1505.
- [31] M. Kubus, K. Levin, S. Kroeker, D. Enseling, T. Jüstel, H.-J. Meyer, *Dalton Trans.* **2015**, 44, 2819.
- [32] M. Ströbele, K. Dolabdjian, D. Enseling, D. Dutczak, B. Mihailova, T. Jüstel, H.-J. Meyer, *Eur. J. Inorg. Chem.* **2015**, 1716.
- [33] L. Unverfehrt, M. Ströbele, H.-J. Meyer, *Z. Anorg. Allg. Chem.* **2013**, 639, 1722.
- [34] B. Blaschkowski, H. Jing, H.-J. Meyer, *Angew. Chem. Int. Ed.* **2002**, 41, 3322; *Angew. Chem.* **2002**, 114, 3468.
- [35] T. M. Gesing, W. Jeitschko, *J. Solid State Chem.* **1998**, 140, 396.
- [36] C. Poesl, W. Schnick, *Z. Anorg. Allg. Chem.* **2016**, 642, 882.
- [37] J. Thewlis, *Acta Crystallogr.* **1955**, 8, 36.
- [38] E. Broch, *Z. Phys. Chem.* **1927**, 127, 446.
- [39] M. C. Verbraeken, E. Suard, *J. Mater. Chem.* **2009**, 19, 2766.
- [40] F. Liebau, *Structural Chemistry of Silicates*, Springer, Berlin, **1985** (the terms *dreier* ring and *sechser* ring was coined by Liebau and are derived from the German words *drei* = 3 and *sechs* = 6; a *dreier* ring comprises three tetrahedron centers).
- [41] H. Hiraguchi, H. Hashizume, *J. Appl. Crystallogr.* **1991**, 24, 286.
- [42] W. H. Baur, *Crystallogr. Rev.* **1987**, 1, 59.
- [43] A. S. Wills, *VaList*, v. 4.0.7, Universtiy College London: UK, **2010**.
- [44] S. J. Clarke, F. J. DiSalvo, *J. Alloys Compd.* **1998**, 274, 118.
- [45] M. S. Bailey, F. J. DiSalvo, *J. Alloys Compd.* **2006**, 417, 50.
- [46] V. A. Blatov, A. P. Shevchenko, D. M. Proserpio, *Cryst. Growth Des.* **2014**, 14, 3576.
- [47] S. C. Neumair, J. S. Knyrim, O. Oeckler, R. Glaum, R. Kaindl, R. Stalder, H. Huppertz, *Chem. Eur. J.* **2010**, 16, 13659.

- [48] M. v. Stackelberg, E. Schnorrenberg, R. Paulus, K. F. Spiess, *Z. Phys. Chem. Abt. A* **1935**, 175, 127.
- [49] J. David, Y. Laurent, J. Lang, *J. Bull. Soc. Fr. Mineral. Cristallogr.* **1970**, 93, 153.
- [50] A. G. Petukhov, W. R. L. Lambrecht, B. Segall, *Phys. Rev. B* **1994**, 49, 4549.
- [51] O. Reckeweg, F. J. DiSalvo, *Z. Anorg. Allg. Chem.* **2001**, 627, 371.
- [52] P. V. D. Sluis, A. L. Spek, *Acta Crystallogr., Sect. A: Found. Crystallogr.* **1990**, 46, 194.
- [53] A. L. Spek, *Acta Crystallogr., Sect. D: Biol. Crystallogr.* **2009**, 65, 148.
- [54] V. Petricek, M. Dusek, L. Palatinus, *Z. Kristallogr.* **2014**, 229, 345.
- [55] T. Brokamp, *Dissertation*, Universität Dortmund, **1991**.
- [56] Gatan Software Team, DigitalMicrograph, 3.6.1, **1999**.
- [57] J. L. Lábár, *Ultramicroscopy* **2005**, 103, 237.
- [58] P. A. Stadelmann, JEMS, 3.3425, **2008**.
- [59] EDAX, TEAM, 3.4.1, **2013**.
- [60] G. M. Sheldrick, *SADABS, Multi-Scan Absorption Correction*, v.2, Bruker-AXS, Madison, WI, USA, **2012**.
- [61] G. M. Sheldrick, *Acta Crystallogr., Sect. A: Found. Crystallogr.* **2008**, 64, 112.
- [62] *WinXPOW, Program for Powder Data Handling* v. 2.21, Stoe & Cie GmbH, Darmstadt, Germany, **2007**.
- [63] A. Coelho, *TOPAS - Academic*, Coelho Software, Brisbane, **2007**.
- [64] A. A. Coelho, *J. Appl. Crystallogr.* **2003**, 36, 86.
- [65] G. Oszlányi, A. Sütö, *Acta Crystallogr., Sect. A: Found. Crystallogr.* **2004**, 60, 134.
- [66] G. Oszlányi, A. Sütö, *Acta Crystallogr., Sect. A: Found. Crystallogr.* **2008**, 64, 123.
- [67] A. A. Coelho, *Acta Crystallogr., Sect. A: Found. Crystallogr.* **2007**, 63, 400.
- [68] R. W. Cheary, A. Coelho, *J. Appl. Crystallogr.* **1992**, 25, 109.
- [69] R. W. Cheary, A. A. Coelho, J. P. Cline, *J. Res. Natl. Inst. Stand. Technol.* **2004**, 190, 1.
- [70] M. Järvinen, *J. Appl. Crystallogr.* **1993**, 26, 525.

2.3 $\text{Ca}_2\text{Mg}_5\text{GeN}_6$ – A Layered Nitridomagnesogermanate

published in: *Z. Anorg. Allg. Chem.* **2016**, 642, 882-886

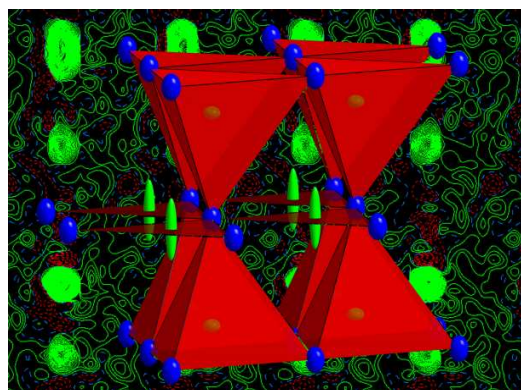
authors: Christine Poesl and Wolfgang Schnick

DOI: 10.1002/zaac.201600200

Copyright © 2016 Wiley-VCH Verlag GmbH & Co. KGaA, Weinheim

<http://onlinelibrary.wiley.com/doi/10.1002/zaac.201600200/full>

Abstract. The nitridomagnesogermanate $\text{Ca}_2\text{Mg}_5\text{GeN}_6$ was synthesized at 780 °C using a sodium flux in sealed tantalum ampules. Pure metals were used as starting materials and sodium azide NaN_3 was added as nitrogen source. $\text{Ca}_2\text{Mg}_5\text{GeN}_6$ was obtained as a byproduct in the form of colorless platelet-like crystals. Solution and refinement of the crystal structure [space group $P6_3/mmc$ (no. 194), $Z = 1$, $a = 3.453(2)$, $c = 17.506(13)$ Å and $V = 180.8(2)$ Å³] were performed on the basis of single-crystal X-ray diffraction data. $\text{Ca}_2\text{Mg}_5\text{GeN}_6$ represents the first



layered nitridogermanate. Its structure is made up of corner-sharing $(\text{Mg}/\text{Ge})\text{N}_4$ tetrahedra and corner-sharing trigonal planar $(\text{Mg}/\text{Ge})\text{N}_3$ units with mixed occupancy of Mg and Ge. Ca^{2+} ions are located in between the sheets. The crystal structure is closely related to that of the nitridomagnesooaluminate $\text{CaMg}_2\text{AlN}_3$ as well as to the carbides ScAl_3C_3 and UAl_3C_3 .

2.3.1 Introduction

There are structural relations between nitridogermanates and nitridogallates on one hand and nitrodoaluminates and -silicates on the other.^[1-3] Doped with Eu^{2+} or Ce^{3+} , the two latter ones are widely applied as luminescent materials in high performance light-emitting diodes.^[4-6] In general, the number of known nitrides increased significantly during the last decade. Especially, ternary and quaternary compounds were in the focus of interest, most of them containing heavier alkaline earth ions. One reason is the quite similar ionic radius of these ions, especially Sr^{2+} , with respect to the dopant Eu^{2+} as well as the higher solubility of nitrogen in sodium melts in the presence of alkaline earth metals during synthesis.^[7] Nitridogallates and nitridogermanates have predominantly been synthesized from elements in sealed Ta or Nb ampoules. They were fired at around 760 °C employing molten sodium as flux and Na azide supplying nitrogen pressure by thermal dissociation. Whereas GaN_4 tetrahedra and trigonal planar GaN_3 units are the most common structural motifs found in the class of nitridogallates,^[1,2,8-17] Ge shows more varieties of building blocks. Sr_2GeN_2 ^[18] is an example for Ge in oxidation state +II and its crystal structure is containing isolated dumbbell-shaped $[\text{GeN}_2]^{4-}$ units. Furthermore, extended Zintl anions $[\text{Ge}]^{2-}$ forming zigzag chains occur e.g. in $\text{Sr}_3\text{Ge}_2\text{N}_2$ ^[18] and isotypic $\text{Ba}_3\text{Ge}_2\text{N}_2$ ^[19] as well as in $\text{Sr}_6\text{Ge}_5\text{N}_2$.^[20] Additionally, nitridogermanates are known containing Ge in oxidation state +IV with GeN_4 tetrahedra or trigonal planar GeN_3 units as structural motifs. Whereas compounds containing Ge in different oxidation states are mostly metallic and of black appearance,^[20-22] compounds containing Ge^{4+} are translucent crystals of different color and shape.^[22-24] The structures of nitridogermanates are typically built up of more or less condensed nitridometallate anions coordinated by alkaline earth atoms as counterions. This results in different dimensionalities, ranging from 0D anion structures up to 3D networks. Ca_4GeN_4 ,^[22] $\text{Sr}_5\text{Ge}_2\text{N}_6$,^[23] and $\text{Ba}_9\text{Ge}_3\text{N}_{10}$ ^[25] are examples containing less condensed building units of either $[\text{GeN}_4]^{8-}$ tetrahedra, $[\text{Ge}_2\text{N}_6]^{10-}$ double-tetrahedra or trigonal planar $[\text{GeN}_3]^{5-}$ units. Examples of 1D condensed nitridomagnesogermanates are isostructural $\text{Sr}_3\text{GeMgN}_4$ ^[26] and $\text{Ba}_3\text{GeMgN}_4$ ^[27] with infinite chains of edge-sharing alternating GeN_4 and MgN_4 tetrahedra as well as $\text{Ca}_5\text{Ge}_2\text{N}_6$.^[22] Additionally, there is only one 3D condensed nitridomagnesogermanate known so far, namely $\text{SrMg}_3\text{GeN}_4$.^[1]

In summary, there are only four compounds within the class of nitridogermanates with higher dimensional nitridometallate networks so far. Three of them contain both Ge and Mg as center ions of the building blocks. As none of the quaternary 1D and 3D nitridogermanates contain Ca as counterion, it is focused on the synthesis of Ca-containing nitridomagnesogermanates with

the aim of a new, highly condensed compound whose structure could be transferred to nitridoaluminates or -silicates. In this way it is hit upon $\text{Ca}_2\text{Mg}_5\text{GeN}_6$, the first layered (2D) Mg-containing nitridogermanate. In this contribution, the synthesis and crystal-structure elucidation of the compound crystallizing isotypically to the nitridomagnesaluminate $\text{CaMg}_2\text{AlN}_3$ [28] and homeotypically to the carbides ScAl_3C_3 and UAl_3C_3 is reported. [29]

2.3.2 Results and Discussion

$\text{Ca}_2\text{Mg}_5\text{GeN}_6$ was obtained as colorless platelets with hexagonal shape, which were isolated from a heterogeneous product. The compound is sensitive towards air and moisture. SEM measurements indicated a new composition with atomic ratio $\text{Ca}:\text{Mg}:\text{Ge}:\text{N} = 1.9:5:1:4.6$ that corresponds approximately to the composition of $\text{Ca}_2\text{Mg}_5\text{GeN}_6$. Due to unavoidable manipulations of the sample carrier in air for a short time, the product was partially hydrolyzed. Small amounts of oxygen were detected. Even though EuF_3 was added as reactant with intention to investigate luminescence properties of the Eu-doped material, no luminescence could be observed and no Eu was detected by EDX measurements.

Single-Crystal Structure Analysis

The crystal structure of $\text{Ca}_2\text{Mg}_5\text{GeN}_6$ was solved and refined using single-crystal X-ray diffraction data. The compound crystallizes in the hexagonal space group $P6_3/mmc$ (no. 194) with $a = 3.453(2)$ and $c = 17.506(13)$ Å. All atoms were refined anisotropically. Crystallographic data as well as atomic coordinates and anisotropic displacement parameters are given in Table 1, Table 2, and Table 3. Besides one octahedrally coordinated Ca-site there are two crystallographic sites with mixed occupation of Mg and Ge. Whereas Mg1/Ge1 shows tetrahedral environment, the coordination of Mg2/Ge2 can be described as trigonal planar with two additional nitrogen atoms in enlarged distance, resulting in an elongated trigonal bipyramidal coordination (see Figure 1). Selected bond lengths and angles are shown in Table 4. Free refinement of the occupancy of both crystallographic sites leads to 84% Mg and 16% Ge on Mg1/Ge1 site and 82% Mg and 18% Ge on Mg2/Ge2 site. This corresponds to electrostatic neutrality.

Table 1. Crystallographic data for $\text{Ca}_2\text{Mg}_5\text{GeN}_6$.

	$\text{Ca}_2\text{Mg}_5\text{GeN}_6$
Molar Mass / $\text{g}\cdot\text{mol}^{-1}$	358.36
Crystal system	Hexagonal
Space group	$P6_3/mmc$ (no. 194)
Cell parameters / Å	$a = 3.453(2)$ $c = 17.506(13)$
Cell volume / Å ³	180.8(2)
Formula units per unit cell	1
Density / $\text{g}\cdot\text{cm}^{-3}$	3.292
Abs. coefficient μ / mm^{-1}	6.031
$F(000)$	174
Temperature	293(2)
Diffractometer	Bruker D8 Quest
Radiation / Å	Mo- K_α ($\lambda = 0.71073$)
θ range / °	$4.657 \leq \theta \leq 31.437$
Total no. of reflections	2943
Independent reflections	150
Refined parameters	13
Goodness of fit	1.153
R_1 (all data) / $R_1 [F > 2\sigma(F)]$	0.0588/0.0399
wR_2 (all data) / $wR_2 [F > 2\sigma(F)]$	0.0963/0.0873
$\Delta\rho_{\text{max}}, \Delta\rho_{\text{min}}$ / $\text{e}\cdot\text{\AA}^{-3}$	1.469, -1.547

Aside from $\text{Ca}_2\text{Mg}_5\text{GeN}_6$ there are further examples of quaternary compounds containing mixed occupation of network-building cations. $\text{Ca}_2\text{Ga}_3\text{MgN}_5$ [8] and $\text{SrMg}_2\text{Ga}_2\text{N}_4$ [1] represent some examples within nitridogallates, $\text{SrMg}_3\text{GeN}_4$ [1] is the only known example of a nitridogermanate so far. Further compounds crystallizing with UCr_4C_4 structure type, [30] namely $\text{MMg}_2\text{Al}_2\text{N}_4$ ($M = \text{Ca}, \text{Sr}, \text{Ba}, \text{Eu}$), [2] also show mixed occupancy. The bond lengths (Mg/Ge)–N found in $\text{Ca}_2\text{Mg}_5\text{GeN}_6$ range from 1.9936(12) to 2.110(3) Å. Due to mixed occupancy, those are averaged values of Ge–N and Mg–N bond lengths. This is in good agreement with the averaged bond length (Mg/Ge)–N of 2.04 Å in $\text{SrMg}_3\text{GeN}_4$. Furthermore, it is likewise similar to the respective value of 2.03 Å in $\text{Ca}_2\text{Ga}_3\text{MgN}_5$. It also complies to Mg–N and Ge–N distances observed in other

known ternary or quaternary nitrides (2.04 to 2.30 Å for Mg–N and 1.84 to 1.99 Å for Ge–N) as well as to the sum of the ionic radii pursuant to Baur.^[22,23,26,27,31-33]

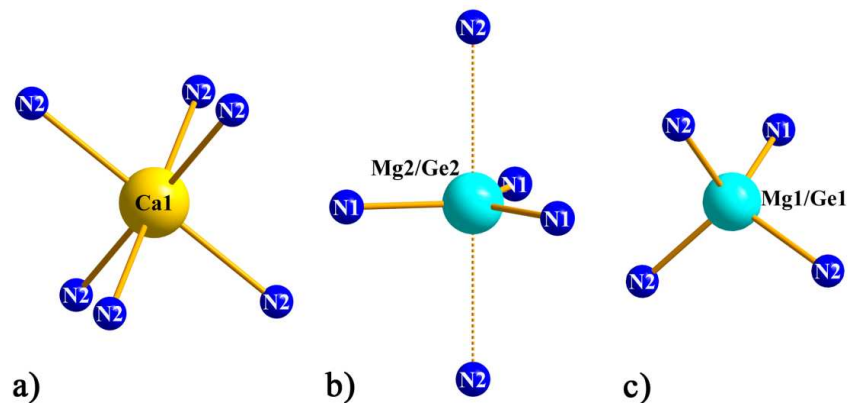


Figure 1. Coordination of cation sites. (a) Octahedral coordination of Ca1; (b) trigonal planar coordination of Mg2/Ge2 in combination with elongated bond lengths Mg2/Ge2–N2, resulting in trigonal bipyramidal coordination; (c) tetrahedral coordination of Mg1/Ge1.

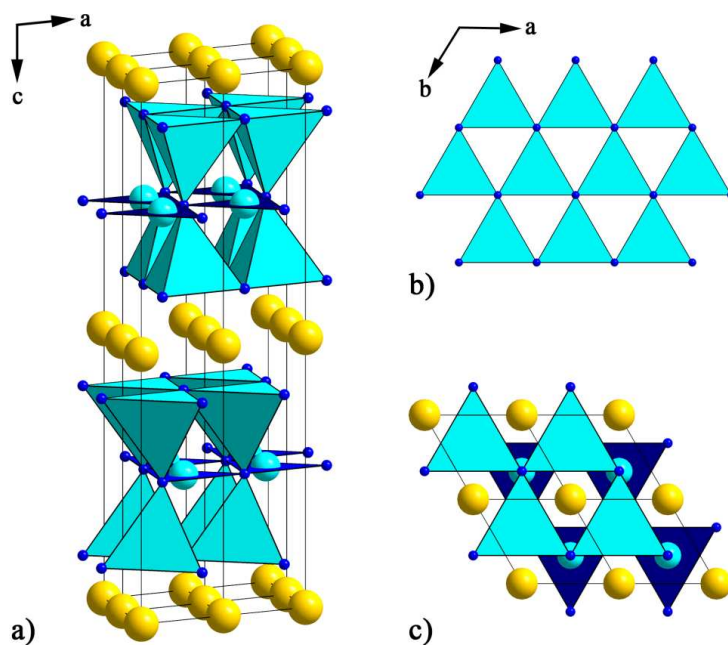


Figure 2. Crystal structure of $\text{Ca}_2\text{Mg}_5\text{GeN}_6$ with (Mg/Ge) N_4 tetrahedra (turquoise), trigonal planar (Mg/Ge) N_3 units (blue). Atom types: Ca (yellow), Mg/Ge (turquoise), N (dark blue). a) Viewing direction along [010]; b) condensed *dreier* rings of one double layer; c) viewing direction along [001].

According to the degree of condensation (i.e. the atomic ratio (Mg/Ge):N) of $\kappa = 1$, a three-dimensional anionic network of $\text{Ca}_2\text{Mg}_5\text{GeN}_6$ could be expected. In contrast to expectations, the nitridogermanate shows a two-dimensional anionic substructure. The crystal structure is closely related to that of $\text{CaMg}_2\text{AlN}_3$, ScAl_3C_3 , and UAl_3C_3 [29] It is the first layered structure known for a nitridogermanate. Its layers are built up of highly condensed planar double layers of corner-sharing (Mg/Ge) N_4 tetrahedra, forming condensed *dreier* rings (see Figure 2a and b). [34] Each nitrogen atom on the exterior of the double layer connects three neighboring Mg/Ge tetrahedron centers. N atoms in the midst of the sheets connect two Mg/Ge tetrahedron centers, one of every sublayer. These N atoms additionally form *dreier* rings, centered by a second site with mixed occupation Mg/Ge. Trigonal planar coordination of Ge^{4+} and Mg^{2+} ions can be found in $\text{Ba}_9\text{Ge}_3\text{N}_{10}$, [35] or Mg_3BN_3 , [31] the latter is structurally related to $\text{Ca}_2\text{Mg}_5\text{GeN}_6$. Thus, mixed occupancy of trigonal planar coordinated ions are conceivable for further compounds. Besides, there is one Ca site, octahedrally coordinated by N. These cations separate the sheets built up of tetrahedra and trigonal planar units. Figure 2c shows the crystal structure along [001]. In this viewing direction, hexagonal channels containing Ca^{2+} ions can be seen. The sheets are stacked along [001].

As already mentioned, there is one peculiarity concerning trigonal planar coordinated Mg2/Ge2 site in $\text{Ca}_2\text{Mg}_5\text{GeN}_6$. It shows a large displacement parameter, comparable to one Al site in $\text{CaMg}_2\text{AlN}_3$, ScAl_3C_3 and UAl_3C_3 after structure refinement in the space group $P6_3/mmc$, respectively. [28,36] In case of the carbides, its coordination is described as trigonal bipyramidal, alternatively as a split position with tetrahedral environment of adjacent Al atoms. [37] Subsequent studies with structural refinements in the space group $P6_3mc$ resulted in tetrahedrally coordinated Al atoms. [29] Structural studies on the nitridomagnesioaluminate resulted in ordering of Mg and Al sites, also with a split Al position or rather a large displacement parameter of Al in the space group $P6_3/mmc$ as well as tetrahedral environment of all network building ions Mg^{2+} and Al^{3+} after refinement in the space group $P6_3mc$. [28] Even with calculations of the Madelung part of the lattice energy (MAPLE) for both structural models, none of the structural models could be validated.

In contrast to these three compounds, analysis of the electron density of $\text{Ca}_2\text{Mg}_5\text{GeN}_6$ in PLATON, plotted in $P1$, does not show any signs of a split position (see Figure 3). Crystal structure refinement in space group $P6_3mc$, as reported by Meyer et al. for $\text{CaMg}_2\text{AlN}_3$ as well as for ScAl_3C_3 and UAl_3C_3 was not successful. In contrast to the nitridomagnesioaluminate, $\text{Ca}_2\text{Mg}_5\text{GeN}_6$ does not show ordering of Ge and Mg.

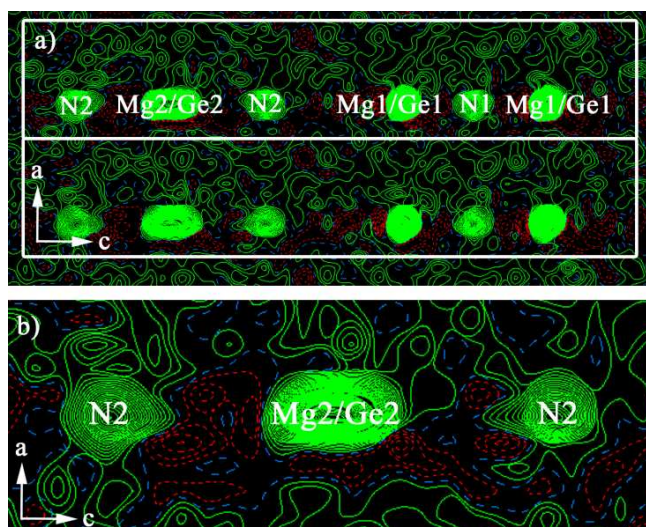


Figure 3. Electron density map of $\text{Ca}_2\text{Mg}_5\text{GeN}_6$ without symmetry restraints on the planes (010) with $y = 2.9904$ and contour level $0.8 \text{ e}^- \text{Å}^3$ (green = positive electron density, red = negative electron density). (a) two unit cells highlighted; (b) enlarged Mg2/Ge2 site.

Table 2. Atomic coordinates and equivalent isotropic displacement parameters $/\text{Å}^2$ of $\text{Ca}_2\text{Mg}_5\text{GeN}_6$.

Atom	Wyckoff-site	x	y	z	U_{eq}	$s.o.f.$
Ca1	2a	0	0	0	0.0085(5)	1
Mg1/Ge1	4f	$\frac{2}{3}$	$\frac{1}{3}$	0.13226(10)	0.0101(5)	0.841(9)/0.159(9)
Mg2/Ge2	2c	$\frac{1}{3}$	$\frac{2}{3}$	$\frac{1}{4}$	0.0551(18)	0.82(2)/0.18(2)
N1	2d	$\frac{2}{3}$	$\frac{1}{3}$	$\frac{1}{4}$	0.019(2)	1
N2	4f	$\frac{1}{3}$	$\frac{2}{3}$	0.0928(4)	0.0195(16)	1

Table 3. Anisotropic displacement parameters $/\text{Å}^2$ of $\text{Ca}_2\text{Mg}_5\text{GeN}_6$.

Atom	U_{11}	U_{22}	U_{33}	U_{23}	U_{13}	U_{12}
Ca1	0.0078(6)	0.0078(6)	0.0103(8)	0	0	0.0039(3)
Mg1/Ge1	0.0113(6)	0.0113(6)	0.0065(7)	0	0	0.0056(3)
Mg2/Ge2	0.0063(10)	0.0063(10)	0.157(5)	0	0	0.0031(5)
N1	0.014(3)	0.014(3)	0.030(5)	0	0	0.0071(16)
N2	0.015(2)	0.015(2)	0.029(4)	0	0	0.0075(11)

Table 4. Selected bond lengths /Å and angles /° in $\text{Ca}_2\text{Mg}_5\text{GeN}_6$.

Bond lengths			Bond angles	
Ca1–	N2	2.572(5) (6x)	N2–Ca1–N2	84.3(2)
(Mg1/Ge1)–	N1	2.061(2)	N2–Ca1–N2	95.7(2)
	N2	2.110(3) (3x)	N2–Ca1–N2	180.0(3)
(Mg2/Ge2)–	N1	1.9936(12) (3x)	N1–(Mg1/Ge1)–N2	109.1(2)
	N2	2.752(1) (2x)	N2–(Mg1/Ge1)–N2	109.9(2)
			N1–(Mg2/Ge2)–N1	120.0
			N2–(Mg2/Ge2)–N2	180.0
			N2–(Mg2/Ge2)–N1	90.0

2.3.3 Conclusions

Reaction of pure elements (Ca, Mg, Ge) and NaN_3 in molten sodium yielded the new quaternary compound $\text{Ca}_2\text{Mg}_5\text{GeN}_6$. As both Mg and Ge are part of the network, the compound can be classified as nitridomagnesogermanate. It is the first layered compound within nitridogermanates known so far. Furthermore, there are only three examples of quaternary nitridogermanates containing alkaline earth elements as counterions, namely $\text{Sr}_3\text{GeMgN}_4$, $\text{Ba}_3\text{GeMgN}_4$, and $\text{SrMg}_3\text{GeN}_4$. Those compounds, including ternary $\text{Ca}_5\text{Ge}_2\text{N}_6$, represent the only examples within nitridogermanates with a 1D or higher-dimensional anionic substructure. Quaternary nitridogermanates containing Ca are not known to date.

The crystal structure of $\text{Ca}_2\text{Mg}_5\text{GeN}_6$ contains highly condensed planar double layers, which in turn are built up of tetrahedra and trigonal planar units with mixed occupation of Mg^{2+} and Ge^{4+} as center ions. The sheets are stacked along [001] forming hexagonal channels containing Ca^{2+} as counterions, which concurrently separate the sheets from each other. The crystal structure is closely related to that of $\text{CaMg}_2\text{AlN}_3$, ScAl_3C_3 , and UAl_3C_3 . All of them show a large displacement parameter for trigonal coordinated crystallographic site. But in contrast to the carbides and the nitridoaluminate, for $\text{Ca}_2\text{Mg}_5\text{GeN}_6$ a split position can be excluded.

Despite different charges of center ions ($\text{Al}^{3+}/\text{Ge}^{4+}$), both nitridogermanates and nitridoaluminates show similarities in their crystal structures and thus to nitridosilicates. As Eu^{2+} -doped nitridoaluminates and -silicates are suitable for application in high-performance pc-LEDs, research on novel structures within the class of nitridogermanates is quite promising. These can

be transferred to nitridoaluminates and -silicates, and thus pave the way to new host lattices with possible application in pc-LEDs.

2.3.4 Experimental Section

2.3.4.1 Synthesis of $\text{Ca}_2\text{Mg}_5\text{GeN}_6$

$\text{Ca}_2\text{Mg}_5\text{GeN}_6$ was synthesized in sealed Ta ampules (30 mm length, 10 mm diameter, 0.5 mm thickness) using NaN_3 (0.306 mmol, 19.9 mg), Ca (0.237 mmol, 9.5 mg), Mg (0.712 mmol, 17.3 mg), Ge (0.237 mmol, 17.2 mg), and EuF_3 ($4.31 \cdot 10^{-3}$ mmol, 0.9 mg) as starting materials in Na-flux (2.13 mmol, 48.9 mg). All manipulations were done in an argon filled glove box (Unilab, MBraun, Garching; $\text{O}_2 < 1$ ppm, $\text{H}_2\text{O} < 1$ ppm). In order to prevent the ampule from oxidation, the weld shut crucible was placed in a quartz tubing under vacuum. It was fired to 780 °C at a rate of 50 K/h and after holding at 780 °C for 48 h, the reaction mixture was cooled down to 200 °C with a rate of 3 K/h. Afterwards the tube furnace was switched off. The Ta ampule was opened in a glove box and Na melt was removed via sublimation at 320 °C under vacuum.

2.3.4.2 Single-Crystal X-ray Diffraction

Under a microscope, single-crystals were isolated from the heterogeneous product mixture and sealed within glass capillaries to avoid hydrolysis. Measurements were performed on a Bruker D8 Quest diffractometer (PHOTON 199 CMOS detector, Mo- K_α radiation). Absorption correction was done using multi-scan methods (SADABS).^[38] The structure was solved by direct methods implemented in SHELXS, structure refinement with anisotropic displacement parameters for all atoms by full-matrix least-squares calculation on $|F|^2$ were done in SHELXL-97.^[39]

Further details of the crystal structure investigations may be obtained from the Fachinformationszentrum Karlsruhe, 76344 Eggenstein-Leopoldshafen, Germany (Fax: +49-7247-808-666; e-Mail: crysdata@fiz-karlsruhe.de) on quoting the depository number CSD-431362.

2.3.4.3 Scanning Electron Microscopy

To determine both chemical composition and morphology, the product was prepared on an adhesive conductive carbon pad and coated with a conductive carbon film (BAL-TEC MED 020, Bal Tec AG). Within a FEI Helios G3 UC equipped with an EDX detector, scanning transmission detector and Focused Ion Beam, the chemical composition of the reported product could be confirmed.

2.3.4.4 Powder X-ray Diffraction

The reaction product was pulverized in an agate mortar and enclosed in a glass capillary. Powder diffraction data were recorded on a STOE STADI P diffractometer (Cu- $K_{\alpha 1}$ radiation, Ge(111) monochromator, Mythen1K detector) in Debye-Scherrer set-up. The WinXPOW program package^[40] served to identify secondary phases as well as simulation of powder diffraction pattern, calculated on the basis of single-crystal structure data. The content of the different phases were determined using the Rietveld method. Refinement was carried out using the TOPAS package.^[41]

2.3.5 References

- [1] D. G. Park, Y. Dong, F. J. DiSalvo, *Solid State Sci.* **2008**, 10, 1846.
- [2] P. Pust, F. Hintze, C. Hecht, V. Weiler, A. Locher, D. Zitnanska, S. Harm, D. Wiechert, P. J. Schmidt, W. Schnick, *Chem. Mater.* **2014**, 26, 6113.
- [3] S. Schmiechen, H. Schneider, P. Wagatha, C. Hecht, P. J. Schmidt, W. Schnick, *Chem. Mater.* **2014**, 26, 2712.
- [4] H. A. Höpfe, H. Lutz, P. Morys, W. Schnick, A. Seilmeier, *J. Phys. Chem. Solids* **2000**, 61, 2001.
- [5] K. Uheda, N. Hirotsaki, H. Yamamoto, *Phys. Status Solidi A* **2006**, 203, 2712.
- [6] P. Pust, V. Weiler, C. Hecht, A. Tücks, A. S. Wochnik, A.-K. Henß, D. Wiechert, C. Scheu, P. J. Schmidt, W. Schick, *Nat. Mater.* **2014**, 13, 891.
- [7] P. E. Rauch, A. Simon, *Angew. Chem.* **1992**, 104, 1505; *Angew. Chem. Int. Ed. Engl.* **1992**, 31, 1519.
- [8] F. Hintze, W. Schnick, *Z. Anorg. Allg. Chem.* **2012**, 638, 2243.
- [9] G. Cordier, P. Höhn, R. Kniep, A. Rabenau, *Z. Anorg. Allg. Chem.* **1990**, 591, 58.
- [10] S. J. Clarke, F. J. DiSalvo, *J. Alloys Compd.* **1998**, 274, 118.
- [11] M. S. Bailey, F. J. DiSalvo, *J. Alloys Compd.* **2006**, 417, 50.
- [12] S. J. Clarke, F. J. DiSalvo, *Inorg. Chem.* **1997**, 36, 1143.
- [13] D. G. Park, Z. A. Gál, F. J. DiSalvo, *Inorg. Chem.* **2003**, 42, 1779.
- [14] D. G. Park, Z. A. Gál, F. J. DiSalvo, *J. Alloys Compd.* **2003**, 353, 107.
- [15] H. Yamane, F. J. DiSalvo, *Acta Crystallogr., Sect. C* **1996**, 52, 760.
- [16] F. Hintze, F. Hummel, P. J. Schmidt, D. Wiechert, W. Schnick, *Chem. Mater.* **2012**, 24, 402.
- [17] F. Hintze, W. Schnick, *Solid State Sci.* **2010**, 12, 1368.
- [18] S. J. Clarke, G. R. Kowach, F. J. DiSalvo, *Inorg. Chem.* **1996**, 35, 7009.
- [19] H. Yamane, F. J. DiSalvo, *J. Alloys Compd.* **1996**, 241, 69.
- [20] D. G. Park, Z. A. Gál, F. J. DiSalvo, *Bull. Korean Chem. Soc.* **2005**, 26, 1543.
- [21] M. Y. Chern, D. A. Vennos, F. J. DiSalvo, *J. Solid State Chem.* **1992**, 96, 415.
- [22] S. J. Clarke, F. J. DiSalvo, *Inorg. Chem.* **2000**, 39, 2631.
- [23] S. C. Junggeburth, O. Oeckler, W. Schnick, *Z. Anorg. Allg. Chem.* **2008**, 634, 1309.
- [24] S. C. Junggeburth, O. Oeckler, D. Johrendt, W. Schnick, *Inorg. Chem.* **2008**, 47, 12018.
- [25] D. G. Park, F. J. DiSalvo, *Bull. Korean Chem. Soc.* **2008**, 29, 2413.
- [26] D. G. Park, Z. A. Gál, F. J. DiSalvo, *J. Alloys Compd.* **2003**, 360, 85.

- [27] D. G. Park, F. J. DiSalvo, *Bull. Korean Chem. Soc.* **2011**, 32, 353.
- [28] M. Kubus, K. Levin, S. Kroeker, D. Enseling, T. Jüstel, H.-J. Meyer, *Dalton Trans.* **2015**, 44, 2819.
- [29] T. M. Gesing, W. Jeitschko, *J. Solid State Chem.* **1998**, 140, 396.
- [30] L. G. Akselrud, O. I. Bodak, E. O. Marusin, *Sov. Phys. Crystallogr. (Engl. Transl.)* **1989**, 34, 289.
- [31] H. Hiraguchi, H. Hashizume, O. Fukunaga, A. Takenaka, M. Sakata, *J. Appl. Crystallogr.* **1991**, 24, 286.
- [32] V. Schultz-Coulon, W. Schnick, *Z. Naturforsch.* **1995**, 50b, 619.
- [33] W. H. Baur, *Crystallogr. Rev.* **1987**, 1, 59.
- [34] The terms *dreier* ring was coined by Liebau and is derived from the German word *drei* = 3. A *dreier* ring comprises three tetrahedron centers.
- [35] D. G. Park, D. J. DiSalvo, *Bull. Korean Chem. Soc.* **2008**, 29, 2413.
- [36] A. O. Tsokol', O. I. Bodak, E. P. Marusin, M. G. Baivel'man, *Sov. Phys. Crystallogr. (Engl. Transl.)* **1986**, 31, 467.
- [37] T. M. Gesing, R. Pöttgen, W. Jeitschko, U. Wortmann, *J. Alloys Compd.* **1992**, 186, 321.
- [38] G. M. Sheldrick, *SADABS*, Multi-Scan Absorption Correction, v.2, Bruker-AXS, Madison, WI, USA, **2012**.
- [39] G. M. Sheldrick, *Acta Crystallogr., Sect. A* **2008**, 64, 112.
- [40] *WinXPow*, Program for Powder Data Handling v. 2.21, Stoe & Cie GmbH, Darmstadt, Germany, **2007**.
- [41] A. Coelho, *TOPAS - Academic*, Coelho Software, Brisbane, Australia, **2007**.

2.4 $\text{Ca}_4\text{Mg}_5\text{Ge}_3\text{N}_{10}$ and $\text{Sr}_2\text{Mg}_3\text{GaN}_{4.33}$ – Two Mg-Containing Nitrides and Their Structural Relation to $(\text{Sr},\text{Ba})_2\text{Si}_5\text{N}_8$

published in: *Eur. J. Inorg. Chem.* **2017**, 1498-1503

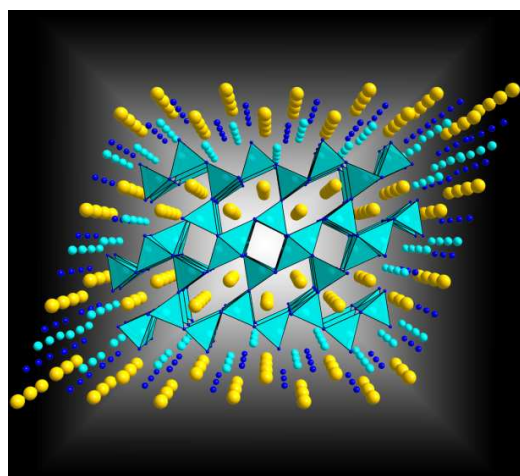
authors: Christine Poesl and Wolfgang Schnick

DOI: 10.1002/ejic.201601532

Copyright © 2017 Wiley-VCH Verlag GmbH & Co. KGaA, Weinheim

<http://onlinelibrary.wiley.com/doi/10.1002/ejic.201601532/abstract>

Abstract: The quaternary nitrides $\text{Ca}_4\text{Mg}_5\text{Ge}_3\text{N}_{10}$ and $\text{Sr}_2\text{Mg}_3\text{GaN}_{4.33}$ were synthesized employing the Na azide route in weld-shut Ta ampules. The two compounds are homeotypic and crystallize in the monoclinic space group $C2/m$ (no. 12). The crystal structures were solved and refined on the basis of single-crystal X-ray diffraction data [$\text{Ca}_4\text{Mg}_5\text{Ge}_3\text{N}_{10}$: $a = 11.269(3)$, $b = 3.3267(11)$, $c = 8.008(3)$ Å, $\beta = 109.80(2)^\circ$, $V = 282.44(16)$ Å³, $Z = 1$; $\text{Sr}_2\text{Mg}_3\text{GaN}_{4.33}$: $a = 11.737(2)$, $b = 3.4610(7)$, $c = 7.8610(16)$ Å, $\beta = 108.03(3)^\circ$, $V = 303.65(12)$ Å³, $Z = 1$]. The



three-periodic anionic substructures of both nitrides are made up of MN_4 tetrahedra with mixed occupation of central atoms $M = \text{Mg}/\text{Ge}$ and Mg/Ga , respectively. Corner- and edge-sharing of MN_4 tetrahedra results in *vierer* and *sechser* ring channels along $[010]$. Alkaline earth metal ions are located within *sechser* ring channels. The crystal structures are also homeotypic with that of known $\text{Ca}_2\text{MgGa}_3\text{N}_5$ and represent a more highly condensed variant of the $M^{\text{II}}_2\text{Si}_5\text{N}_8$ ($M^{\text{II}} = \text{Sr}, \text{Ba}$) type of structure.

2.4.1 Introduction

Understanding of the structural characteristics of nitrides is of growing importance, since they are an interesting class of materials regarding their outstanding chemical and physical properties.^[1-15] Especially Mg-containing nitrides are of key interest, since they play an important role as host lattices for lanthanide-doped luminescent materials such as $\text{Sr}[\text{Mg}_3\text{SiN}_4]:\text{Eu}^{2+}$,^[16] $\text{Ba}[\text{Mg}_3\text{SiN}_4]:\text{Eu}^{2+}$,^[17] $M[\text{Mg}_2\text{Al}_2\text{N}_4]:\text{Eu}^{2+}$ ($M = \text{Ca}, \text{Sr}, \text{Ba}$) and $\text{Ba}[\text{Mg}_2\text{Ga}_2\text{N}_4]:\text{Eu}^{2+}$.^[1] Up to now, only a small number of quaternary compounds containing Ge or Ga have been reported, and only a few also contain Mg.^[1,18-25]

Most syntheses of nitridogermanates and nitridogallates start from the pure elements and employ the Na azide route.^[19-22,26-30] Therefore, the starting materials as well as NaN_3 and Na were filled into Ta or Nb ampules, which were hermetically closed by arc welding and fired at around 760 °C. By thermal dissociation, NaN_3 supplies an increased nitrogen pressure in the ampule. Due to enhanced solubility of nitrogen in liquid Na on addition of alkaline earth metals, most nitridogermanates and nitridogallates contain Ca, Sr, or Ba as one of the constituent elements.

The crystal structures of previously known Mg-containing compounds in both classes of nitrides are built up of tetrahedra that are connected through common corners and/or edges to form anionic substructures. Tetrahedral centers are thereby occupied by Ge/Mg or Ga/Mg and the compounds can therefore be classified as nitridomagnesogermanates and nitridomagnesogallates, respectively. Electropositive alkaline earth metals balance the charges and are distributed among the cavities of the anionic framework.

The dimensionality of nitridomagnesogermanates is diverse. There are anionic substructures of infinite chains ($M_3\text{MgGeN}_4$ with $M = \text{Sr}, \text{Ba}$),^[18,20] layers ($\text{Ca}_2\text{Mg}_5\text{GeN}_6$),^[22] and three-periodic networks ($\text{Sr}[\text{Mg}_3\text{GeN}_4]$).^[19] In case of nitridomagnesogallates, only layered ($\text{CaMg}_2\text{GaN}_3$ and $\text{CaMg}_2\text{Ga}_2\text{N}_4$)^[31] and three-periodic anionic frameworks ($\text{Ca}_2\text{MgGa}_3\text{N}_5$, $M[\text{Mg}_2\text{Ga}_2\text{N}_4]$ with $M = \text{Sr}, \text{Ba}$) are known.^[1,19,21] Since the homeotypic nitrides $\text{Sr}[\text{Mg}_3\text{GeN}_4]$ and $M[\text{Mg}_2\text{Ga}_2\text{N}_4]$ illustrate the structural similarities between the two compound classes, we assume that further compounds exist that are structurally related to already known nitridomagnesogermanates and -gallates, respectively.

Herein, we report on the synthesis and structure elucidation of the nitrides $\text{Ca}_4\text{Mg}_5\text{Ge}_3\text{N}_{10}$ and $\text{Sr}_2\text{Mg}_3\text{GaN}_{4.33}$, which are closely related to $\text{Ca}_2\text{MgGa}_3\text{N}_5$. Similarities between these compounds

2.4 $\text{Ca}_4\text{Mg}_5\text{Ge}_3\text{N}_{10}$ and $\text{Sr}_2\text{Mg}_3\text{GaN}_{4.33}$ – Two Mg-Containing Nitrides and Their Structural Relation to $(\text{Sr},\text{Ba})_2\text{Si}_5\text{N}_8$

and particular structural features of $\text{Sr}_2\text{Mg}_3\text{GaN}_{4.33}$ are discussed in detail. Structural analogies to thoroughly investigated $M_2\text{Si}_5\text{N}_8$ ($M = \text{Sr}, \text{Ba}$) are also presented.

2.4.2 Results and Discussion

2.4.2.1 Synthesis

$\text{Ca}_4\text{Mg}_5\text{Ge}_3\text{N}_{10}$ as well as $\text{Sr}_2\text{Mg}_3\text{GaN}_{4.33}$ were synthesized by employing the NaN_3 route from the pure elements with sodium azide NaN_3 as nitrogen source and sodium as fluxing agent in weld-shut tantalum ampules at 780 and 760 °C, respectively. Both nitrides could be isolated as crystalline side phases from heterogeneous reaction mixtures. Rod-shaped single crystals of $\text{Ca}_4\text{Mg}_5\text{Ge}_3\text{N}_{10}$ and $\text{Sr}_2\text{Mg}_3\text{GaN}_{4.33}$ show yellow to red body colors and are sensitive to air and moisture. Energy-dispersive X-ray (EDX) analyses yielded an average atomic ratio of $\text{Ca}/\text{Mg}/\text{Ge} = 3.9:5.4:3.0$ for $\text{Ca}_4\text{Mg}_5\text{Ge}_3\text{N}_{10}$ (normalized according to the Ge content) and an average atomic ratio of $\text{Sr}/\text{Mg}/\text{Ga} = 2.0:3.2:1.2$ for $\text{Sr}_2\text{Mg}_3\text{GaN}_{4.33}$ (normalized according to the Sr content). Besides a small amount of oxygen, which can be attributed to the high sensitivity of the products to air and moisture, no further elements were detected.

2.4.2.2 Single-Crystal Structure Analysis

The crystal structures of $\text{Ca}_4\text{Mg}_5\text{Ge}_3\text{N}_{10}$ and $\text{Sr}_2\text{Mg}_3\text{GaN}_{4.33}$ were solved and refined by using single-crystal X-ray diffraction data. Both compounds crystallize in the monoclinic space group $C2/m$ (no. 12). Crystallographic data are summarized in Table 1, and atomic coordinates and isotropic displacement parameters are given in Table 2. Table 3 lists selected bond lengths of $\text{Ca}_4\text{Mg}_5\text{Ge}_3\text{N}_{10}$ and $\text{Sr}_2\text{Mg}_3\text{GaN}_{4.33}$; selected bond angles of both compounds can be found in the Supporting Information.

2.4 $\text{Ca}_4\text{Mg}_5\text{Ge}_3\text{N}_{10}$ and $\text{Sr}_2\text{Mg}_3\text{GaN}_{4.33}$ –
Two Mg-Containing Nitrides and Their Structural Relation to $(\text{Sr},\text{Ba})_2\text{Si}_5\text{N}_8$

Table 1. Crystallographic data for $\text{Ca}_4\text{Mg}_5\text{Ge}_3\text{N}_{10}$ and $\text{Sr}_2\text{Mg}_3\text{GaN}_{4.33}$.

Formula	$\text{Ca}_4\text{Mg}_5\text{Ge}_3\text{N}_{10}$	$\text{Sr}_2\text{Mg}_3\text{GaN}_{4.33}$
Crystal system	Monoclinic	Monoclinic
Space group	$C2/m$ (No. 12)	$C2/m$ (No. 12)
Lattice parameter /Å, °	$a = 11.269(3)$	$a = 11.737(2)$
	$b = 3.3267(11)$	$b = 3.4610(7)$
	$c = 8.008(3)$	$c = 7.8610(16)$
	$\beta = 109.80(2)$	$\beta = 108.03(3)$
Cell volume /Å ³	282.44(16)	303.65(12)
Formula units per unit cell	1	2
Density /g·cm ⁻³	3.761	4.138
μ /mm ⁻¹	10.027	22.243
T /K	293(2)	293(2)
Diffractometer	Bruker D8 Quest	Bruker D8 Quest
Radiation	Mo- K_α ($\lambda = 0.71073$ Å)	Mo- K_α ($\lambda = 0.71073$ Å)
$F(000)$	306	346
θ range /°	$2.703 \leq \theta \leq 29.114$	$2.725 \leq \theta \leq 33.781$
Total no. of reflections	2312	4631
Independent reflections	435	698
Refined parameters	35	33
Goodness of fit	1.142	1.071
R_1 (all data) / $R_1 [F^2 > 2\sigma(F^2)]$	0.0586/0.0416	0.0738/0.0545
wR_2 (all data) / $wR_2 [F^2 > 2\sigma(F^2)]$	0.1108/0.0998	0.0956/0.0901
$\Delta\rho_{\min}/\Delta\rho_{\max}$ / e·Å ³	-1.290/1.138	-1.447/2.715

$\text{Ca}_4\text{Mg}_5\text{Ge}_3\text{N}_{10}$ is homeotypic with $\text{Ca}_2\text{MgGa}_3\text{N}_5$ [21] and also exhibits disordering of tetrahedrally coordinated Mg^{2+} and Ge^{4+} ions on the same site. An analogous situation was observed for the quaternary compounds $\text{Ca}_2\text{Mg}_5\text{GeN}_6$ [22] and $\text{Sr}[\text{Mg}_3\text{GeN}_4]$. [19] Since Mg^{2+} and Ge^{4+} are both part of the tetrahedral network, the compounds can be classified as nitridomagnesogermanates.

In $\text{Ca}_4\text{Mg}_5\text{Ge}_3\text{N}_{10}$, there are two crystallographic tetrahedral positions. The (Mg/Ge)–N distances vary between 1.954(2) and 2.115(8) Å and are in good agreement with the (Mg/Ge)–N bond

2.4 $\text{Ca}_4\text{Mg}_5\text{Ge}_3\text{N}_{10}$ and $\text{Sr}_2\text{Mg}_3\text{GaN}_{4.33}$ – Two Mg-Containing Nitrides and Their Structural Relation to $(\text{Sr},\text{Ba})_2\text{Si}_5\text{N}_8$

lengths found in $\text{Ca}_2\text{Mg}_5\text{GeN}_6$ and $\text{Sr}[\text{Mg}_3\text{GeN}_4]$ [1.99 to 2.11 Å] as well as to averaged Mg–N and Ge–N bond lengths known from other ternary or quaternary nitrides.^[18-20,27,28,32-35] $(\text{Mg1}/\text{Ge1})\text{N}_4$ tetrahedra are linked through common corners to adjacent tetrahedra. In contrast, $(\text{Mg2}/\text{Ge2})\text{N}_4$ units are connected through common corners and edges, whereby edge-sharing can solely be observed between $(\text{Mg2}/\text{Ge2})\text{N}_4$ tetrahedra. The linkage of tetrahedra results in *vierer* ring^[36] channels and *sechser* ring channels along [010], and the respective ring types alternate vertically and iterate horizontally (see Figure 1). Ca ions are located within *sechser* ring channels, coordinated by seven N atoms. The Ca–N distances range from 2.437(1) to 2.820(7) Å, in compliance with Ca–N bond lengths of other Ca-containing nitrides { $\text{Ca}_2\text{MgGa}_3\text{N}_5$: 2.41-2.61 Å, $\text{Ca}_2\text{Mg}_5\text{GeN}_6$: 2.57 Å, $\text{Ca}[\text{LiAl}_3\text{N}_4]$: 2.52-2.91 Å}^[3,21,22] and the sum of ionic radii reported by Baur.^[37]

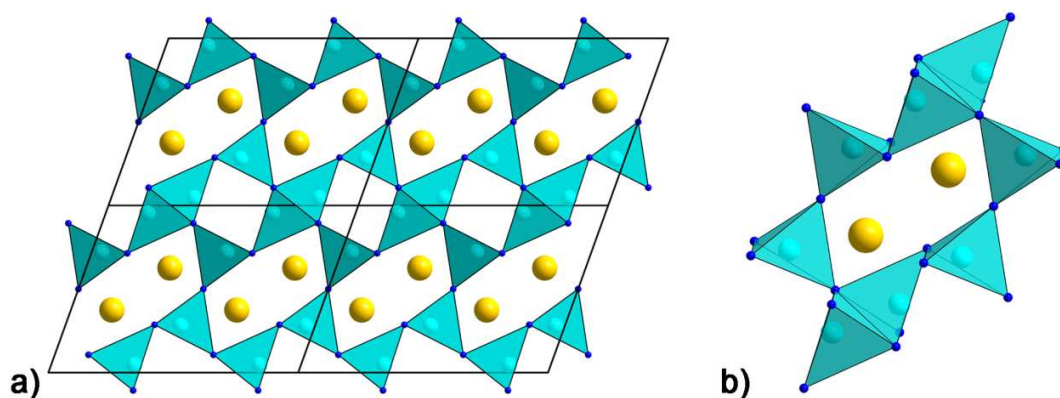


Figure 1. (a) Crystal structure of $\text{Ca}_4\text{Mg}_5\text{Ge}_3\text{N}_{10}$, viewed along [010]. (b) Corner- and edge-sharing $(\text{Mg}/\text{Ge})\text{N}_4$ tetrahedra building *sechser* rings. Atom types: Ca (yellow), Mg/Ge (turquoise), N (dark blue).

The crystal structure of $\text{Ca}_4\text{Mg}_5\text{Ge}_3\text{N}_{10}$ is closely related to that of $M_2\text{Si}_5\text{N}_8$ ($M = \text{Sr}, \text{Ba}$),^[38] as has previously been reported for $\text{Ca}_2\text{MgGa}_3\text{N}_5$.^[21] $M_2\text{Si}_5\text{N}_8$ crystallizes in the orthorhombic space group $Pmn2_1$ (no. 31), and its crystal structure consists of SiN_4 tetrahedra that are connected via common vertices, forming *vierer* and *sechser* ring channels, the latter of which contain alkaline earth metal ions. In contrast to $\text{Ca}_4\text{Mg}_5\text{Ge}_3\text{N}_{10}$ and $\text{Ca}_2\text{MgGa}_3\text{N}_5$, network-building SiN_4 tetrahedra in $M_2\text{Si}_5\text{N}_8$ are linked solely through vertices, and this results in a different order of *vierer* and *sechser* ring channels (see Figure 2). Additional edge sharing in the crystal structures of $\text{Ca}_4\text{Mg}_5\text{Ge}_3\text{N}_{10}$ and $\text{Ca}_2\text{MgGa}_3\text{N}_5$ leads to a higher degree of condensation (i.e., the atomic

ratio of the number of network-building ions to the number of nitrogen atoms surrounding them) compared with that of $M_2\text{Si}_5\text{N}_8$ [$\text{Ca}_4\text{Mg}_5\text{Ge}_3\text{N}_{10}$ and $\text{Ca}_2\text{MgGa}_3\text{N}_5$: $\kappa = 8:10$, $M_2\text{Si}_5\text{N}_8$: $\kappa = 5:8$]. In general, a higher degree of condensation is closely associated with an increase in the stability and rigidity of the anionic network, which is of great interest, for example, regarding application of rare earth doped nitrides of p-block elements as luminescent materials in phosphor-converted light-emitting diodes.^[2,3,17,39] Therefore, further investigations of compounds crystallizing isostructural to $\text{Ca}_4\text{Mg}_5\text{Ge}_3\text{N}_{10}$ and $\text{Ca}_2\text{MgGa}_3\text{N}_5$ are one subject of our research.

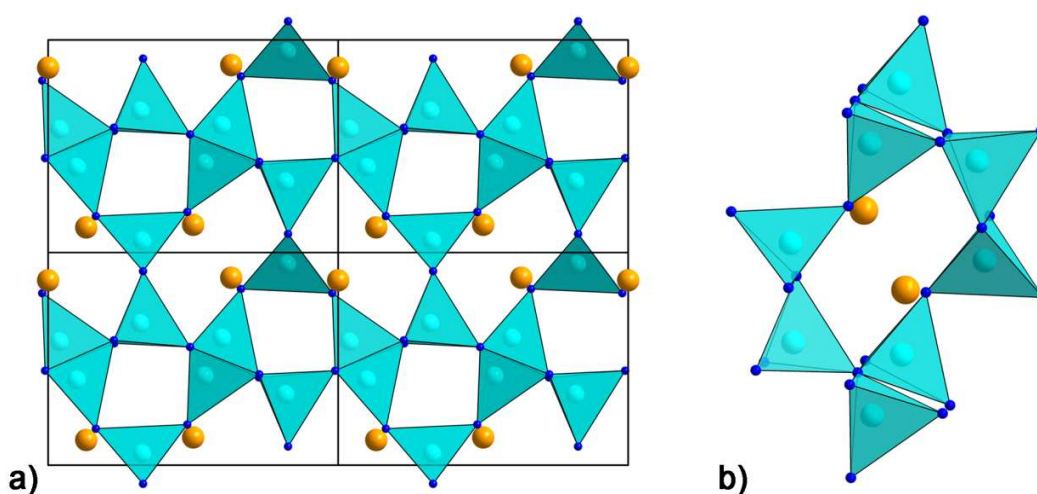


Figure 2. (a) Crystal structure of $(\text{Sr,Ba})_2\text{Si}_5\text{N}_8$ with a corrugated arrangement of *vierer* ring channels and neighboring *sechser* ring channels with different orientation of inclination. Viewing direction [100]; (b) edge-sharing SiN_4 tetrahedra building *sechser* rings. Atom types: Sr,Ba (orange), Si (turquoise), N (dark blue).

$\text{Sr}_2\text{Mg}_3\text{GaN}_{4.33}$ is homeotypic with $\text{Ca}_4\text{Mg}_5\text{Ge}_3\text{N}_{10}$, is another nitride isostructural to $\text{Ca}_2\text{MgGa}_3\text{N}_5$, and therefore also exhibits strong relations to $M_2\text{Si}_5\text{N}_8$. The crystal structure contains two crystallographically independent sites with mixed occupancy Mg/Ga. The sites Mg2/Ga2 and N2/N3 were described with split positions (see Table 2) with site occupation factors of 0.844(3)/0.156(3) and 0.35(8)/0.65(8), respectively. N4 is partially occupied; free refinement led to an occupation factor of 0.22(2). Within the standard deviations of site occupation factors [Mg: 2.97(2), Ga: 1.03(2), N: 2.2(7)], the chemical composition $\text{Sr}_2\text{Mg}_{2.97}\text{Ga}_{1.03}\text{N}_{4.2}$ resulting from single-crystal X-ray diffraction data complies with charge-balanced formula $\text{Sr}_2\text{Mg}_3\text{GaN}_{4.33}$.

2.4 $\text{Ca}_4\text{Mg}_5\text{Ge}_3\text{N}_{10}$ and $\text{Sr}_2\text{Mg}_3\text{GaN}_{4.33}$ – Two Mg-Containing Nitrides and Their Structural Relation to $(\text{Sr},\text{Ba})_2\text{Si}_5\text{N}_8$

Mg/Ga sites are tetrahedrally surrounded by four N atoms. The (Mg/Ga)–N bond lengths [1.97(3)-2.19(3) Å] correspond to the sum of the ionic radii and to those of other nitrido(magnesio)gallates.^[1,19,21,26,30,40-43] According to $\text{Ca}_4\text{Mg}_5\text{Ge}_3\text{N}_{10}$ and $\text{Ca}_2\text{MgGa}_3\text{N}_5$, the alkaline earth metal ion is located within *sechser* ring channels and sevenfold-coordinated by N. The distances Sr–N range from 2.60(1) to 2.94(6) Å, which is in good agreement with those in other Sr nitridogallates and with the calculated sum of the ionic radii.^[26,37,44,45]

Figure 3 shows the unit cell of $\text{Sr}_2\text{Mg}_3\text{GaN}_{4.33}$ with exemplary coordination spheres of the split positions Mg2/Ga2. Since the occupation factors of N4 and Ga2 are in the same range, tetrahedral coordination of Ga2 as well as trigonal (Mg2)N₃ units can be assumed.

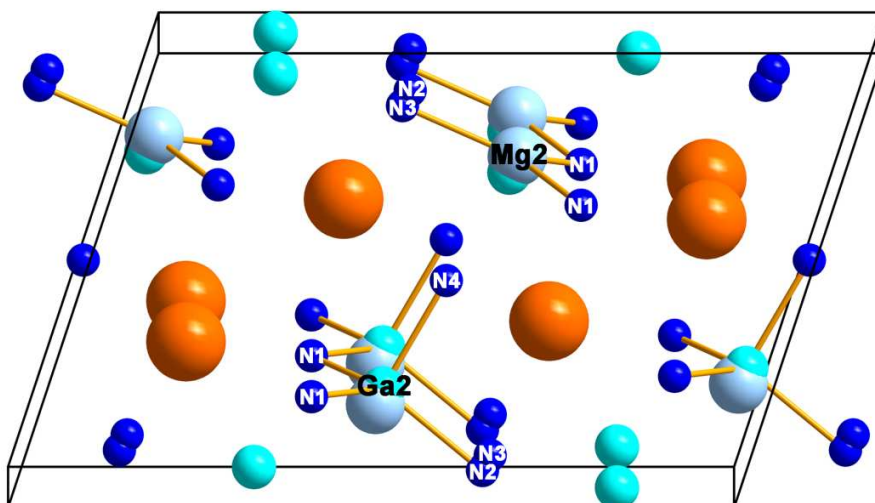


Figure 3. Perspective view of a unit cell of $\text{Sr}_2\text{Mg}_3\text{GaN}_{4.33}$. Mg2/Ga2 and N2/N3 are split positions; N4 is partially occupied. Atom types: Sr (orange), Mg (light blue), Ga and Mg/Ga (turquoise), N (dark blue).

A trigonal coordination environment of Mg ions is unusual, but has already been reported for Mg_3BN_3 .^[46] Additionally, further nitrides, namely, $\text{CaMg}_2\text{GaN}_3$ and $\text{CaMg}_2\text{Ga}_2\text{N}_4$,^[31] exhibit comparable surroundings of disordered Mg/Ga sites. In $\text{CaMg}_2\text{GaN}_3$, the coordination of one Mg/Ga site can be described as 3+2 (trigonal planar with two long distances to N atoms parallel to the *c*-axis direction). Moreover, Mg/Ga coordination spheres in $\text{CaMg}_2\text{Ga}_2\text{N}_4$ exhibit one elongated (Mg/Ga)–N bond length in (Mg/Ga)N₄ tetrahedra and can also be described as nonplanar, pyramidal (Mg/Ga)N₃ units. In accordance with $M_6\text{B}_{22}\text{O}_{39}\cdot\text{H}_2\text{O}$ (*M* = Fe, Co),^[47] these

2.4 $\text{Ca}_4\text{Mg}_5\text{Ge}_3\text{N}_{10}$ and $\text{Sr}_2\text{Mg}_3\text{GaN}_{4.33}$ – Two Mg-Containing Nitrides and Their Structural Relation to $(\text{Sr},\text{Ba})_2\text{Si}_5\text{N}_8$

units are considered to be an intermediate state between a trigonal-planar $(\text{Mg}/\text{Ga})\text{N}_3$ group and an $(\text{Mg}/\text{Ga})\text{N}_4$ tetrahedron.

Reciprocal lattice sections, reconstructed from single-crystal X-ray data, helped to further investigate the crystal structure of $\text{Sr}_2\text{Mg}_3\text{GaN}_{4.33}$. Thereby, splitting of reflections, iterating along c^* , could be observed in reciprocal lattice sections hnl ($-2 \leq n \leq 2$). This is an indication for the coexistence of two crystal structures with almost identical metrics, which might be caused by segregation of a high-temperature modification while cooling. The crystal structure presented here is therefore an average structural model of both crystal structures. Occurrence of lamellar domain structures is typical for segregation in solid-state materials. At sufficient size of these domains, the layered morphology can be visualized with the aid of electron microscopy. Figure 4 shows SEM images of rod-shaped single crystals of $\text{Sr}_2\text{Mg}_3\text{GaN}_{4.33}$. Both images clearly show the platelike assembly of single crystals, which corroborates previous assumptions.

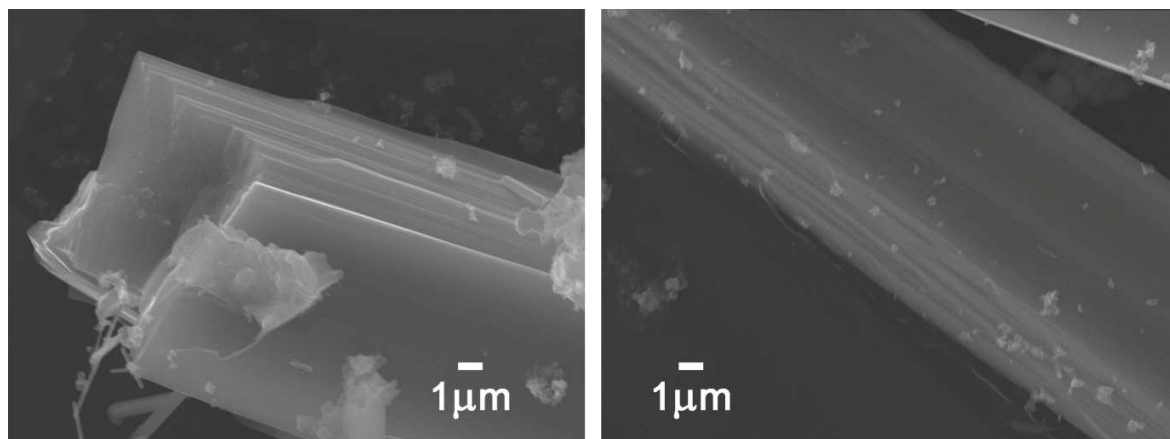


Figure 4. SEM images of rod-shaped single crystals of $\text{Sr}_2\text{Mg}_3\text{GaN}_{4.33}$.

Up to now, there are only two examples of isotypic nitridogallates with equal sum formulas known in the literature, namely, $\text{Sr}_3\text{Ga}_2\text{N}_4$ [26] and $\text{Ba}_3\text{Ga}_2\text{N}_4$ [42] as well as $\text{Sr}[\text{Mg}_2\text{Ga}_2\text{N}_4]$ [19] and $\text{Ba}[\text{Mg}_2\text{Ga}_2\text{N}_4]$. [1] The crystal structures of corresponding Ca analogues are rather different. [26,31,40] Conversely, it can be stated that Sr and Ba compounds isotypic with known Ca nitridogallates are lacking. This may be explained by differences in the ionic radii of alkaline earth metal ions, which act as counterions and therefore stabilize the anionic network. With regard to $\text{Ca}_2\text{MgGa}_3\text{N}_5$ and structurally related $\text{Sr}_2\text{Mg}_3\text{GaN}_{4.33}$, an exchange of Ca^{2+} by Sr^{2+} simultaneously requires an expansion of the anionic network. As observed in $\text{Sr}_2\text{Mg}_3\text{GaN}_{4.33}$, this

2.4 $\text{Ca}_4\text{Mg}_5\text{Ge}_3\text{N}_{10}$ and $\text{Sr}_2\text{Mg}_3\text{GaN}_{4.33}$ –

Two Mg-Containing Nitrides and Their Structural Relation to $(\text{Sr},\text{Ba})_2\text{Si}_5\text{N}_8$

can be realized by inversion of the atomic ratio Mg/Ga (ionic radii of fourfold-coordinated ions $\text{Mg}^{2+}/\text{Ga}^{3+}$: 0.64/0.48 Å).^[37] However, due to different charges of the ions ($\text{Mg}^{2+}/\text{Ga}^{3+}$) and in order to maintain electroneutrality, this inversion must be accompanied by modifications in the anionic network.

However, a similar phenomenon is also known from nitridogermanates. Since the ionic radii of Ca^{2+} and Ba^{2+} are rather different, there are no examples of isotypic Ca- and Ba-containing nitridogermanates. Depending on the anionic network, Sr^{2+} can be isotypic with its corresponding Ca analogue or Ba analogue, respectively, as has been observed for Ca_7GeN_6 and Sr_7GeN_6 as well as for the isotypic compounds $\text{Sr}_3\text{Ge}_2\text{N}_2$ and $\text{Ba}_3\text{Ge}_2\text{N}_2$.^[28,48,49]

Table 2. Atomic coordinates and equivalent isotropic displacement parameters $/\text{\AA}^2$ of $\text{Ca}_4\text{Mg}_5\text{Ge}_3\text{N}_{10}$ and $\text{Sr}_2\text{Mg}_3\text{GaN}_{4.33}$.

$\text{Ca}_4\text{Mg}_5\text{Ge}_3\text{N}_{10}$						
Atom	Wyck.	x	y	z	U_{eq}	s.o.f.
Ca1	4 <i>i</i>	0.16409(14)	0	0.6256(2)	0.0090(4)	1
Mg1/Ge1	4 <i>i</i>	0.53857(12)	0	0.2799(2)	0.0143(4)	½ / ½
Mg2/Ge2	4 <i>i</i>	0.16711(17)	0	0.0454(2)	0.0127(4)	¾ / ¼
N1	4 <i>i</i>	0.3650(7)	0	0.1065(11)	0.0258(18)	1
N2	2 <i>d</i>	0	½	½	0.0115(18)	1
N3	4 <i>i</i>	0.1440(7)	0	0.2861(10)	0.0192(15)	1
$\text{Sr}_2\text{Mg}_3\text{GaN}_{4.33}$						
Atom	Wyck.	x	y	z	U_{eq}	s.o.f.
Sr1	4 <i>i</i>	0.16929(6)	0	0.63436(9)	0.0093(2)	1
Mg1/Ga1	4 <i>i</i>	0.17047(12)	0	0.0445(2)	0.0090(4)	0.641(6)/0.359(6)
Mg2 ^a	4 <i>i</i>	0.5411(3)	0	0.2271(6)	0.0083(7)	0.844(6)
Ga2 ^a	4 <i>i</i>	0.5376(6)	0	0.2625(10)	0.0083(7)	0.156(6)
N1	4 <i>i</i>	0.1420(5)	0	0.2893(8)	0.0123(11)	1
N2 ^a	4 <i>i</i>	0.364(2)	0	0.082(9)	0.114(17)	0.35(16)
N3 ^a	4 <i>i</i>	0.3598(13)	0	0.115(5)	0.114(17)	0.65(16)
N4	2 <i>d</i>	0	½	½	0.0123(11)	0.22(2)

^a Split positions

2.4 $\text{Ca}_4\text{Mg}_5\text{Ge}_3\text{N}_{10}$ and $\text{Sr}_2\text{Mg}_3\text{GaN}_{4.33}$ –
Two Mg-Containing Nitrides and Their Structural Relation to $(\text{Sr},\text{Ba})_2\text{Si}_5\text{N}_8$

Table 3. Selected bond lengths in the crystal structures of $\text{Ca}_4\text{Mg}_5\text{Ge}_3\text{N}_{10}$ and $\text{Sr}_2\text{Mg}_3\text{GaN}_{4.33}$. Standard deviations are given in parantheses.

$\text{Ca}_4\text{Mg}_5\text{Ge}_3\text{N}_{10}$			
Ca1–N1 (2x)	2.820(7)	Mg1/Ge1–N2	1.954(2)
Ca1–N2 (2x)	2.437(1)	Mg1/Ge1–N3 (2x)	2.035(4)
Ca1–N3 (2x)	2.628(6)	Mg2/Ge2–N1 (2x)	2.020(5)
Ca1–N3	2.650(8)	Mg2/Ge2–N1	2.115(8)
Mg1/Ge1–N1	1.978(8)	Mg2/Ge2–N3	2.031(7)
$\text{Sr}_2\text{Mg}_3\text{GaN}_{4.33}$			
Sr1–N1 (2x)	2.727(5)	Mg1/Ga1–N2,N3	2.19(3), 2.12(2)
Sr1–N1	2.631(6)	Mg2–N1 (2x)	2.068(4)
Sr1–N2,N3 (2x)	2.94(6), 2.72(3)	Mg2–N2,N3	2.10(3), 2.04(1)
Sr2–N4 (2x)	2.560(1)	Ga2–N1 (2x)	2.093(5)
Mg1/Ga1–N1	2.053(6)	Ga2–N2,N3	2.10(3), 2.05(1)
Mg1/Ga1–N2,N3 (2x)	1.97(3), 2.10(2)	Ga2–N4	2.048(8)

2.4.3 Conclusions

$\text{Ca}_4\text{Mg}_5\text{Ge}_3\text{N}_{10}$ and $\text{Sr}_2\text{Mg}_3\text{GaN}_{4.33}$ are new Mg-containing nitrides with a three-periodic anionic network. By employing the Na azide synthesis route, single crystals of the title compounds could be obtained and isolated. Both nitrides are homeotypic to $\text{Ca}_2\text{MgGa}_3\text{N}_5$ and show structural similarities to $M_2\text{Si}_5\text{N}_8$ ($M = \text{Sr}, \text{Ba}$). The anionic network consists of corner- and edge-sharing tetrahedra with Mg/Ga or Mg/Ge mixed occupation on tetrahedral sites. The tetrahedra build *vierer* and *sechser* rings, which are stacked along [010], forming channels. Alkaline earth metal ions are located inside the channels of *sechser* rings; *vierer* ring channels are not filled. In $\text{Sr}_2\text{Mg}_3\text{GaN}_{4.33}$, one tetrahedra site with mixed occupancy Mg/Ga was described with a split position. Additionally, one nitrogen atom position is also split and another N site is partially occupied. SEM images, which show a platelike assembly of single crystals of $\text{Sr}_2\text{Mg}_3\text{GaN}_{4.33}$, and investigations of reciprocal lattice sections, suggest the coexistence of two crystal structures with almost identical metrics. Additional studies with the aid of electron diffraction would lead to more detailed information about the crystal structure and its domains. Tempering of the reaction product containing $\text{Sr}_2\text{Mg}_3\text{GaN}_{4.33}$ and high cooling rates during synthesis are two possibilities to

2.4 $\text{Ca}_4\text{Mg}_5\text{Ge}_3\text{N}_{10}$ and $\text{Sr}_2\text{Mg}_3\text{GaN}_{4.33}$ – Two Mg-Containing Nitrides and Their Structural Relation to $(\text{Sr,Ba})_2\text{Si}_5\text{N}_8$

avoid segregation. First experiments regarding these considerations led to average structure models as described here. However, since $\text{Ca}_4\text{Mg}_5\text{Ge}_3\text{N}_{10}$ and $\text{Sr}_2\text{Mg}_3\text{GaN}_{4.33}$ can be viewed as more highly condensed variants of the $M_2\text{Si}_5\text{N}_8$ structure, the title compounds illustrate the strong relationship between nitridogermanates, nitridogallates and nitridosilicates. The higher degree of condensation is possibly caused by incorporation of additional Mg atoms in the tetrahedral network, which modifies the charge and covalency of the anionic substructure. Since nitridosilicates are known as highly efficient luminescent materials when doped with Eu^{2+} and due to their strong relationship to nitrido(magnesio)germanates and –gallates, the latter are interesting candidates as host lattices for Eu^{2+} doping. Recently investigated $\text{Ba}_3\text{Ga}_3\text{N}_5\text{:Eu}^{2+}$ as well as $\text{Ba}[\text{Mg}_2\text{Ga}_2\text{N}_4]\text{:Eu}^{2+}$ demonstrate the potential as luminescent materials.

2.4.4 Experimental Section

2.4.4.1 General

To avoid oxidation and hydrolysis of starting materials and products, all manipulations were done under inert-gas conditions by using a combined Schlenk/vacuum line and an argon-filled glove box (Unilab, MBraun, Garching; $\text{O}_2 < 1$ ppm, $\text{H}_2\text{O} < 1$ ppm). Ar was dried and purified by passage through glass tubes filled with silica gel (Merck), molecular sieves (Fluka, 4 Å), KOH (Merck, $\geq 85\%$), P_4O_{10} (Roth, $\geq 99\%$), and titanium sponge (Johnsen Matthey, 99.5%). Under Ar, arc-welded Ta ampules (length 30 mm, diameter 10 mm, wall thickness 0.5 mm) were used as reaction containers. Two at a time were transferred into a silica tube and heated under vacuum.

2.4.4.2 Synthesis of $\text{Ca}_4\text{Mg}_5\text{Ge}_3\text{N}_{10}$

Single crystals of $\text{Ca}_4\text{Mg}_5\text{Ge}_3\text{N}_{10}$ were obtained by reaction of NaN_3 (0.46 mmol, 29.9 mg, Acros, 99%), Ca (0.80 mmol, 32.1 mg, Sigma-Aldrich, 99.99%), Mg (0.79 mmol, 19.3 mg, Alfa Aesar, 99.9%), Ge (0.40 mmol, 29.1 mg, Sigma-Aldrich, 99.99%) and EuF_3 ($1.63 \cdot 10^{-2}$ mmol, 3.4 mg, Sigma-Aldrich, 99.99%) in Na flux (2.21 mmol, 50.7 mg, Sigma-Aldrich, 99.95%). The starting materials were heated to 780 °C at a rate of 50 °C · h⁻¹, maintained at that temperature for 48 h, and subsequently cooled to 500 °C at a rate of 3 °C · h⁻¹. Subsequently, the reaction mixture was quenched to room temperature and the Ta ampule was opened in a glove box. Excess of the Na flux was removed by sublimation at 320 °C under vacuum.

2.4.4.3 Synthesis of $\text{Sr}_2\text{Mg}_3\text{GaN}_{4.33}$

$\text{Sr}_2\text{Mg}_3\text{GaN}_{4.33}$ was synthesized by heating a mixture of NaN_3 (0.46 mmol, 29.9 mg, Acros, 99%), Sr (0.55 mmol, 48.4 mg, Sigma-Aldrich, 99.99%), Mg (0.28 mmol, 6.7 mg, Alfa Aesar, 99.9%), and Ga (0.14 mmol, 9.6 mg, Alusuisse, 99.999%) in Na flux (1.96 mmol, 45.0 mg, Sigma-Aldrich, 99.95%) at a rate of $50\text{ }^\circ\text{C}\cdot\text{h}^{-1}$ to $760\text{ }^\circ\text{C}$. The temperature was maintained for 48 h before cooling to $200\text{ }^\circ\text{C}$ at a rate of $3.4\text{ }^\circ\text{C}\cdot\text{h}^{-1}$. After quenching to room temperature and opening the Ta ampule in a glove box, the Na melt was removed by sublimation at $320\text{ }^\circ\text{C}$ under vacuum.

2.4.4.4 Single-Crystal X-ray Diffraction

Single crystals of $\text{Ca}_4\text{Mg}_5\text{Ge}_3\text{N}_{10}$ and $\text{Sr}_2\text{Mg}_3\text{GaN}_{4.33}$ were isolated from the respective products, washed with dry paraffin oil, and enclosed in glass capillaries. To prevent hydrolysis of single crystals, the glass capillaries were sealed under argon. Single-crystal X-ray diffraction data were collected with a Bruker D8 Quest diffractometer (PHOTON 199 CMOS detector, $\text{Mo-}K_\alpha$ radiation). Absorption effects were corrected by using the multiscan method (SADABS).^[50] The structures were solved by direct methods in SHELXS-97, structure refinements were carried out by full-matrix least-squares calculation on $|F|^2$ in SHELXL-97.^[51]

Further details of the crystal structure investigations may be obtained from the Fachinformationszentrum Karlsruhe, 76344 Eggenstein-Leopoldshafen, Germany (Fax: +49-7247-808-666; E-Mail: crysdata@fiz-karlsruhe.de) on quoting the depository numbers CSD-432308 (for $\text{Ca}_4\text{Mg}_5\text{Ge}_3\text{N}_{10}$) and CSD-432309 (for $\text{Sr}_2\text{Mg}_3\text{GaN}_{4.33}$).

2.4.5 References

- [1] P. Pust, F. Hintze, C. Hecht, V. Weiler, A. Locher, D. Zitnanska, S. Harm, D. Wiechert, P. J. Schmidt, W. Schnick, *Chem. Mater.* **2014**, 26, 6113.
- [2] P. Pust, V. Weiler, C. Hecht, A. Tücks, A. S. Wochnik, A.-K. Henß, D. Wiechert, C. Scheu, P. J. Schmidt, W. Schnick, *Nat. Mater.* **2014**, 13, 891.
- [3] P. Pust, A. S. Wochnik, E. Baumann, P. J. Schmidt, D. Wiechert, C. Scheu, W. Schnick, *Chem. Mater.* **2014**, 26, 3544.
- [4] H. Yamane, S. Kikkawa, M. Koizumi, *Solid State Ionics* **1987**, 25, 183.
- [5] K. Kim, W. R. L. Lambrecht, B. Segall, *Phys. Rev. B: Condens. Matter* **1996**, 53, 16310.
- [6] H. Lange, G. Wötting, G. Winter, *Angew. Chem. Int. Ed. Engl.* **1991**, 30, 1579; *Angew. Chem.* **1991**, 103, 1606.
- [7] W. Schnick, *Angew. Chem. Int. Ed. Engl.* **1993**, 32, 806; *Angew. Chem.* **1993**, 105, 846.
- [8] A. Ziegler, J. C. Idrobo, M. K. Cinibulk, C. Kisielowski, N. D. Browning, R. O. Ritchie, *Science* **2004**, 306, 1768.
- [9] R. J. Bruls, Doctoral Thesis, Eindhoven University of Technology, **2000**.
- [10] G. A. Slack, R. A. Tanzilli, R. O. Pohl, J. W. Vandersande, *J. Phys. Chem. Solids* **1987**, 48, 641.
- [11] M. P. Borom, G. A. Slack, J. W. Szymaszek, *Am. Ceram. Soc. Bull.* **1972**, 51, 852.
- [12] K. H. Jack, *J. Mater. Sci.* **1976**, 11, 1135.
- [13] W. Schnick, *Phys. Status Solidi RRL* **2009**, 3, A113.
- [14] R. Juza, H. H. Weber, E. Meyer-Simon, *Z. Anorg. Allg. Chem.* **1953**, 273, 48.
- [15] H. Yamane, S. Kikkawa, M. Koizumi, *J. Power Sources* **1987**, 20, 311.
- [16] S. Schmiechen, H. Schneider, P. Wagatha, C. Hecht, P. J. Schmidt, W. Schnick, *Chem. Mater.* **2014**, 26, 2712.
- [17] S. Schmiechen, P. Strobel, C. Hecht, T. Reith, M. Siegert, P. J. Schmidt, P. Huppertz, D. Wiechert, W. Schnick, *Chem. Mater.* **2015**, 27, 1780.
- [18] D. G. Park, Z. A. Gál, F. J. DiSalvo, *J. Alloys Compd.* **2003**, 360, 85.
- [19] D. G. Park, Y. Dong, F. J. DiSalvo, *Solid State Sci.* **2008**, 10, 1846.
- [20] D. G. Park, F. J. DiSalvo, *Bull. Korean Chem. Soc.* **2011**, 32, 353.
- [21] F. Hintze, W. Schnick, *Z. Anorg. Allg. Chem.* **2012**, 638, 2243.
- [22] C. Poesl, W. Schnick, *Z. Anorg. Allg. Chem.* **2016**, 642, 882.
- [23] D. G. Park, Z. A. Gál, F. J. DiSalvo, *J. Alloys Compd.* **2003**, 353, 107.
- [24] D. G. Park, F. J. DiSalvo, *Bull. Korean Chem. Soc.* **2012**, 33, 1759.

2.4 $\text{Ca}_4\text{Mg}_5\text{Ge}_3\text{N}_{10}$ and $\text{Sr}_2\text{Mg}_3\text{GaN}_{4.33}$ –
Two Mg-Containing Nitrides and Their Structural Relation to $(\text{Sr},\text{Ba})_2\text{Si}_5\text{N}_8$

- [25] O. Boudrifa, A. Bouhemadou, N. Guechi, S. Bin-Omran, Y. Al-Douri, R. Khenata, *J. Alloys Compd.* **2015**, 618, 84.
- [26] S. J. Clarke, F. J. DiSalvo, *Inorg. Chem.* **1997**, 36, 1143.
- [27] S. J. Clarke, F. J. DiSalvo, *Inorg. Chem.* **2000**, 39, 2631.
- [28] S. C. Junggeburth, O. Oeckler, D. Johrendt, W. Schnick, *Inorg. Chem.* **2008**, 47, 12018.
- [29] D. G. Park, D. J. DiSalvo, *Bull. Korean Chem. Soc.* **2008**, 29, 2413.
- [30] F. Hintze, F. Hummel, P. J. Schmidt, D. Wiechert, W. Schnick, *Chem. Mater.* **2012**, 24, 402.
- [31] C. Poesl, L. Neudert, W. Schnick, *Eur. J. Inorg. Chem.* **2017**, 1067.
- [32] V. Schultz-Coulon, W. Schnick, *Z. Naturforsch. B* **1995**, 50, 619.
- [33] O. Reckeweg, F. J. DiSalvo, *Z. Anorg. Allg. Chem.* **2001**, 627, 371.
- [34] S. C. Junggeburth, O. Oeckler, W. Schnick, *Z. Anorg. Allg. Chem.* **2008**, 634, 1309.
- [35] D. G. Park, Z. A. Gál, F. J. DiSalvo, *J. Solid State Chem.* **2003**, 172, 166.
- [36] F. Liebau, *Structural Chemistry of Silicates*, Springer, Berlin, **1985** (the terms *vierer* ring and *sechser* ring was coined by Liebau and is derived from the German words *vier* = four and *sechs* = six. A *vierer* ring comprises four tetrahedra).
- [37] W. H. Baur, *Crystallogr. Rev.* **1987**, 1, 59.
- [38] T. Schlieper, W. Schnick, *Z. Anorg. Allg. Chem.* **1995**, 621, 1037.
- [39] J. Brgoch, S. P. DenBaars, R. Seshadri, *J. Phys. Chem. C* **2013**, 117, 17955.
- [40] S. J. Clarke, F. J. DiSalvo, *J. Alloys Compd.* **1998**, 274, 118.
- [41] F. Hintze, N. W. Johnson, M. Seibald, D. Muir, A. Moewes, W. Schnick, *Chem. Mater.* **2013**, 25, 4044.
- [42] H. Yamane, F. J. DiSalvo, *Acta Crystallogr., Sect. C: Cryst. Struct. Commun.* **1996**, 52, 760.
- [43] R. Juza, F. Hund, *Z. Anorg. Allg. Chem.* **1948**, 257, 13.
- [44] P. M. Mallinson, Z. A. Gál, S. J. Clarke, *Inorg. Chem.* **2006**, 45, 419.
- [45] D. G. Park, Z. A. Gál, F. J. DiSalvo, *Inorg. Chem.* **2003**, 42, 1779.
- [46] H. Hiraguchi, H. Hashizume, O. Fukunaga, A. Takenaka, M. Sakata, *J. Appl. Crystallogr.* **1991**, 24, 286.
- [47] S. C. Neumair, J. S. Knyrim, O. Oeckler, R. Glaum, R. Kaindl, R. Stalder, H. Huppertz, *Chem. Eur. J.* **2010**, 16, 13659.
- [48] S. J. Clarke, G. R. Kowach, F. J. DiSalvo, *Inorg. Chem.* **1996**, 35, 7009.
- [49] H. Yamane, F. J. DiSalvo, *J. Alloys Compd.* **1996**, 241, 69.

2.4 $\text{Ca}_4\text{Mg}_5\text{Ge}_3\text{N}_{10}$ and $\text{Sr}_2\text{Mg}_3\text{GaN}_{4.33}$ –

Two Mg-Containing Nitrides and Their Structural Relation to $(\text{Sr},\text{Ba})_2\text{Si}_5\text{N}_8$

- [50] G. M. Sheldrick, *SADABS*, Multi-Scan Absorption Correction, v.2, Bruker-AXS, Madison, WI, USA, **2012**.
- [51] G. M. Sheldrick, *Acta Crystallogr., Sect. A: Found. Crystallogr.* **2008**, 64, 112.

2.5 The Crystal Structure of Nitridomagnesogermanate $\text{Ba}[\text{Mg}_3\text{GeN}_4]:\text{Eu}^{2+}$ and Theoretical Calculations of Its Electronic Properties

published in: *Eur. J. Inorg. Chem.* **2017**, 2422-2427

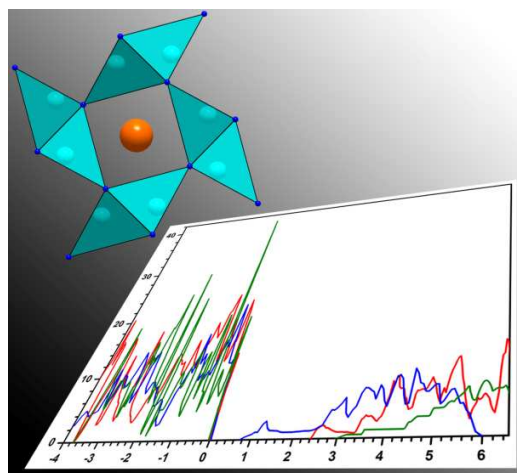
authors: Christine Poesl, Robin Niklaus, and Wolfgang Schnick

DOI: 10.1002/ejic.201700096

Copyright © 2017 Wiley-VCH Verlag GmbH & Co. KGaA, Weinheim

<http://onlinelibrary.wiley.com/doi/10.1002/ejic.201700096/abstract>

Abstract: Nitridomagnesogermanate $\text{Ba}[\text{Mg}_3\text{GeN}_4]:\text{Eu}^{2+}$ was synthesized by the NaN_3 route in weld-shut tantalum ampules by reaction of the elements in molten sodium with NaN_3 as nitrogen source at 780 °C. The crystal structure was solved and refined on the basis of single-crystal X-ray diffraction data. $\text{Ba}[\text{Mg}_3\text{GeN}_4]:\text{Eu}^{2+}$ crystallizes in the UCr_4C_4 structure type [space group $I4/m$ (no. 87), $a = 8.3921(12)$, $c = 3.4813(7)$ Å, $Z = 2$] and exhibits a highly condensed anionic network made up of statistically disordered (Mg/Ge) N_4 tetrahedra, which are connected to each



other by common vertices and edges to form *vierer* ring channels along [001]. Ba^{2+} is located in every second channel and has cubelike coordination by eight N atoms. Theoretical calculations of the electronic properties of $\text{Ba}[\text{Mg}_3\text{GeN}_4]:\text{Eu}^{2+}$ are discussed to understand the absence of photoluminescence in the visible range and for comparison with other luminescent materials that are structurally related to $\text{Ba}[\text{Mg}_3\text{GeN}_4]:\text{Eu}^{2+}$.

2.5.1 Introduction

Nitrides have gained significant importance during the last decades, since they are suitable for a variety of technological applications, such as nonlinear optical materials, lithium solid electrolytes, and efficient luminescent materials for phosphor-converted light-emitting diodes (pc-LEDs).^[1-14] Due to the sensitivity of nitride compounds towards hydrolysis, their synthesis and characterization are challenging. Recently, a number of new ternary or higher nitrides have been synthesized via different synthetic routes, for example, solid-state reactions, flux methods, precursor routes, and ammonothermal syntheses.^[15,16] Despite these differing synthetic approaches, nitridogermanates have been exclusively synthesized by employing the NaN₃ route starting from the pure elements in sodium flux with NaN₃ as nitrogen source. Minor variations of the syntheses have been reported, for example, by substituting Ge metal through GeO₂, or addition of small amounts of Li to facilitate crystal growth.^[17-22] Nevertheless, the class of nitridogermanates is quite unexplored, and only a small number of compounds has been described so far.

Almost all nitridogermanates contain Ge with oxidation state +IV and alkaline earth metal ions. Alkaline earth metals are supposed to enhance solubility of nitrogen in the flux. Most common structural motifs are GeN₄ tetrahedra and trigonal-planar GeN₃ units, forming more or less condensed nitridometallate anions surrounded by electropositive alkaline earth metal ions. Besides, Ge may also occur in oxidation states –IV (no coordination to nitrogen),^[23,24] –II (Zintl anions $\infty^1[\text{Ge}]^{2-}$)^[25-27] and +II (dumbbell shaped anions $[\text{GeN}_2]^{4-}$).^[25,26,28]

Yet, only four Mg-containing nitridogermanates have been reported: $M_3[\text{MgGeN}_4]$ with $M = \text{Sr}, \text{Ba}$,^[18,29] $\text{Ca}_2[\text{Mg}_5\text{GeN}_6]$,^[19] and $\text{Sr}[\text{Mg}_3\text{GeN}_4]$.^[17] Since Mg and Ge are both part of the tetrahedral network, the compounds can be more accurately classified as nitridomagnesogermanates. $\text{Sr}[\text{Mg}_3\text{GeN}_4]$ crystallizes in the UCr_4C_4 structure type^[30] and exhibits a three-periodic anionic network of vertex- and edge-sharing (Mg/Ge)N₄ tetrahedra resulting in a highly symmetrical coordination of Sr²⁺ by N. Furthermore, some other nitrides are isostructural with UCr_4C_4 , namely, $M[\text{Mg}_2\text{Ga}_2\text{N}_4]$ ($M = \text{Sr}, \text{Ba}$), $M[\text{Mg}_2\text{Al}_2\text{N}_4]$,^[31] $M[\text{Mg}_3\text{SiN}_4]$ ($M = \text{Ca}, \text{Sr}, \text{Ba}$),^[32-33] and $M[\text{LiAl}_3\text{N}_4]$ ($M = \text{Ca}, \text{Sr}$).^[1,34] All of these compounds, except for $\text{Sr}[\text{Mg}_2\text{Ga}_2\text{N}_4]$, show red emission with rather narrow bandwidths on doping with Eu²⁺ and after irradiation with UV-to-green light.^[1,31-34]

2.5 The Crystal Structure of Nitridomagnesogermanate Ba[Mg₃GeN₄]:Eu²⁺ and Theoretical Calculations of Its Electronic Properties

Herein, we report on the synthesis and structural elucidation of Ba[Mg₃GeN₄]:Eu²⁺, a new nitridomagnesogermanate with UCr₄C₄ structure type. Since Ba[Mg₃GeN₄]:Eu²⁺ does not show luminescence within the range of visible light after irradiation with UV-to-green light, theoretical calculations of electronic properties were performed. These findings, as well as the coherences and differences with regard to the aforementioned Eu²⁺-doped compounds crystallizing isostructural to UCr₄C₄, are discussed in detail.

2.5.2 Results and Discussion

2.5.2.1 Synthesis

Ba[Mg₃GeN₄]:Eu²⁺ was synthesized by solid-state reaction at 780 °C with molten sodium as flux, NaN₃ as nitrogen source, and EuF₃ as dopant. In the absence of EuF₃ as starting material, formation of undoped Ba[Mg₃GeN₄] was not observed. Synthesis yielded a heterogeneous product mixture, from which the title compound was isolated in the form of stretched double-pyramids with orange body color. Due to sensitivity to air and moisture, decomposition of Ba[Mg₃GeN₄]:Eu²⁺ starts immediately when it is exposed to air. Energy-dispersive X-ray spectroscopy (EDX) was used to investigate elemental composition. This resulted in a Ba/Mg/Ge atomic ratio of 8/30/8, which is in fair agreement with the sum formula determined from single-crystal structure analysis. Due to the method, accurate determination of light elements such as N next to heavier elements is not possible. As the concentration of Eu²⁺ in Ba[Mg₃GeN₄]:Eu²⁺ is quite low, it could not be detected with certainty by EDX analysis. Since EuF₃ seems to be essential for successful synthesis of Ba[Mg₃GeN₄]:Eu²⁺ and obtained crystals show an orange body color, we assume incorporation of Eu²⁺ in its crystal structure.

2.5.2.2 Single-Crystal Structure Analysis

The structure of Ba[Mg₃GeN₄]:Eu²⁺ was solved and refined in tetragonal space group *I4/m* (no. 87) with *a* = 8.3921(12) and *c* = 3.4813(7) Å. Eu²⁺ was neglected during structure refinement because of its low concentration and its insignificant contribution to scattering intensity. Crystallographic data and further details of the structure determination are listed in Table 1. The site occupation factor was refined by assuming full occupancy of Mg1/Ge1 site and led to Mg/Ge = 0.759(6)/0.241(6). According to electroneutrality, the occupancy was fixed at

2.5 The Crystal Structure of Nitridomagnesogermanate Ba[Mg₃GeN₄]:Eu²⁺ and Theoretical Calculations of Its Electronic Properties

$\frac{3}{4}/\frac{1}{4}$. All atoms were refined anisotropically. Table 2 lists atomic coordinates and isotropic displacement parameters. Selected bond lengths and angles in the crystal structure of Ba[Mg₃GeN₄]:Eu²⁺ are listed in Table 3. Rietveld refinement based on powder X-ray diffraction data of finely ground single crystals of Ba[Mg₃GeN₄]:Eu²⁺ is shown in the Supporting Information. It confirmed the results of the single-crystal structure analysis.

Table 1. Crystallographic data of Ba[Mg₃GeN₄]:Eu²⁺.

Formula	Ba[Mg ₃ GeN ₄]:Eu ²⁺
Crystal system	tetragonal
Space group	<i>I</i> 4/ <i>m</i> (no. 87)
Lattice parameter /Å	<i>a</i> = 8.3921(12) <i>c</i> = 3.4813(7)
Cell volume /Å ³	245.18(9)
Formula units per unit cell	2
Density /g·cm ⁻³	4.591
μ /mm ⁻¹	14.360
T /K	293(2)
Diffractometer	Bruker D8 Quest
Radiation	Mo-K α (λ = 0.71073 Å)
<i>F</i> (000)	304
θ range /°	3.433 $\leq \theta \leq$ 28.480
Total reflections	1076
Independent reflections	180
Refined parameters	15
Goodness of fit	1.330
<i>R</i> ₁ (all data) / <i>R</i> ₁ [<i>F</i> ² > 2σ(<i>F</i> ²)]	0.0215 / 0.0201
<i>wR</i> ₂ (all data) / <i>wR</i> ₂ [<i>F</i> ² > 2σ(<i>F</i> ²)]	0.0456 / 0.0451
$\Delta\rho_{\min}/\Delta\rho_{\max}$ / e·Å ³	-0.468/0.825

2.5 The Crystal Structure of Nitridomagnesogermanate Ba[Mg₃GeN₄]:Eu²⁺ and Theoretical Calculations of Its Electronic Properties

Table 2. Atomic coordinates and equivalent isotropic displacement parameters /Å² of Ba[Mg₃GeN₄]:Eu²⁺, standard deviations in parentheses.

Atom	Wyckoff	<i>x</i>	<i>y</i>	<i>z</i>	<i>U</i> _{eq}	<i>s.o.f.</i>
Ba1	2 <i>a</i>	0	0	0	0.0142(2)	1
Mg1/Ge1	8 <i>h</i>	0.18582(13)	0.36290(12)	0	0.0144(3)	3/4/1/4
N1	8 <i>h</i>	0.4007(5)	0.2338(6)	0	0.0221(10)	1

Table 3. Selected bond lengths and angles in the crystal structure of Ba[Mg₃GeN₄]:Eu²⁺, standard deviations in parentheses.

Bond length /Å		Bond angle /°	
Ba1–N1	2.952(4) (8x)	N1–Ba1–N1	110.35(6)
Mg1/Ge1–N1	2.024(4)	N1–Ba1–N1	69.65(6)
Mg1/Ge1–N1	2.053(3) (2x)	N1–Ba1–N1	180
Mg1/Ge1–N1	2.104(4)	N1–Ba1–N1	107.73(12)
		N1–Ba1–N1	72.27(12)
		N1–Mg1/Ge1–N1	117.3(1)
		N1–Mg1/Ge1–N1	115.9(3)
		N1–Mg1/Ge1–N1	109.5(3)
		N1–Mg1/Ge1–N1	95.7(1)

2.5.2.3 Crystal-Structure Description

Ba[Mg₃GeN₄]:Eu²⁺ crystallizes in the UCr₄C₄ structure type^[30] and is isotypic with Sr[Mg₃GeN₄] and homeotypic with *M*[Mg₂Al₂N₄] (*M* = Ca, Sr, Ba, Eu) and *M*[Mg₂Ga₂N₄] (*M* = Sr, Ba).^[17,31] It consists of a highly condensed anionic network of (Mg/Ge)N₄ tetrahedra with a degree of condensation (i.e. the (Mg/Ge)/N atomic ratio) of $\kappa = 1$. As shown in Figure 1, (Mg/Ge)N₄ tetrahedra are linked through edges to form strands along *c*. These strands are connected through corners to one another, resulting in *vierer* ring^[35] channels along [001]. Ba²⁺ ions are located in every second channel and have cubelike coordination by N (Figure 2b). The Ba–N bond length is 2.952(4) Å, which corresponds to the sum of the ionic radii and to the distances in

2.5 The Crystal Structure of Nitridomagnesogermanate Ba[Mg₃GeN₄]:Eu²⁺ and Theoretical Calculations of Its Electronic Properties

other Ba-containing nitrides.^[18,31,33,36] The central Mg²⁺ and Ge⁴⁺ ions of the tetrahedra are statistically disordered. Figure 2a shows tetrahedral coordination of the Mg/Ge site. Since Mg²⁺ and Ge⁴⁺ are both part of the tetrahedral network, the compound can be classified as a nitridomagnesogermanate.^[37] The (Mg/Ge)–N distances range from 2.024(4) to 2.104(4) Å, and correspond to averaged Mg–N and Ge–N bond lengths of other nitrides and to the calculated sum of the ionic radii according to Baur (Ge⁴⁺ 0.41; Mg²⁺ 0.64; N^{3–} 1.46 Å).^[18,28,36,38,39] The N–Mg/Ge–N bond angles in (Mg/Ge)N₄ tetrahedra range from 95.7(1) to 117.3(1)°. Similar distortions of tetrahedra can be found in Sr[Mg₃GeN₄] (97–119°), (Sr,Ba)₃MgGeN₄ (90–119°), or CaMg₂Ga₂N₄ (99–118°),^[40] and may be due to strong interactions resulting from edge sharing of neighboring tetrahedra. Mixed Mg/Ge occupancy of tetrahedral sites also appears in Sr[Mg₃GeN₄] and Ca₂[Mg₅GeN₆].^[17,19] The (Mg/Ge)–N bond lengths vary between 1.990(6) and 2.057(6) Å in Sr[Mg₃GeN₄] and 1.994(1) and 2.110(3) Å in Ca₂[Mg₅GeN₆] and resemble the (Mg/Ge)–N bond lengths in Ba[Mg₃GeN₄]:Eu²⁺.

Table 4 gives an overview of nitrides with structural features identical to those of UCr₄C₄, including Na[Li₃SiO₄] and Cs[Na₃PbO₄] structure types, which resemble the UCr₄C₄ structure type quite closely.^[1,17,31–34] M[Mg₃SiN₄] and M[LiAl₃N₄] (M = Ca, Sr) are isotypic with Na[Li₃SiO₄] and Cs[Na₃PbO₄], respectively. In contrast to nitrides with UCr₄C₄ structure type, the latter show crystallographic ordering of the tetrahedrally coordinated network atoms Mg/Si and Li/Al, respectively. This ordering is quite likely due to the marked differences in the ionic radii of fourfold-coordinated Si⁴⁺ (0.29 Å) and Mg²⁺ (0.64 Å) as well as Li⁺ (0.62 Å) and Al³⁺ (0.41 Å). However, nitrides crystallizing in the UCr₄C₄ structure type described here and also Ba[Mg₃SiN₄], which crystallizes in a triclinic variant of the UCr₄C₄ structure type, show disordering of tetrahedrally coordinated central ions despite comparable differences in ionic radii. In M[Mg₂Al₂N₄] (M = Ca, Sr, Ba), the difference in Mg²⁺/Al³⁺ ionic radii is 0.23 Å, which is even slightly larger than the differences of Li⁺/Al³⁺ (0.21 Å) in M[LiAl₃N₄] (M = Ca, Sr). Thus, a reason for crystallographic disorder is not obvious.

2.5 The Crystal Structure of Nitridomagnesogermanate $\text{Ba}[\text{Mg}_3\text{GeN}_4]\cdot\text{Eu}^{2+}$ and Theoretical Calculations of Its Electronic Properties

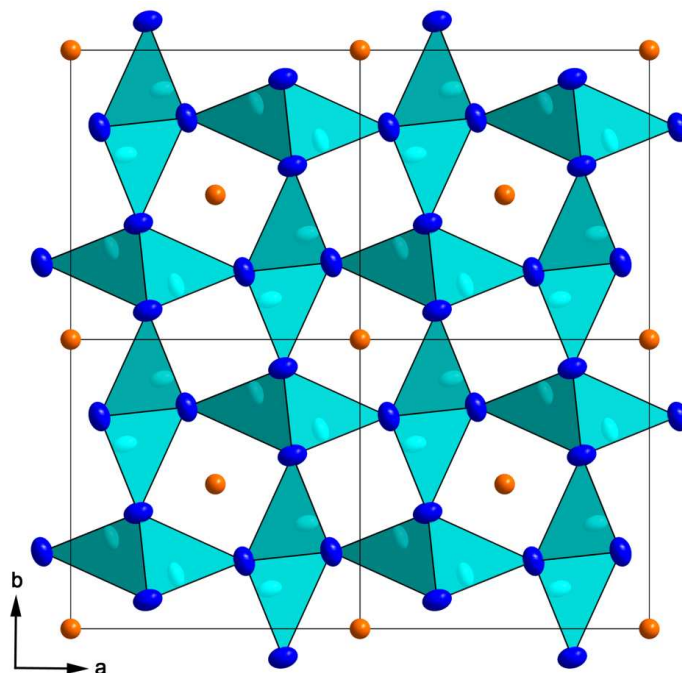


Figure 1. Crystal structure of $\text{Ba}[\text{Mg}_3\text{GeN}_4]\cdot\text{Eu}^{2+}$ along [001]. Ba (orange), Mg/Ge (turquoise), N (blue). All atoms are shown as ellipsoids with 90% probability.

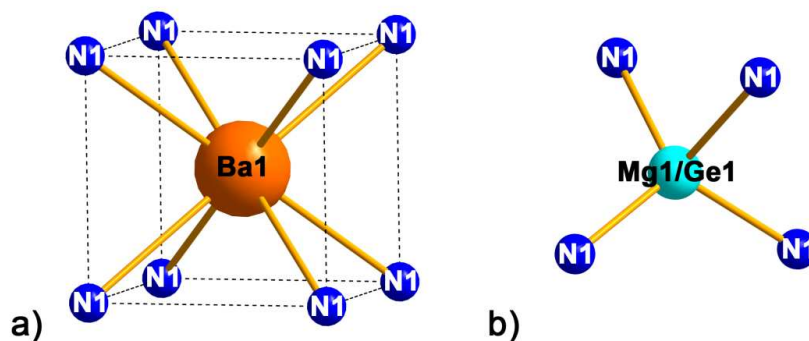


Figure 2. (a) Cubic coordination of Ba1 (orange) by nitrogen atoms (blue). (b) Tetrahedral coordination of Mg1/Ge1 site (turquoise) by four nitrogen atoms (blue).

The aforementioned $\text{AB}_2\text{C}_2\text{X}_4$ and AB_3CX_4 structures also illustrate the substitutability of network-building ions B and C, provided that their total number (B+C) of four atoms with a positive charge of 10+ remains unchanged. As can be seen from Table 4, unlike

2.5 The Crystal Structure of Nitridomagnesogermanate Ba[Mg₃GeN₄]:Eu²⁺ and Theoretical Calculations of Its Electronic Properties

nitridomagnesioaluminates and -silicates, corresponding Ca analogues “Ca[Mg₃GeN₄]” and Ca[Mg₂Ga₂N₄] are either still lacking or show marked differences in their crystal structures, respectively. There are further examples in the classes of nitridogallates and nitridogermanates showing this phenomenon, for instance, Sr₃Ga₂N₄ and Ba₃Ga₂N₄ as well as Sr₃[MgGeN₄] and Ba₃[MgGeN₄]. Whereas the Sr and Ba compounds are isotypic, corresponding Ca analogues are not known so far. One explanation might be that an increase in the radius of network-building ions^[36] within one main group of the periodic table (Al³⁺/Ga³⁺: 0.41/0.48 Å, Si⁴⁺/Ge⁴⁺: 0.29/0.41 Å) accompanied by a decrease in the radius of counterions (Ba²⁺: 1.54, Sr²⁺: 1.23, Ca²⁺: 1.05 Å) may lead to a crystal structure that is not isotypic or rather may not exist. Ba[Mg₃GeN₄]:Eu²⁺ can therefore be designated as one of the last missing compounds in this compound class crystallizing in the UCr₄C₄ structure type.

Table 4. Overview of nitrides with identic structural features. Compounds with the UCr₄C₄ type of structure are marked with asterisks.

AB ₂ C ₂ X ₄ structures		AB ₃ CX ₄ structures		
Ca[Mg ₂ Al ₂ N ₄]*		Ca[Mg ₃ SiN ₄]		Ca[LiAl ₃ N ₄]
Sr[Mg ₂ Al ₂ N ₄]*	Sr[Mg ₂ Ga ₂ N ₄]*	Sr[Mg ₃ SiN ₄]	Sr[Mg ₃ GeN ₄]*	Sr[LiAl ₃ N ₄]
Ba[Mg ₂ Al ₂ N ₄]*	Ba[Mg ₂ Ga ₂ N ₄]*	Ba[Mg ₃ SiN ₄] ^(*)	Ba[Mg ₃ GeN ₄]*	

2.5.2.4 Luminescence

Eu²⁺-doped samples of Ba[Mg₃GeN₄] exhibit orange body color but show no luminescence under UV-to-green irradiation, neither at room temperature or on cooling with liquid nitrogen. Generally, emission of Eu²⁺-doped nitrides is derived from parity-allowed 4f – 5d broad-band transitions when excited by UV or blue light. Since the lowest 5d levels of Eu²⁺ are assumed to be located in or rather close to the conduction band of the host lattice, the band gap of the host lattice is decisive for emission characteristics of the Eu²⁺-doped compound. Therefore, to study the absence of luminescence, investigations on the band gap of Ba[Mg₃GeN₄] are of special interest. Since synthesis yielded a heterogeneous product with Ba[Mg₃GeN₄] as side phase, accurate separation of the title compound out of the reaction batch was not possible. Hence, DFT calculations utilizing the generalized gradient approximation (GGA) on the density of states

(DOS) were conducted instead of UV/Vis measurements. Thus, the approximate electronic band gap was evaluated from differently ordered models of $\text{Ba}[\text{Mg}_3\text{GeN}_4]$. Chosen models are shown in Figure 3. The resulting values range from 0.2 in model B to 1.5 eV in model A, while the band gap of a supercell (see Figure 4), comprising a number of different Mg/Ge arrangements, amounts to 0.6 eV. This corresponds to the value calculated for model B. Thus, edge-sharing GeN_4 tetrahedra appear to limit the electronic gap of the ordering models.

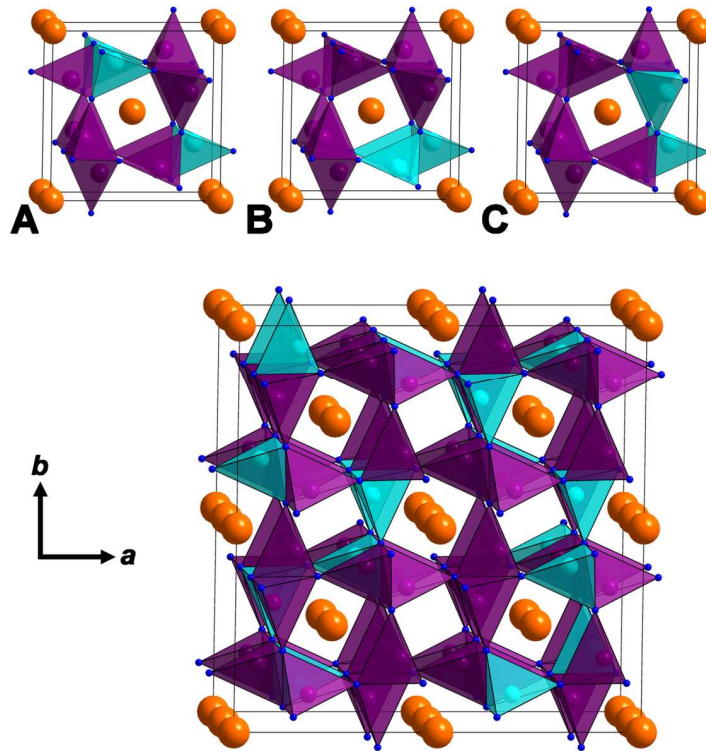


Figure 3. Chosen models for the ordering of Mg/Ge in $\text{Ba}[\text{Mg}_3\text{GeN}_4]$ (A-C) and a supercell combining different arrangements. MgN_4 tetrahedra (violet), GeN_4 tetrahedra (turquoise).

GGA is typically observed to underestimate the electronic band gap for nitride phosphor materials. Small band gaps in luminescent materials are often associated with increased thermal quenching behavior due to location of the Eu 5d state within or sufficiently close to the conduction band.^[33,41] Additionally, we conducted meta-GGA calculations with the modified Becke-Johnson potential (mbj) (see Figure 5),^[42] which yield band gaps closer to the experiment.^[43] Resulting mbj values for E_g are 2.45 eV (model A), 0.65 eV (model B), and 2.8 eV (model C). Hence, the absence of luminescence in $\text{Ba}[\text{Mg}_3\text{GeN}_4]\text{:Eu}^{2+}$ appears conclusive from the calculated band gap values. The experimentally observed orange body color of the crystals

2.5 The Crystal Structure of Nitridomagnesogermanate $\text{Ba}[\text{Mg}_3\text{GeN}_4]\text{:Eu}^{2+}$ and Theoretical Calculations of Its Electronic Properties

would suggest an E_g value around 2.3 eV and is further in line with the mbj-corrected values suggesting that the disordered material would mainly consist of ordered variants A and C without the presence of edge-sharing GeN_4 tetrahedra.

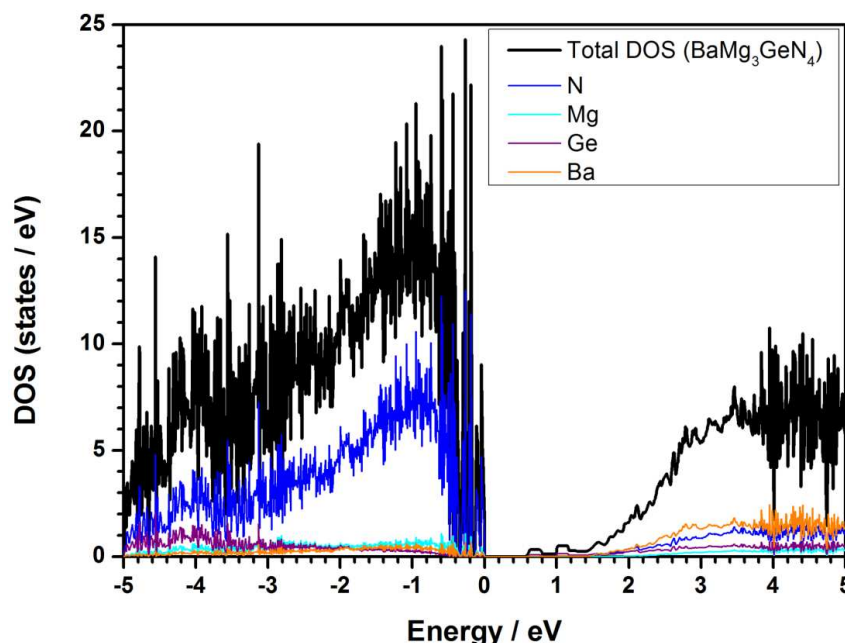


Figure 4. DOS for an ordered $2 \times 2 \times 2$ supercell of $\text{Ba}[\text{Mg}_3\text{GeN}_4]$ comprising different Mg/Ge arrangements.

Up to now, there are no investigations concerning luminescence properties of Eu^{2+} -doped nitridogermanates in the literature. As there are many examples of nitrides crystallizing in UCr_4C_4 or closely related structure types, luminescence investigations on $\text{Ba}[\text{Mg}_3\text{GeN}_4]\text{:Eu}^{2+}$ are well suited for comparison between different compound classes.

The crystal structures as well as luminescence properties of Eu^{2+} -doped compounds with general formula $\text{AB}_2\text{C}_2\text{X}_4$ and AB_3CX_4 listed in Table 4 have precisely been described in the literature. Important characteristics are summarized in Table 5. Compounds in the UCr_4C_4 structure type show rather broader bandwidths than those with $\text{Na}[\text{Li}_3\text{SiO}_4]$ and $\text{Cs}[\text{Na}_3\text{PbO}_4]$ structure types, respectively. A close relation between luminescence and structural features can be inferred.

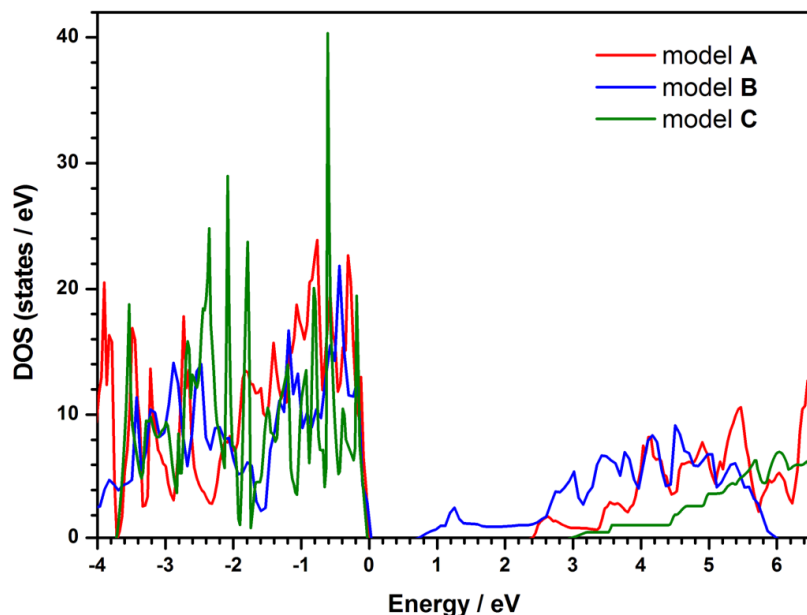


Figure 5. Density of states (mbj-GGA) for the different Mg/Ge ordering models (A-C) of disordered $\text{Ba}[\text{Mg}_3\text{GeN}_4]$.

Generally, the number of crystallographic sites for the activator ion and its direct surroundings influence the bandwidth of the emission. An isomorphic and highly symmetrical crystal field for all crystallographic activator sites, ideally only one site, in a rigid host lattice has so far been expected to be beneficial for narrow emission. In the herein-presented $\text{AB}_2\text{C}_2\text{X}_4$ and AB_3CX_4 structures, Eu^{2+} is expected to occupy the single alkaline earth atom site having cubelike coordination by N. Thus, all of them provide promising conditions for narrow-band emission. The differences in the full widths at half-maximum (fwhm) may be explained by the occupancy of tetrahedral central ions. Unlike $\text{Na}[\text{Li}_3\text{SiO}_4]$ and $\text{Cs}[\text{Na}_3\text{PbO}_4]$, compounds with UCr_4C_4 structure type show disordering of tetrahedral central ions $\text{Mg}^{2+}/\text{Al}^{3+}$, $\text{Mg}^{2+}/\text{Ga}^{3+}$, $\text{Mg}^{2+}/\text{Ge}^{4+}$ or $\text{Mg}^{2+}/\text{Si}^{4+}$. Larger values of the fwhm of compounds with UCr_4C_4 structure type are presumably caused by varying distances of network-building ions to N, which entail differing in Eu–N distances and therefore a broad range of crystal fields, which directly causes inhomogeneous line broadening of the emission band. Ordering of central ions is consequently an important characteristic for host lattices of narrow-band-emitting phosphor materials. Since $\text{Ba}[\text{Mg}_3\text{GeN}_4]:\text{Eu}^{2+}$ also shows disordering of Mg^{2+} and Ge^{4+} network ion positions, broad-band red emission may be assumed. Due to the small band gap, no luminescence of $\text{Ba}[\text{Mg}_3\text{GeN}_4]:\text{Eu}^{2+}$ was observed.

2.5 The Crystal Structure of Nitridomagnesogermanate Ba[Mg₃GeN₄]:Eu²⁺ and Theoretical Calculations of Its Electronic Properties

Table 5. Emission data of compounds isostructural to Ba[Mg₃GeN₄]:Eu²⁺. Compounds with disordering of tetrahedrally coordinated network ions are marked with asterisks.

Compound	λ_{em} / nm	$fwhm$ / cm ⁻¹	λ_{exc} / nm
Ca[Mg ₂ Al ₂ N ₄]:Eu ²⁺ (0.1%) *	607	1815	440
Sr[Mg ₂ Al ₂ N ₄]:Eu ²⁺ (0.1%) *	612	1823	440
Ba[Mg ₂ Al ₂ N ₄]:Eu ²⁺ (0.1%) *	666	2331	440
Ba[Mg ₂ Ga ₂ N ₄]:Eu ²⁺ (2.0%) *	649	2168	440
Sr[Mg ₃ SiN ₄]:Eu ²⁺ (2.0%)	615	1170	440
Ba[Mg ₃ SiN ₄]:Eu ²⁺ (0.5%) *	670	1970	450
Ca[LiAl ₃ N ₄]:Eu ²⁺ (5.0%)	668	1333	470
Sr[LiAl ₃ N ₄]:Eu ²⁺ (0.4%)	650	1180	466

2.5.3 Conclusions

Ba[Mg₃GeN₄]:Eu²⁺ was synthesized by solid-state reaction in weld-shut Ta ampules. The compound crystallizes in the UCr₄C₄ structure type and shows disordering of Mg and Ge atoms in the highly condensed rigid tetrahedra network. Ba²⁺ is located in *vierer* ring channels running along *c* and has cubelike coordination by N. At room temperature or under cooling with liquid nitrogen Ba[Mg₃GeN₄]:Eu²⁺ does not show luminescence in the visible region after irradiation with UV-to-green light. Theoretical investigations of the DOS corroborate this observation: the band gap for different ordering variants of statistically disordered Ba[Mg₃GeN₄] was calculated to be 2.45-2.8 eV.

In general, it is the aim to draw conclusions on the relation between structures and their luminescence properties. Thus, target-oriented research of new phosphors could be improved in an efficient way. Since commercially available phosphor materials that are currently applied in warm-white pc-LEDs show substantial energy loss in the IR region of the emission spectrum, further investigations on narrow-band red-emitting phosphors are one focus of current research.

2.5 The Crystal Structure of Nitridomagnesogermanate Ba[Mg₃GeN₄]:Eu²⁺ and Theoretical Calculations of Its Electronic Properties

The UCr₄C₄ structure type seems to fulfil major requirements for narrow-band red-emitting phosphors. It shows a rigid framework of highly condensed tetrahedra and only one crystallographic site for the alkaline earth atom with a highly symmetric eightfold environment. Both properties are expected to reduce inhomogeneous line broadening, which is caused by different crystal fields around the activator site, which is expected to occupy the alkaline earth atom site.

Despite the small band gap of Ba[Mg₃GeN₄]:Eu²⁺, research on nitridogermanates is of interest for investigation of new host lattices for Eu²⁺-doped phosphors. As substitutability of ions on tetrahedra positions within structure types UCr₄C₄ and ordered variants Na[Li₃SiO₄] and Cs[Na₃PbO₄] demonstrate, interesting structures of new nitridogermanates may be transferred to nitridoaluminates or nitridosilicates. Previous works show that host lattices of these two compound classes have potential for application in high-power phosphor-converted white-light-emitting diodes.

2.5.4 Experimental Section

2.5.4.1 General

To protect starting materials and products from both hydrolization and oxidation, all manipulations were performed under inert-gas conditions. A combined Schlenk/vacuum line and an argon-filled glove box (Unilab, MBraun, Garching; O₂ < 1 ppm, H₂O < 1 ppm) were used. Ar was purified over silica gel (Merck), molecular sieves (Fluka, 4 Å), KOH (Merck, ≥85%), P₄O₁₀ (Roth, ≥99%), and titanium sponge (Johnsen Matthey, 99.5%). Starting materials were weighed into Ta ampules (length 30 mm, diameter 10 mm, wall thickness 0.5 mm), which were arc-welded under argon atmosphere. Ta ampules were transferred into silica tubes and heated under vacuum.

2.5.4.2 Synthesis

Ba[Mg₃GeN₄]:Eu²⁺ was synthesized by firing Ba (0.24 mmol, 32.4 mg, Sigma-Aldrich, 99.99%), Mg (0.47 mmol, 11.4 mg, Alfa Aesar, 99.9%), Ge (0.24 mmol, 17.2 mg, Smart Elements, 99.9999%), 2.6 mol-% EuF₃ (6.24·10⁻³ mmol, 1.3 mg, Sigma-Aldrich, 99.99%), NaN₃

2.5 The Crystal Structure of Nitridomagnesogermanate Ba[Mg₃GeN₄]:Eu²⁺ and Theoretical Calculations of Its Electronic Properties

(0.31 mmol, 20.1 mg, Acros, 99%) and Na (2.1 mmol, 48.3 mg, Sigma-Aldrich, 99.95%) in weld-shut Ta ampules to 780 °C. The temperature was held for 48 h, subsequently decreased to 200 °C at a rate of 3 °C/h, and finally quenched to room temperature. NaN₃ decomposes with loss of N₂ while heating, which leads to increased pressure in the ampule. Liquid sodium enhances solubility of nitrogen, which is further increased by the presence of Ba, and formation of nitrides is facilitated. Orange crystals of Ba[Mg₃GeN₄]:Eu²⁺ were isolated from the inhomogeneous product mixture.

2.5.4.3 Single-Crystal X-ray Diffraction

Single crystals of Ba[Mg₃GeN₄]:Eu²⁺ were selected under a microscope, washed with dry paraffin oil, enclosed in glass capillaries, and sealed under argon to avoid hydrolysis. X-ray diffraction data were collected with a Bruker D8 Quest diffractometer (PHOTON 199 CMOS detector, Mo-K_α radiation), and absorption correction was by multi-scan methods (SADABS).^[44] The crystal structure was solved by direct methods implemented in SHELXS. Structure refinement with anisotropic displacement parameters for all atoms by full-matrix least-squares calculation on $|F|^2$ were done in SHELXL-97.^[45]

Further details of the crystal structure investigations may be obtained from the Fachinformationszentrum Karlsruhe, 76344 Eggenstein-Leopoldshafen, Germany (Fax: +49-7247-808-666; E-Mail: crysdata@fiz-karlsruhe.de) on quoting the depository number CSD-432528.

2.5.4.4 Powder X-ray Diffraction

Single crystals of Ba[Mg₃GeN₄]:Eu²⁺ were selected under a microscope, pulverized in an agate mortar, enclosed in glass capillaries, and sealed under argon. Powder diffraction data were recorded with a STOE STADI P diffractometer (Cu-K_{α1} radiation, Ge(111) monochromator, MYTHEN 1 K detector) in Debye-Scherrer geometry. Simulated powder diffraction patterns were calculated with the aid of WinXPOW, on the basis of single-crystal structure data.^[46] Rietveld refinement was carried out with the TOPAS package.^[47]

2.5.4.5 Theoretical Calculations

Structural relaxations were conducted for all chosen ordering variants of Ba[Mg₃GeN₄] with respect to all internal cell parameters and internal coordinates by using the Vienna ab initio simulation package (VASP).^[48-50] To ensure high precision, the total energy of the unit cell was converged to 10⁻⁷ eV/atom with residual atomic forces below 3×10⁻⁴ eV/Å. For the exchange correlation we used the generalized gradient approximations of Perdew, Burke, and Ernzerhof (PBE)^[51,52] with the projector-augmented-wave (PAW) method.^[53,54] For all electronic calculations including those of the density of states a plane-wave cut-off of 535 eV and a Brillouin zone sampling on a Γ -centered k -mesh of 7 × 7 × 15 (4 × 4 × 8 for the respective supercell) produced by the method of Monkhorst and Pack was chosen.^[55] Additional meta-GGA calculations were performed with the modified Becke-Johnson formalism (GGA-mbj).^[42]

2.5.5 References

- [1] P. Pust, V. Weiler, C. Hecht, A. Tücks, A. S. Wochnik, A.-K. Henß, D. Wiechert, C. Scheu, P. J. Schmidt, W. Schnick, *Nat. Mater.* **2014**, 13, 891.
- [2] H. Yamane, S. Kikkawa, M. Koizumi, *Solid State Ionics* **1987**, 25, 183.
- [3] J. David, Y. Laurent, J. Lang, *J. Bull. Soc. Fr. Mineral. Cristallogr.* **1970**, 93, 153.
- [4] D. R. MacFarlane, J. Huang, M. Forsyth, *Nature* **1999**, 402, 792.
- [5] H. Yamane, S. Kikkawa, M. Koizumi, *J. Power Sources* **1987**, 20, 311.
- [6] M. S. Bhamra, D. J. Fray, *J. Mater. Sci.* **1995**, 30, 5381.
- [7] H. Hillebrecht, J. Churda, L. Schröder, H. G. v. Schnering, *Z. Kristallogr. Suppl.* **1993**, 6, 80.
- [8] Z. Wen, K. Wang, L. Chen, J. Xie, *Electrochem. Commun.* **2006**, 8, 1349.
- [9] H. Lutz, S. Joosten, J. Hoffmann, P. Lehmeier, A. Seilmeier, H. A. Höppe, W. Schnick, *J. Phys. Chem. Solids* **2004**, 65, 1285.
- [10] R.-J. Xie, N. Hiroaki, *Sci. Technol. Adv. Mater.* **2007**, 8, 588.
- [11] S. Nakamura, M. Senoh, T. Mukai, *Appl. Phys. Lett.* **1993**, 62, 2390.
- [12] H. Huppertz, *Doctoral Thesis*, University of Bayreuth, **1997**.
- [13] H. A. Höppe, H. Lutz, P. Morys, W. Schnick, A. Seilmeier, *J. Phys. Chem. Solids* **2000**, 61, 2001.
- [14] J. W. H. v. Krevel, H. T. Hintzen, R. Metselaar, A. Meijerink, *J. Alloys Compd.* **1998**, 268.
- [15] M. Zeuner, S. Pagano, W. Schnick, *Angew. Chem.* **2011**, 123, 7898; *Angew. Chem. Int. Ed.* **2011**, 50, 7754.
- [16] T. M. M. Richter, R. Niewa, *Inorganics* **2014**, 2, 29.
- [17] D. G. Park, Y. Dong, F. J. DiSalvo, *Solid State Sci.* **2008**, 10, 1846.
- [18] D. G. Park, F. J. DiSalvo, *Bull. Korean Chem. Soc.* **2011**, 32, 353.
- [19] C. Poesl, W. Schnick, *Z. Anorg. Allg. Chem.* **2016**, 642, 882.
- [20] D. G. Park, F. J. DiSalvo, *Bull. Korean Chem. Soc.* **2012**, 33, 1759.
- [21] D. G. Park, F. J. DiSalvo, *Bull. Korean Chem. Soc.* **2008**, 29, 2413.
- [22] S. C. Junggeburth, O. Oeckler, D. Johrendt, W. Schnick, *Inorg. Chem.* **2008**, 47, 12018.
- [23] Z. A. Gál, S. J. Clarke, *Chem. Commun.* **2005**, 728.
- [24] S. J. Clarke, F. J. DiSalvo, *J. Alloys Compd.* **1997**, 259, 158.
- [25] H. Yamane, F. J. DiSalvo, *J. Alloys Compd.* **1996**, 241, 69.
- [26] S. J. Clarke, G. R. Kowach, F. J. DiSalvo, *Inorg. Chem.* **1996**, 35, 7009.
- [27] D. G. Park, Z. A. Gál, F. J. DiSalvo, *Bull. Korean Chem. Soc.* **2005**, 26, 1543.

2.5 The Crystal Structure of Nitridomagnesogermanate Ba[Mg₃GeN₄]:Eu²⁺ and Theoretical Calculations of Its Electronic Properties

- [28] S. J. Clarke, F. J. DiSalvo, *Inorg. Chem.* **2000**, 39, 2631.
- [29] D. G. Park, Z. A. Gál, F. J. DiSalvo, *J. Alloys Compd.* **2003**, 360, 85.
- [30] L. G. Akselrud, O. I. Bodak, E. P. Marusin, *Sov. Phys. Crystallogr. (Engl. Transl.)* **1989**, 34, 289.
- [31] P. Pust, F. Hintze, C. Hecht, V. Weiler, A. Locher, D. Zitnanska, S. Harm, D. Wiechert, P. J. Schmidt, W. Schnick, *Chem. Mater.* **2014**, 26, 6113.
- [32] S. Schmiechen, H. Schneider, P. Wagatha, C. Hecht, P. J. Schmidt, W. Schnick, *Chem. Mater.* **2014**, 26, 2712.
- [33] S. Schmiechen, P. Strobel, C. Hecht, T. Reith, M. Siegert, P. J. Schmidt, P. Huppertz, D. Wiechert, W. Schnick, *Chem. Mater.* **2015**, 27, 1780.
- [34] P. Pust, A. S. Wochnik, E. Baumann, P. J. Schmidt, D. Wiechert, C. Scheu, W. Schnick, *Chem. Mater.* **2014**, 26, 3544.
- [35] S. J. Clarke, F. J. DiSalvo, *Inorg. Chem.* **1997**, 36, 1143.
- [36] W. H. Baur, *Crystallogr. Rev.* **1987**, 1, 59.
- [37] B. Nowitzki, R. Hoppe, *Rev. Chim. Miner.* **1986**, 23, 217.
- [38] F. Hintze, N. W. Johnson, M. Seibald, D. Muir, A. Moewes, W. Schnick, *Chem. Mater.* **2013**, 25, 4044.
- [39] M. Kubus, K. Levin, S. Kroeker, D. Enseling, T. Jüstel, H.-J. Meyer, *Dalton Trans.* **2015**, 44, 2819.
- [40] C. Poesl, L. Neudert, W. Schnick, *Eur. J. Inorg. Chem.* **2017**, 1067.
- [41] P. Dorenbos, *J. Phys.: Condens. Matter* **2003**, 15, 2645.
- [42] F. Tran, P. Blaha, *Phys. Rev. Lett.* **2009**, 102, 226401.
- [43] J. A. Camargo-Martínez, R. Baquero, *Phys. Rev. B: Condens. Matter* **2012**, 86, 195106.
- [44] G. M. Sheldrick, *SADABS*, Multi-Scan Absorption Correction, v.2, Bruker-AXS, Madison, WI, USA, **2012**.
- [45] G. M. Sheldrick, *Acta Crystallogr., Sect. A: Found. Crystallogr.* **2008**, 64, 112.
- [46] *WinXPOW*, Program for Powder Data Handling v. 2.21, Stoe & Cie GmbH, Darmstadt, Germany, **2007**.
- [47] A. Coelho, *TOPAS - Academic*, Coelho Software, Brisbane, **2007**.
- [48] G. Kresse, J. Hafner, *Phys. Rev. B: Condens. Matter* **1993**, 47, 558.
- [49] G. Kresse, J. Hafner, *Phys. Rev. B: Condens. Matter* **1994**, 49, 14251.
- [50] G. Kresse, J. Furthmüller, *Comput. Mater. Sci.* **1996**, 6, 15.
- [51] J. P. Perdew, K. Burke, M. Ernzerhof, *Phys. Rev. Lett.* **1997**, 78, 1396.
- [52] J. P. Perdew, K. Burke, M. Ernzerhof, *Phys. Rev. Lett.* **1996**, 77, 3865.

2.5 The Crystal Structure of Nitridomagnesogermanate Ba[Mg₃GeN₄]:Eu²⁺ and Theoretical Calculations of Its Electronic Properties

- [53] P. E. Blöchl, *Phys. Rev. B: Condens. Matter* **1994**, 50, 17953.
- [54] G. Kresse, D. Joubert, *Phys. Rev. B: Condens. Matter* **1999**, 59, 1758.
- [55] H. J. Monkhorst, J. D. Pack, *Phys. Rev. B: Condens. Matter* **1976**, 13, 5188.

3 Nitridosilicates

3.1 Introduction

During the last decades, Eu^{2+} -doped nitridosilicates emerged as highly efficient optical materials. $M_2\text{Si}_5\text{N}_8:\text{Eu}^{2+}$ ($M = \text{Sr}, \text{Ba}$)^[1-3] represents one prominent example, which already finds application as luminescent material in phosphor-converted (pc)-LEDs. In recent years, further investigations have shown that, in particular, Mg- or Li-containing nitridosilicates (e.g. $\text{Sr}[\text{LiAl}_3\text{N}_4]:\text{Eu}^{2+}$ and $\text{Sr}[\text{Mg}_3\text{SiN}_4]:\text{Eu}^{2+}$)^[4,5] exhibit excellent luminescence properties and comply with high demands that are crucial for an application in LED-based lighting products. Several novel nitridosilicates containing Mg and/or Li have been developed, namely, $M[\text{Mg}_3\text{SiN}_4]$ ($M = \text{Ca}, \text{Sr}, \text{Ba}, \text{Eu}$)^[5,6] $\text{Ca}_2\text{Mg}[\text{Li}_4\text{Si}_2\text{N}_6]$, $\text{Li}_2\text{Ca}_2[\text{Mg}_2\text{Si}_2\text{N}_6]$,^[7] $\text{Ba}[(\text{Mg}_{2-x}\text{Li}_x)(\text{Al}_{4-x}\text{Si}_x)\text{N}_6]$ ($x = 0-2$)^[8] $\text{Li}_2(\text{Ca}_{1-x}\text{Sr}_x)_2[\text{Mg}_2\text{Si}_2\text{N}_6]$ ($x = 0-0.06$)^[9] and $\text{Mg}_2\text{Si}_5\text{N}_8$.^[10] Constituting ions Mg^{2+} and Li^+ may thereby be part of the tetrahedral network, or act as counterions that balance the charges of the anionic framework. Additionally, $\text{Ba}[(\text{Mg}_{2-x}\text{Li}_x)(\text{Al}_{4-x}\text{Si}_x)\text{N}_6]$ and $\text{Li}_2(\text{Ca}_{1-x}\text{Sr}_x)_2[\text{Mg}_2\text{Si}_2\text{N}_6]$ clearly illustrate the substitutability of network-building ions or counterions. Nitridosilicates represent therefore an intriguing class of materials with a wide variety of structural features.

The following chapters deal with the novel Mg- and Li-containing nitridosilicate $\text{Ca}_3\text{Mg}[\text{Li}_2\text{Si}_2\text{N}_6]:\text{Eu}^{2+}$. It represents the fourth example of a nitridosilicate that contains both, Li^+ and Mg^{2+} ions. A detailed description of its crystal structure is given and a comparison to structurally related $\text{Ca}_2\text{Mg}[\text{Li}_4\text{Si}_2\text{N}_6]$ is presented. Furthermore, exceptional luminescence properties of $\text{Ca}_3\text{Mg}[\text{Li}_2\text{Si}_2\text{N}_6]:\text{Eu}^{2+}$ are discussed.

References

- [1] H. A. Höpfe, H. Lutz, P. Morys, W. Schnick, A. Seilmeier, *J. Phys. Chem. Solids* **2000**, 61, 2001.
- [2] R. Mueller-Mach, G. Mueller, M. R. Krames, H. A. Höpfe, F. Stadler, W. Schnick, T. Jüstel, P. J. Schmidt, *Phys. Status Solidi A* **2005**, 202, 1727.

- [3] M. Zeuner, P. J. Schmidt, W. Schnick, *Chem. Mater.* **2009**, 21, 2467.
- [4] P. Pust, V. Weiler, C. Hecht, A. Tücks, A. S. Wochnik, A.-K. Henß, D. Wiechert, C. Scheu, P. J. Schmidt, W. Schnick, *Nat. Mater.* **2014**, 13, 891.
- [5] S. Schmiechen, H. Schneider, P. Wagatha, C. Hecht, P. J. Schmidt, W. Schnick, *Chem. Mater.* **2014**, 26, 2712.
- [6] S. Schmiechen, P. Strobel, C. Hecht, T. Reith, M. Siegert, P. J. Schmidt, P. Huppertz, D. Wiechert, W. Schnick, *Chem. Mater.* **2015**, 27, 1780.
- [7] S. Schmiechen, F. Nietschke, W. Schnick, *Eur. J. Inorg. Chem.* **2015**, 1592.
- [8] P. Strobel, S. Schmiechen, M. Siegert, A. Tücks, P. J. Schmidt, W. Schnick, *Chem. Mater.* **2015**, 27, 6109.
- [9] P. Strobel, V. Weiler, C. Hecht, P. J. Schmidt, W. Schnick, *Chem. Mater.* **2017**, 29, 1377.
- [10] P. Bielec, W. Schnick, *Angew. Chem.* **2017**, 129, 4888; *Angew. Chem. Int. Ed.* **2017**, 56, 4810.

3.2 Crystal Structure and Nontypical Deep-Red Luminescence of $\text{Ca}_3\text{Mg}[\text{Li}_2\text{Si}_2\text{N}_6]:\text{Eu}^{2+}$

published in: *Chem. Mater.* **2017**, 29, 3778-3784

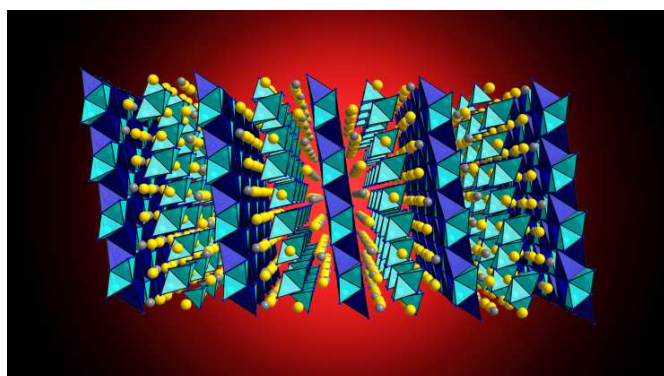
authors: Christine Poesl and Wolfgang Schnick

DOI: 10.1002/acs.chemmater.7b00871

Copyright © 2017 American Chemical Society

<http://pubs.acs.org/doi/abs/10.1021/acs.chemmater.7b00871>

Abstract: Rare-earth-doped nitridosilicates exhibit outstanding luminescence properties and have been intensively studied for solid-state lighting. Here, we describe the new nitridolithosilicate $\text{Ca}_3\text{Mg}[\text{Li}_2\text{Si}_2\text{N}_6]:\text{Eu}^{2+}$ with extraordinary luminescence characteristics. The compound was synthesized by the solid-state metathesis reaction in sealed Ta ampules. The crystal structure was solved and refined on the basis of single-crystal X-ray diffraction data. $\text{Ca}_3\text{Mg}[\text{Li}_2\text{Si}_2\text{N}_6]:\text{Eu}^{2+}$ crystallizes in the monoclinic space group $C2/m$ (no. 12) [$Z = 4$, $a = 5.966(1)$, $b = 9.806(2)$, $c = 11.721(2)$ Å, $\beta = 99.67(3)^\circ$, $V = 675.9(2)$ Å³] and exhibits a layered anionic network made up of edge- and corner-sharing LiN_4 tetrahedra and $[\text{Si}_2\text{N}_6]^{10-}$



bow-tie units. The network charge is compensated by Ca^{2+} and Mg^{2+} ions. Upon irradiation with UV to blue light, red emission at exceptionally long wavelengths ($\lambda_{\text{em}} = 734$ nm, $\text{fwhm} \approx 2293$ nm) is observed. According to emission in the near-infrared, application in LEDs for horticultural lighting appears promising.

3.2.1 Introduction

Nitridosilicates are characterized by their manifold structural chemistry and intriguing materials properties. Because of the high sensitivity to air and moisture of both starting materials and products, synthesis of less-condensed nitridosilicates is quite challenging. Over the last years, different synthetic approaches leading to nitridosilicates have been elaborated. These include high-temperature reactions, precursor routes, ammonothermal syntheses, and flux methods by using, for example, liquid sodium.^[1-9] Solid-state metathesis reactions have gained significant importance as well, because a variety of ternary or higher nitrides have recently been synthesized by this approach.^[10-15] Thereby, a key feature is the employment of reactive starting materials by coproducing a metathesis salt, which on one hand drives the reaction thermodynamically and on the other hand concurrently acts as reactive flux.

Common structural motifs of nitridosilicates are SiN_4 tetrahedra, which may be linked through vertices and/or edges, forming more- or less-condensed anionic substructures ranging up to three-periodic anionic frameworks. The resulting structural diversity of nitridosilicates can be ascribed to the N atoms, which are able to connect up to four adjacent tetrahedral centers. Cations like alkaline earths (AE^{2+}), Li^+ or Mg^{2+} are distributed among the voids of the anionic networks and balance their charges. As some examples in the literature have already shown, the number of new nitrides can be further increased by partial substitution of Si^{4+} by Li^+ , Mg^{2+} , or Al^{3+} .^[12,13,16-19] Complete exchange of Si^{4+} by Ga^{3+} or Ge^{4+} is also possible and results in the strongly related compound classes of nitridogallates and nitridogermanates, respectively (see homeotypical compounds $\text{Ba}[\text{Mg}_3\text{SiN}_4]$, $\text{Sr}[\text{Mg}_3\text{GeN}_4]$, and $M[\text{Mg}_2\text{Ga}_2\text{N}_4]$ with $M = \text{Sr}, \text{Ba}$).^[17,20,21]

Nitridosilicates show a great diversity of interesting materials properties, e.g. high mechanical strength and high thermal stability of silicon nitride ceramics, lithium ion conductivity (e.g. Li_2SiN_2)^[22,23] or luminescence when doped with Eu^{2+} or Ce^{3+} .^[22,24-28] $(\text{Sr},\text{Ba})_2\text{Si}_5\text{N}_8:\text{Eu}^{2+}$,^[29-31] $\text{CaAlSiN}_3:\text{Eu}^{2+}$,^[19] and $\text{Sr}[\text{Mg}_3\text{SiN}_4]:\text{Eu}^{2+}$ ^[16] represent prominent examples of rare-earth doped nitrides, which show strong broadband emission in the red spectral region after irradiation with blue light, originating from parity allowed $4f^65d^1 \rightarrow 4f^7$ transitions in Eu^{2+} and spin and parity allowed $4f^05d^1 \rightarrow 4f^1$ transitions in Ce^{3+} . Warm white light can be generated by a combination of red and green emitting phosphors, both covered on a blue LED chip, which is usually an $(\text{In},\text{Ga})\text{N}$ semiconductor chip.^[32,33] The so-called phosphor-converted light-emitting diodes (pc-LEDs) are highly efficient and, over the past decade, developed into an energy-saving replacement for inefficient incandescent light bulbs. Because most commercially available warm

white pc-LEDs still show a large portion of its emission beyond the sensitivity of the human eye,^[34,35] research for narrow-band red emitting luminescent materials is of particular interest for general illumination purposes.

During our research for innovative red-emitting compounds, we came across $\text{Ca}_3\text{Mg}[\text{Li}_2\text{Si}_2\text{N}_6]:\text{Eu}^{2+}$, a new nitridolithosilicate with outstanding emission properties at fairly long wavelengths. In this contribution, we report on the synthesis, structural elucidation, and optical properties of $\text{Ca}_3\text{Mg}[\text{Li}_2\text{Si}_2\text{N}_6]:\text{Eu}^{2+}$. Unprecedented luminescence properties differ essentially from previously described Eu^{2+} -doped nitridosilicates and are discussed in detail, also in comparison to recently reported narrow-band red emitting Eu^{2+} -doped nitridosilicates.

3.2.2 Experimental Section

3.2.2.1 Synthesis

Because of the sensitivity of the starting materials and the product toward air and moisture, all manipulations were performed under inert-gas conditions using argon filled glove boxes (Unilab, MBraun, Garching, $\text{O}_2 < 1$ ppm, $\text{H}_2\text{O} < 1$ ppm) and combined Schlenk/vacuum lines. Ar was dried and purified by passing it through glass tubes filled with silica gel (Merck), molecular sieve (Fluka, 4 Å), P_4O_{10} (Roth, $\geq 99\%$), and titanium sponge (Johnsen Matthey, 99.5%). $\text{Ca}_3\text{Mg}[\text{Li}_2\text{Si}_2\text{N}_6]:\text{Eu}^{2+}$ was synthesized by solid-state metathesis reaction using $\text{Ca}(\text{NH}_2)_2$ (17.9 mg, 0.25 mmol, synthesized according to Brokamp),^[36] CaH_2 (8.3 mg, 0.20 mmol, Cerac, 99.5%), MgF_2 (15.5 mg, 0.25 mmol, ABCR, 99.99%), Si_3N_4 (6.9 mg, 0.05 mmol, UBE, 99.9%), 1.7 mol% EuF_3 (0.9 mg, $4.3 \cdot 10^{-3}$ mmol, Sigma-Aldrich, 99.99%), and Li (9.8 mg, 1.41 mmol, Alfa Aesar, 99.9%) as starting materials. The powdery reactants were finely ground and placed with metallic Li in a tantalum ampule, which was weld shut in an arc furnace. The reaction mixture was heated up to 950 °C with a rate of 300 °C · h⁻¹, maintained for 24 h, subsequently cooled to 500 °C with a rate of 5 °C · h⁻¹ and finally quenched to room temperature by switching off the furnace. Orange colored single crystals of $\text{Ca}_3\text{Mg}[\text{Li}_2\text{Si}_2\text{N}_6]:\text{Eu}^{2+}$ were obtained embedded in an amorphous powder. Additionally, red rod-shaped crystals of $\text{Ca}[\text{Mg}_3\text{SiN}_4]:\text{Eu}^{2+}$, colorless crystals of LiF, and some metallic residues were found as side phases of the reaction. The sample is sensitive toward air and moisture and partially shows intensive red luminescence under irradiation with ultraviolet (UV) to green light.

3.2.2.2 Single-Crystal X-ray Diffraction

Single crystals of $\text{Ca}_3\text{Mg}[\text{Li}_2\text{Si}_2\text{N}_6]:\text{Eu}^{2+}$ were isolated from the reaction product, washed with dry paraffin oil and enclosed in glass capillaries, which were sealed under argon to avoid hydrolysis. X-ray diffraction data were collected on a Stoe IPDS I diffractometer (Mo- $K\alpha$ radiation, graphite monochromator). Structure solution was performed in SHELXS-97,^[37] by using direct methods. The crystal structure was refined by full-matrix least-squares calculation on $|F|^2$ in SHELXL-97^[38,39] with anisotropic displacement parameters for all atoms. Further details of the crystal-structure refinement may be obtained from the Fachinformationszentrum Karlsruhe, 76344 Eggenstein-Leopoldshafen, Germany (Fax: +49-7247-808-666; E-mail: crysdata@fiz-karlsruhe.de), on quoting the depository number CSD-432605.

3.2.2.3 Scanning Electron Microscopy

The chemical composition of $\text{Ca}_3\text{Mg}[\text{Li}_2\text{Si}_2\text{N}_6]:\text{Eu}^{2+}$ was confirmed by energy dispersive X-ray spectroscopy (FEI Helios G3 UC scanning electron microscope equipped with an EDX detector, scanning transmission detector, and focused ion beam). The reaction product was placed on an adhesive conductive carbon pad and coated with a conductive carbon film (BAL-TEC MED 020, Bal Tec AG).

3.2.2.4 Luminescence

Luminescence investigations on single crystals of $\text{Ca}_3\text{Mg}[\text{Li}_2\text{Si}_2\text{N}_6]:\text{Eu}^{2+}$ were performed using a luminescence microscope, consisting of a HORIBA Fluorimax4 Spectrofluorimeter system, which is attached to an Olympus BX51 microscope via fiber optics. The single crystals were measured in sealed glass capillaries with an excitation wavelength of 440 nm. The emission spectrum was measured between 460 and 800 nm; the excitation spectrum was measured between 380 and 680 nm, with a step size of 2 nm. Because $\text{Ca}_3\text{Mg}[\text{Li}_2\text{Si}_2\text{N}_6]:\text{Eu}^{2+}$ shows emission beyond 800 nm and the spectrometer is only calibrated for wavelengths up to 800 nm, emission peak in the near-infrared was simulated using a Gauss-fit.

3.2.3 Results and Discussion

3.2.3.1 Synthesis and Chemical Analysis

Solid-state metathesis reaction as described above yielded a heterogeneous reaction mixture containing single-crystals of $\text{Ca}_3\text{Mg}[\text{Li}_2\text{Si}_2\text{N}_6]:\text{Eu}^{2+}$. The crystals show orange body color and undergo rapid hydrolysis when exposed to air. The elemental composition was determined by energy-dispersive X-ray spectroscopy (EDX). Using this method, light elements like N cannot be determined with a reasonable degree of accuracy, also Li is not determinable. The atomic ratio Ca/Mg/Si of 3.0/1.1/2.0 (six measurements on different crystals), normalized to the Ca content, is in good agreement with the sum formula obtained from single-crystal structure analysis. Besides a small amount of oxygen, which can be attributed to superficial hydrolysis of the product, no further elements were detected.

3.2.3.2 Single-Crystal Structure Analysis

The crystal structure of $\text{Ca}_3\text{Mg}[\text{Li}_2\text{Si}_2\text{N}_6]:\text{Eu}^{2+}$ was solved and refined in the monoclinic space group $C2/m$ (no. 12) with $a = 5.966(1)$, $b = 9.806(2)$, $c = 11.721(2)$ Å, and $\beta = 99.67(3)^\circ$. The crystallographic data are summarized in Table 1. Atomic coordinates, Wyckoff positions, and isotropic displacement parameters are listed in Table 2. Selected bond lengths and angles as well as anisotropic displacement parameters are given in the Supporting Information (Tables S1-S3). Given the small dopant concentration and, therefore, the insignificant scattering intensity, Eu^{2+} was neglected during structure refinement.

Table 1. Crystallographic Data of the Single-Crystal Structure Determination of $\text{Ca}_3\text{Mg}[\text{Li}_2\text{Si}_2\text{N}_6]:\text{Eu}^{2+}$

formula	$\text{Ca}_3\text{Mg}[\text{Li}_2\text{Si}_2\text{N}_6]:\text{Eu}^{2+}$
crystal system	monoclinic
space group	$C2/m$ (no. 12)
lattice parameters / $\text{\AA},^\circ$	$a = 5.966(1)$ $b = 9.806(2)$ $c = 11.721(2)$ $\beta = 99.67(3)$
cell volume / \AA^3	675.9(2)
formula units / unit cell	4
density / $\text{g}\cdot\text{cm}^{-3}$	2.935
μ / mm^{-1}	2.827
T / K	293(2)
diffractometer	Stoe IPDS I
radiation	$\text{Mo-K}\alpha$ ($\lambda = 0.71073 \text{ \AA}$), graphite monochromator
$F(000)$	592
profile range	$4.04 \leq \theta \leq 29.90$
index ranges	$-8 \leq h \leq 8$ $-13 \leq k \leq 13$ $-16 \leq l \leq 16$
independent reflections	1028 [$R(\text{int}) = 0.0722$]
refined parameters	72
goodness of fit	1.323
R_1 (all data); $R_1 (F^2 > 2\sigma(F^2))$	0.0770, 0.0618
wR_2 (all data); $wR_2 (F^2 > 2\sigma(F^2))$	0.1118, 0.1080
$\Delta\rho_{\text{max}}, \Delta\rho_{\text{min}}$ / $\text{e}\cdot\text{\AA}^{-3}$	0.826, -1.176

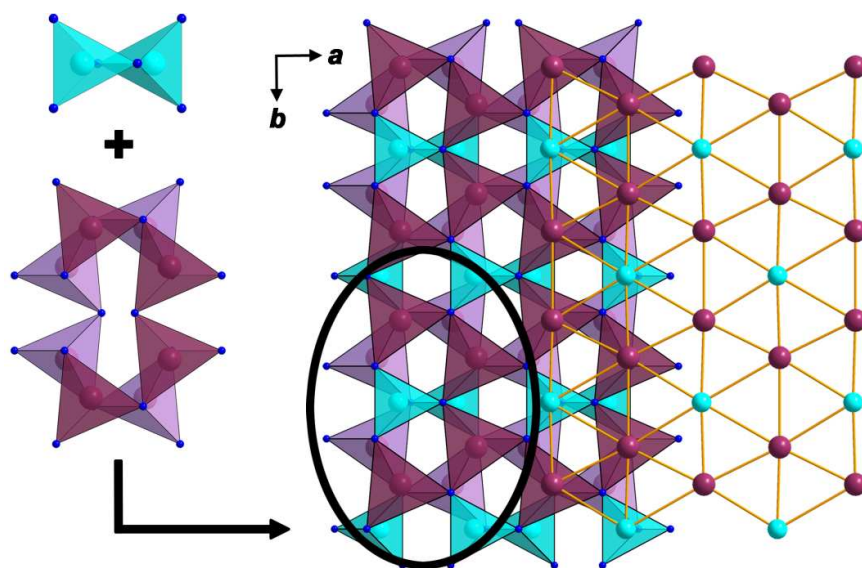


Figure 1. Details of layers in $\text{Ca}_3\text{Mg}[\text{Li}_2\text{Si}_2\text{N}_6]:\text{Eu}^{2+}$. Left: $[\text{Si}_2\text{N}_6]^{10-}$ bow-tie units (turquoise) and *achter* rings of LiN_4 tetrahedra (violet). Right: Layer made up of bow-tie units and *achter* rings forming two sublayers of condensed *dreier* rings; only one of them is shown for reasons of clarity.

The crystal structure of $\text{Ca}_3\text{Mg}[\text{Li}_2\text{Si}_2\text{N}_6]:\text{Eu}^{2+}$ is closely related to that of $\text{Ca}_2\text{Mg}[\text{Li}_4\text{Si}_2\text{N}_6]$,^[12] which has already been reported in literature. Both structures contain identical layers of LiN_4 and SiN_4 tetrahedra as well as Ca and Mg ions, which are located between the layers. Since Li as well as Si are part of the tetrahedral network, the compounds can be more precisely classified as nitridolithosilicates. The arrangement of tetrahedra within one layer is shown in Figure 1. It consists of vertex- and corner-sharing LiN_4 tetrahedra forming *achter* rings,^[40] intercalated by edge-sharing $[\text{Si}_2\text{N}_6]^{10-}$ “bow-tie” units. This results in layers of condensed *dreier* rings in the *ab* plane. The differences between the structurally related compounds $\text{Ca}_2\text{Mg}[\text{Li}_4\text{Si}_2\text{N}_6]$ and $\text{Ca}_3\text{Mg}[\text{Li}_2\text{Si}_2\text{N}_6]:\text{Eu}^{2+}$ are additional $[\text{Si}_2\text{N}_6]^{10-}$ bow-tie units in the crystal structure of $\text{Ca}_3\text{Mg}[\text{Li}_2\text{Si}_2\text{N}_6]:\text{Eu}^{2+}$. Together with the Ca^{2+} and Mg^{2+} ions, these bow-tie units are located between layers of *dreier* rings. A direct comparison of both crystal structures is illustrated in Figure 2.

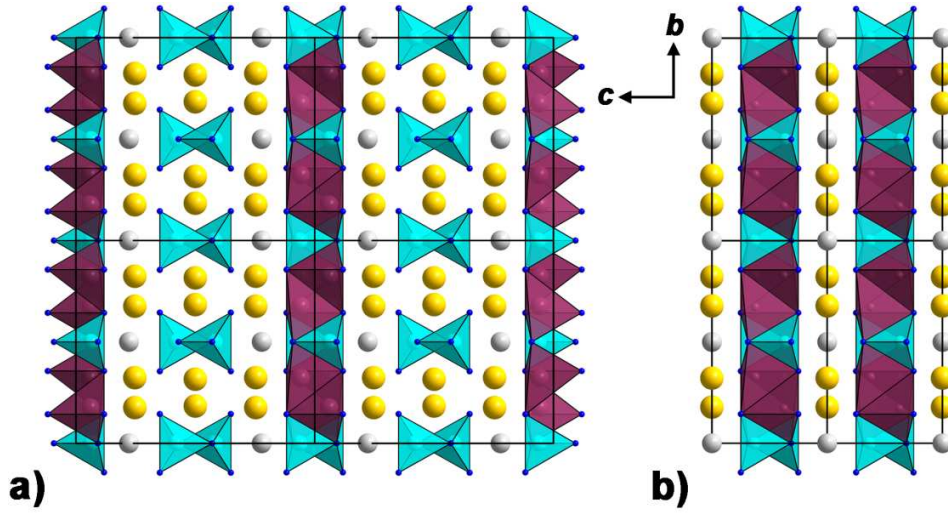


Figure 2. Crystal structures of $\text{Ca}_3\text{Mg}[\text{Li}_2\text{Si}_2\text{N}_6]:\text{Eu}^{2+}$ (a) and $\text{Ca}_2\text{Mg}[\text{Li}_4\text{Si}_2\text{N}_6]$ (b).

$[\text{Si}_2\text{N}_6]^{10-}$ bow-tie units were first described in $\text{Ba}_5\text{Si}_2\text{N}_6$,^[2] and are also known in other nitridosilicates, e.g. $\text{Ca}_2\text{Mg}[\text{Li}_4\text{Si}_2\text{N}_6]$, $\text{Li}_2\text{Ca}_2[\text{Mg}_2\text{Si}_2\text{N}_6]$,^[12] and $\text{Ca}_3[\text{Li}_4\text{Si}_2\text{N}_6]$.^[41,42] Si–N bond lengths in these bow-tie units ($\text{Ca}_3\text{Mg}[\text{Li}_2\text{Si}_2\text{N}_6]:\text{Eu}^{2+}$: 1.719(5)-1.843(7) Å) are slightly larger than distances found in other nitridosilicates.^[1,5,16,43,44] This can be attributed to the repulsion of the Si atoms in the pairs of edge-sharing SiN_4 tetrahedra (Si–Si: 2.363(4)-2.477(4) Å), which in turn is related to a reduced angle N–Si–N. Li–N distances range from 2.088(11) to 2.225(11) Å and are in good agreement with distances known from other nitrides and with the sum of the ionic radii.^[11,44-46]

Ca^{2+} and Mg^{2+} ions balance the charges of the anionic framework. Its coordination spheres are displayed in Figure 3. Ca^{2+} occupies two different sites with distorted octahedral coordination by N and with distances varying from 2.310(4)-2.744(5) Å. Mg^{2+} exhibits 4-fold rectangular surroundings by N. Mg–N bond lengths are in a range of 2.159(5)-2.199(5) Å. Additionally, there is one further N atom at a distance of 2.693(7) Å, its coordination to Mg1 is illustrated in Figure 3 by a dashed line. Ca–N as well as Mg–N distances correspond to the sums of the ionic radii (2.55 and 2.10 Å, respectively)^[45] as well as to distances known from other nitridosilicates.^[1,12,16] The Madelung part of the lattice energy has been calculated to confirm the crystal structure of $\text{Ca}_3\text{Mg}[\text{Li}_2\text{Si}_2\text{N}_6]:\text{Eu}^{2+}$.^[45,47-49] Therefore, the charge, distance, and coordination spheres of constituting ions were taken into account. MAPLE values for $\text{Ca}_3\text{Mg}[\text{Li}_2\text{Si}_2\text{N}_6]:\text{Eu}^{2+}$ and its

constituting binary and ternary nitrides are given in Table 3. The resulting deviation of 0.31% verifies the electrostatic consistency of the refined structure.

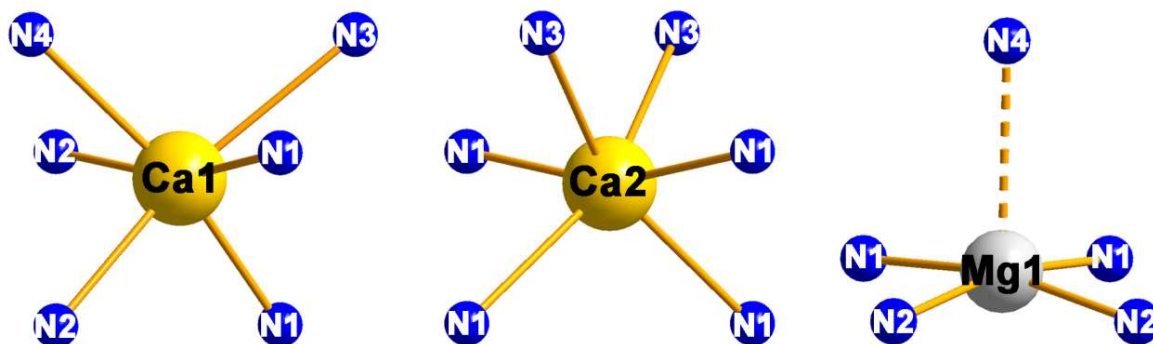


Figure 3. Coordination spheres of counterions Ca^{2+} and Mg^{2+} .

Table 2. Atomic Coordinates, Wyckoff Positions, and Equivalent Isotropic Displacement Parameters of $\text{Ca}_3\text{Mg}[\text{Li}_2\text{Si}_2\text{N}_6]:\text{Eu}^{2+}$

atom	Wyck.	x	y	z	$U_{\text{eq}}/\text{\AA}^2$
Ca1	8j	0.0500(2)	0.32384(11)	0.24678(9)	0.0068(2)
Ca2	4h	0	0.1840(2)	$\frac{1}{2}$	0.0085(3)
Si1	4i	0.3521(3)	0	0.4192(2)	0.0050(4)
Si2	4i	0.6885(3)	0	0.0632(2)	0.0048(4)
Mg1	4i	0.0623(5)	0	0.2220(2)	0.0094(5)
Li1	8j	0.1731(18)	0.1767(11)	0.0594(8)	0.015(2)
N1	8j	0.2335(7)	0.1447(4)	0.3513(4)	0.0070(8)
N2	8j	0.3413(7)	0.3566(5)	0.1179(4)	0.0064(8)
N3	4i	0.3418(10)	0	0.5703(5)	0.0084(12)
N4	4i	0.3943(11)	0	0.0921(5)	0.0068(11)

3.2 Crystal Structure and Nontypical Deep-Red Luminescence of $\text{Ca}_3\text{Mg}[\text{Li}_2\text{Si}_2\text{N}_6]:\text{Eu}^{2+}$

Table 3. MAPLE Values and MAPLE Sums $/\text{kJ}\cdot\text{mol}^{-1}$ for $\text{Ca}_3\text{Mg}[\text{Li}_2\text{Si}_2\text{N}_6]:\text{Eu}^{2+}$; Δ is the deviation between the MAPLE sum of $\text{Ca}_3\text{Mg}[\text{Li}_2\text{Si}_2\text{N}_6]:\text{Eu}^{2+}$ and the MAPLE sum of constituting binary and ternary nitrides ^[a]

atom	MAPLE	atom	MAPLE	Σ, Δ
$\text{Ca}1^{2+}$	2083	$\text{Li}1^+$	717	
$\text{Ca}2^{2+}$	1812	$\text{N}1^{3-}$	5056	
$\text{Si}1^{4+}$	9201	$\text{N}2^{3-}$	4951	
$\text{Si}2^{4+}$	9202	$\text{N}3^{3-}$	5440	$\Sigma = 58949$
$\text{Mg}1^{2+}$	2241	$\text{N}4^{3-}$	5439	$\Delta = 0.31\%$
Total MAPLE:				
$\text{Ca}_3\text{Mg}[\text{Li}_2\text{Si}_2\text{N}_6] = \text{Ca}_3\text{N}_2 + \frac{1}{3}\cdot\text{Mg}_3\text{N}_2 + \frac{2}{3}\cdot\text{Li}_2\text{SiN}_2 + \frac{2}{3}\cdot\text{LiSi}_2\text{N}_3 = 59131 \text{ kJ}\cdot\text{mol}^{-1}$				
[a] Typical partial MAPLE values $/\text{kJ}\cdot\text{mol}^{-1}$: Ca^{2+} : 1700-2200; Mg^{2+} : 2100-2500; Li^+ : 550-860; Si^{4+} : 9000-10200; N^{3-} : 4300-6200. ^[9, 16, 50-51]				

3.2.3.3 Luminescence

Addition of EuF_3 to the starting materials yielded a gray microcrystalline sample containing orange-colored crystals of $\text{Ca}_3\text{Mg}[\text{Li}_2\text{Si}_2\text{N}_6]:\text{Eu}^{2+}$. Under blue irradiation, the sample shows luminescence in the red spectral region. Because of inhomogeneity of the sample, luminescence investigations have been performed on single crystals of $\text{Ca}_3\text{Mg}[\text{Li}_2\text{Si}_2\text{N}_6]:\text{Eu}^{2+}$ in sealed silica glass capillaries. All crystals show comparable red emission under blue irradiation. Excitation of the title compound with a nominal dopant concentration of 1.7 mol% at 440 nm yields an emission band with a maximum at 734 nm and a full width at half-maximum (fwhm) of 2293 cm^{-1} (124 nm). The Eu^{2+} -doped compound exhibits a maximum absorption around 450 nm and is therefore efficiently excitable with UV to blue light, as provided, for example, by (In,Ga)N-LEDs. Excitation and emission spectra are illustrated in Figure 4.

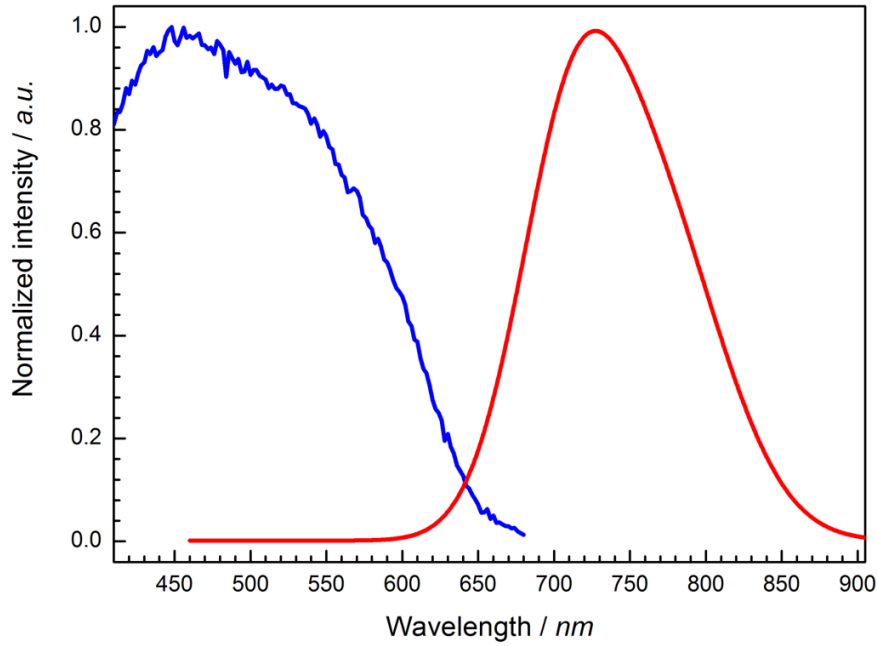


Figure 4. Excitation (blue) and emission (red) spectra of $\text{Ca}_3\text{Mg}[\text{Li}_2\text{Si}_2\text{N}_6]:\text{Eu}^{2+}$.

The broad emission band of $\text{Ca}_3\text{Mg}[\text{Li}_2\text{Si}_2\text{N}_6]:\text{Eu}^{2+}$ is assigned to parity allowed $4f^65d^1 \rightarrow 4f^7$ transitions in Eu^{2+} .^[33,52,53] Since Eu^{2+} is expected to occupy the Ca site, we assume that luminescence originates from octahedrally coordinated Eu^{2+} ions. The presence of two crystallographically different Ca sites with slightly differing distortion of the octahedra and therefore different interatomic distances influences the width of the emission band by broadening. A comparable 6-fold coordination can also be found in $\text{Ba}_3\text{Si}_6\text{O}_{12}\text{N}_2$ ^[54] and its solid-solution series $\text{Ba}_{1-x}\text{Sr}_x\text{Si}_6\text{O}_{12}\text{N}_2$ with $x \approx 0.4$ and 1. These compounds doped with 2 mol% Eu^{2+} exhibit broad emission bandwidth maxima between 523 and 549 nm (green luminescence) when irradiated with near-UV to blue light. In general, both the spectral position and the band width of the emission strongly depend on the energy level of 5d states of the activator ion, which in turn is influenced by the host lattice. The stronger the covalent interactions between Eu^{2+} and its surroundings, the smaller is the transition energy between 4f and 5d orbitals of the activator ion (nephelauxetic effect). For this reason and because of the higher formal charge of N^{3-} compared to O^{2-} , the 5d states of Eu^{2+} in $\text{Ca}_3\text{Mg}[\text{Li}_2\text{Si}_2\text{N}_6]:\text{Eu}^{2+}$ are at lower energies than those in $\text{Ba}_3\text{Si}_6\text{O}_{12}\text{N}_2:\text{Eu}^{2+}$ and $\text{Ba}_{1-x}\text{Sr}_x\text{Si}_6\text{O}_{12}\text{N}_2:\text{Eu}^{2+}$, respectively, and emission of $\text{Ca}_3\text{Mg}[\text{Li}_2\text{Si}_2\text{N}_6]:\text{Eu}^{2+}$ occurs at longer wavelengths.

Typical Eu^{2+} emission of other compound classes are in a range of 356-461 nm (fluorides), 360-540 nm (oxosilicates), 420-555 nm (aluminates and gallates), 470-660 nm (sulfides) and 529-670 nm (nitrides).^[55,56] The here presented nitridolithosilicate $\text{Ca}_3\text{Mg}[\text{Li}_2\text{Si}_2\text{N}_6]:\text{Eu}^{2+}$ is to the best of our knowledge and, except for $\text{CaO}:\text{Eu}^{2+}$ ($\lambda_{\text{em}} = 733 \text{ nm}$)^[57,58] and $M\text{H}_2:\text{Eu}^{2+}$ ($M = \text{Ca}, \text{Sr}, \text{Ba}$; $\lambda_{\text{em}} = 728\text{-}764 \text{ nm}$)^[59] the first and so far the only example of a Eu^{2+} -doped nitridosilicate that emits at fairly long wavelengths of $>700 \text{ nm}$.

Recently, we reported on luminescence investigations of the nitridomagnesosilicate $\text{Li}_2(\text{Ca}_{1-x}\text{Sr}_x)_2[\text{Mg}_2\text{Si}_2\text{N}_6]:\text{Eu}^{2+}$ ($x = 0$ and 0.06),^[60] with a nominal dopant concentration of 1 mol%. Just as $\text{Ca}_3\text{Mg}[\text{Li}_2\text{Si}_2\text{N}_6]:\text{Eu}^{2+}$, the crystal structure of $\text{Li}_2(\text{Ca}_{1-x}\text{Sr}_x)_2[\text{Mg}_2\text{Si}_2\text{N}_6]:\text{Eu}^{2+}$ contains $[\text{Si}_2\text{N}_6]^{10-}$ bow-tie units. In contrast to the here presented nitridolithosilicate with LiN_4 and SiN_4 tetrahedra as network-building structural motifs and Ca^{2+} and Mg^{2+} as counterions, Li^+ and Ca^{2+} compensate the negative charge of the network, which, in $\text{Li}_2(\text{Ca}_{1-x}\text{Sr}_x)_2[\text{Mg}_2\text{Si}_2\text{N}_6]:\text{Eu}^{2+}$, is made up of MgN_4 and SiN_4 tetrahedra. In the latter compound, chains of edge-sharing MgN_4 tetrahedra are interconnected by bow-tie units, forming *vierer* and *sechser* ring channels along $[100]$. Whereas Li^+ ions are located within *vierer* ring channels, Ca^{2+} (Sr^{2+}) ions, and therefore also Eu^{2+} ions show distorted octahedral coordination by N within *sechser* ring channels. When irradiated with blue light, narrow-band red emission also occurs at rather long wavelengths of 638 nm ($x = 0$) and 634 nm ($x = 0.06$) with $\text{fwhm} = 1513\text{-}1532 \text{ cm}^{-1}$, respectively.

Both $\text{Li}_2(\text{Ca}_{1-x}\text{Sr}_x)_2[\text{Mg}_2\text{Si}_2\text{N}_6]:\text{Eu}^{2+}$ and $\text{Ca}_3\text{Mg}[\text{Li}_2\text{Si}_2\text{N}_6]:\text{Eu}^{2+}$ exhibit similar body colors and show similarities in their absorption bands. The main difference between both nitridosilicates is the Stokes shift, which is larger for $\text{Ca}_3\text{Mg}[\text{Li}_2\text{Si}_2\text{N}_6]:\text{Eu}^{2+}$. This can be attributed to differences in the chemical surroundings of Eu^{2+} , which in each case is expected to occupy the Ca^{2+} (Sr^{2+}) site, and also to differences in the phonon frequencies of respective host lattices. $\text{Li}_2(\text{Ca}_{1-x}\text{Sr}_x)_2[\text{Mg}_2\text{Si}_2\text{N}_6]:\text{Eu}^{2+}$ exhibits only one crystallographic Ca site (Wyckoff position $4g$ of space group $C2/m$) with three different Ca–N distances between 2.49 and 2.75 Å. In $\text{Ca}_3\text{Mg}[\text{Li}_2\text{Si}_2\text{N}_6]:\text{Eu}^{2+}$, nine interatomic distances Ca–N of two Ca sites (Wyckoff positions $8j$ and $4h$ of space group $C2/m$) vary between 2.31 and 2.74 Å. This is, in comparison, a significantly larger spread and entails chemical differentiation of both sites, which eventually leads to a composed emission band of Eu^{2+} on either of the crystallographic sites. Moreover, the shorter bond lengths Ca–N in $\text{Ca}_3\text{Mg}[\text{Li}_2\text{Si}_2\text{N}_6]:\text{Eu}^{2+}$, especially occurring on the lowest symmetry Ca1 site, may entail efficient energy transfer from Eu^{2+} incorporated on the larger higher symmetry Ca2 site and thus also leads to a more pronounced red shift of the emission band for the Eu doping concentration investigated in this report. Whereas in $\text{Li}_2(\text{Ca}_{1-x}\text{Sr}_x)_2[\text{Mg}_2\text{Si}_2\text{N}_6]:\text{Eu}^{2+}$, infinite chains of edge-sharing MgN_4 tetrahedra are interconnected by $[\text{Si}_2\text{N}_6]^{10-}$ bow-tie units leading to

a three-periodic network, $\text{Ca}_3\text{Mg}[\text{Li}_2\text{Si}_2\text{N}_6]:\text{Eu}^{2+}$ consists of layers made up of LiN_4 and SiN_4 tetrahedra and isolated bow-tie units. Consequently, because of the lower degree of condensation and also the lower symmetry of the Ca1 site with its short Ca-N contact lengths, local lattice relaxation of Eu^{2+} in its excited state in $\text{Ca}_3\text{Mg}[\text{Li}_2\text{Si}_2\text{N}_6]:\text{Eu}^{2+}$ is expected to be larger than in $\text{Li}_2(\text{Ca}_{1-x}\text{Sr}_x)_2[\text{Mg}_2\text{Si}_2\text{N}_6]:\text{Eu}^{2+}$,^[61] resulting in a larger Stokes shift of the title compound.

Red emission and extremely narrow band widths with fwhm $<1200\text{ cm}^{-1}$ have been reported for $\text{Sr}[\text{Mg}_3\text{SiN}_4]:\text{Eu}^{2+}$ (1170 cm^{-1}) and $\text{Sr}[\text{LiAl}_3\text{N}_4]:\text{Eu}^{2+}$ (1180 cm^{-1}).^[16,34] Both compounds show a highly symmetric cube-like coordination of the alkaline earth ion by N.

3.2.4 Conclusions

In this contribution, we report on $\text{Ca}_3\text{Mg}[\text{Li}_2\text{Si}_2\text{N}_6]:\text{Eu}^{2+}$, a new nitridolithosilicate with exceptional luminescence properties. The compound was synthesized by solid-state metathesis reaction and could be obtained as orange-colored single crystals within an amorphous powder. The crystal structure of $\text{Ca}_3\text{Mg}[\text{Li}_2\text{Si}_2\text{N}_6]:\text{Eu}^{2+}$ is related to that of $\text{Ca}_2\text{Mg}[\text{Li}_4\text{Si}_2\text{N}_6]$. It consists of corner- and edge-sharing LiN_4 tetrahedra, intercalated by $[\text{Si}_2\text{N}_6]^{10-}$ bow-tie units forming anionic layers, which are separated by isolated $[\text{Si}_2\text{N}_6]^{10-}$ bow-tie units and Ca^{2+} and Mg^{2+} ions. The latter two act as counterions and compensate the negative charge of the anionic framework. Up to now, only a small number of nitridosilicates containing Li^+ and Mg^{2+} ions are known from literature, namely $\text{Ca}_2\text{Mg}[\text{Li}_4\text{Si}_2\text{N}_6]$, $\text{Li}_2\text{Ca}_2[\text{Mg}_2\text{Si}_2\text{N}_6]$, and $\text{Li}_2(\text{Ca}_{1.88}\text{Sr}_{0.12})[\text{Mg}_2\text{Si}_2\text{N}_6]$.^[12,60] Thereby, Li^+ and Mg^{2+} ions may either be part of the tetrahedral network or act as counterions. This behavior may significantly increase the variety of possible structures within the class of nitridosilicates.

Recently, the quest for narrow-band red-emitting phosphors has been triggered by attempts to improve luminescence properties of commercially available pc-LEDs for general illumination and signaling purposes.^[16,34,62] Meanwhile, LED technology for other specific applications is on the advance and will increasingly be pursued. This includes, for example, LED technology for plants, in order to replace currently used lamps to reduce costs and, seen in the long term, improve productivity by optimizing growth environments.^[63] Similar to requirements for LEDs applied for general illumination, LEDs with regard to application in horticulture have to be cheap, environmentally friendly, highly efficient, and reliable. Luminescence investigations on $\text{Ca}_3\text{Mg}[\text{Li}_2\text{Si}_2\text{N}_6]:\text{Eu}^{2+}$ show red emission peaking at 734 nm and a fwhm of 2293 cm^{-1} (124 nm). This represents an unexpected emission at fairly long wavelengths, not yet known for Eu^{2+} -doped nitrides. Despite emission $>700\text{ nm}$ and, therefore, too high energy loss beyond the

3.2 Crystal Structure and Nontypical Deep-Red Luminescence of $\text{Ca}_3\text{Mg}[\text{Li}_2\text{Si}_2\text{N}_6]:\text{Eu}^{2+}$

sensitivity of the human eye when applied in pc-LEDs, $\text{Ca}_3\text{Mg}[\text{Li}_2\text{Si}_2\text{N}_6]:\text{Eu}^{2+}$ may find application in more specialized fields like horticultural lighting.

3.2.5 References

- [1] Z. A. Gál, P. M. Mallinson, H. J. Orchard, S. J. Clarke, *Inorg. Chem.* **2004**, 43, 3998.
- [2] H. Yamane, F. J. DiSalvo, *J. Alloys Compd.* **1996**, 240, 33.
- [3] T. Watanabe, K. Nonaka, J. Li, K. Kishida, M. Yoshimura, *J. Ceram. Soc. Jpn.* **2012**, 120, 500.
- [4] T. M. M. Richter, R. Niewa, *Inorganics* **2014**, 2, 29.
- [5] T. Schlieper, W. Schnick, *Z. Anorg. Allg. Chem.* **1995**, 621, 1037.
- [6] W. Schnick, H. Huppertz, *Chem. - Eur. J.* **1997**, 3, 679.
- [7] D. Durach, W. Schnick, *Eur. J. Inorg. Chem.* **2015**, 4095.
- [8] M. Woike, W. Jeitschko, *Inorg. Chem.* **1995**, 34, 5105.
- [9] M. Zeuner, S. Pagano, W. Schnick, *Angew. Chem.* **2011**, 123, 7898; *Angew. Chem., Int. Ed.* **2011**, 50, 7754.
- [10] M. Kubus, H.-J. Meyer, *Z. Anorg. Allg. Chem.* **2013**, 639, 669.
- [11] P. Pust, A. S. Wochnik, E. Baumann, P. J. Schmidt, D. Wiechert, C. Scheu, W. Schnick, *Chem. Mater.* **2014**, 26, 3544.
- [12] S. Schmiechen, F. Nietschke, W. Schnick, *Eur. J. Inorg. Chem.* **2015**, 1592.
- [13] P. Strobel, S. Schmiechen, M. Siegert, A. Tücks, P. J. Schmidt, W. Schnick, *Chem. Mater.* **2015**, 27, 6109.
- [14] C. Poesl, L. Neudert, W. Schnick, *Eur. J. Inorg. Chem.* **2017**, 1067.
- [15] H.-J. Meyer, *Dalton Trans.* **2010**, 39, 5973.
- [16] S. Schmiechen, H. Schneider, P. Wagatha, C. Hecht, P. J. Schmidt, W. Schnick, *Chem. Mater.* **2014**, 26, 2712.
- [17] S. Schmiechen, P. Strobel, C. Hecht, T. Reith, M. Siegert, P. J. Schmidt, P. Huppertz, D. Wiechert, W. Schnick, *Chem. Mater.* **2015**, 27, 1780.
- [18] T. Takeda, N. Hirosaki, S. Funahshi, R.-J. Xie, *Chem. Mater.* **2015**, 27, 5892.
- [19] K. Uheda, N. Hirosaki, H. Yamamoto, *Phys. Status Solidi A* **2006**, 203, 2712.
- [20] D. G. Park, Y. Dong, F. J. DiSalvo, *Solid State Sci.* **2008**, 10, 1846.
- [21] P. Pust, F. Hintze, C. Hecht, V. Weiler, A. Locher, D. Zitnanska, S. Harm, D. Wiechert, P. J. Schmidt, W. Schnick, *Chem. Mater.* **2014**, 26, 6113.
- [22] H. Yamane, S. Kikkawa, M. Koizumi, *Solid State Ionics* **1987**, 25, 183.
- [23] M. S. Bhamra, D. J. Fray, *J. Mater. Sci.* **1995**, 30, 5381.
- [24] A. Ziegler, J. C. Idrobo, M. K. Cinibulk, C. Kisielowski, N. D. Browning, R. O. Ritchie, *Science* **2004**, 306, 1768.

- [25] K. H. Jack, *J. Mater. Sci.* **1976**, *11*, 1135.
- [26] H. Yamane, S. Kikkawa, M. Koizumi, *J. Power Sources* **1987**, *20*, 311.
- [27] D. Durach, L. Neudert, P. J. Schmidt, O. Oeckler, W. Schnick, *Chem. Mater.* **2015**, *27*, 4832.
- [28] L. Wang, H. Zhang, X.-J. Wang, B. Dierre, T. Suehiro, T. Takeda, N. Hirotsaki, R.-J. Xie, *Phys. Chem. Chem. Phys.* **2015**, *17*, 15797.
- [29] H. A. Höppe, H. Lutz, P. Morys, W. Schnick, A. Seilmeier, *J. Phys. Chem. Solids* **2000**, *61*, 2001.
- [30] R. Mueller-Mach, G. Mueller, M. R. Krames, H. A. Höppe, F. Stadler, W. Schnick, T. Jüstel, P. J. Schmidt, *Phys. Status Solidi A* **2005**, *202*, 1727.
- [31] M. Zeuner, P. J. Schmidt, W. Schnick, *Chem. Mater.* **2009**, *21*, 2467.
- [32] W. Schnick, *Phys. Status Solidi RRL* **2009**, *3*, A113.
- [33] R.-J. Xie, N. Hirotsaki, T. Takeda, T. Suehiro, *ECS J. Solid State Sci. Technol.* **2013**, *2*, R3031.
- [34] P. Pust, V. Weiler, C. Hecht, A. Tücks, A. S. Wochnik, A.-K. Henß, D. Wiechert, C. Scheu, P. J. Schmidt, W. Schnick, *Nat. Mater.* **2014**, *13*, 891.
- [35] M. Krames, G. O. Müller, R. Mueller-Mach, H.-H. Bechtel, P. J. Schmidt, *PCT Int. Appl. WO2010131133 A1*, **2010**.
- [36] T. Brokamp, Thesis, Universität Dortmund: Germany, **1991**.
- [37] G. M. Sheldrick, University of Göttingen: Germany, **1997**.
- [38] G. M. Sheldrick, *Acta Crystallogr., Sect. A: Found. Crystallogr.* **2008**, *64*, 112.
- [39] G. M. Sheldrick, University of Göttingen: Germany, **1997**.
- [40] F. Liebau, *Structural Chemistry of Silicates*, Springer, Berlin, **1986**. The terms *dreier* ring, *vierer* ring, *sechser* ring and *achter* ring was coined by Liebau and is derived from the German words *drei* = 3, *vier* = 4, *sechs* = 6 and *acht* = 8. A *dreier* ring comprises three tetrahedra centers.
- [41] S. Pagano, S. Lupart, M. Zeuner, W. Schnick, *Angew. Chem.* **2009**, *121*, 6453; *Angew. Chem., Int. Ed.* **2009**, *48*, 6335.
- [42] S. Pagano, S. Lupart, S. Schmichen, W. Schnick, *Z. Anorg. Allg. Chem.* **2010**, *636*, 1907.
- [43] M. Zeuner, S. Pagano, S. Hug, P. Pust, S. Schmichen, C. Scheu, W. Schnick, *Eur. J. Inorg. Chem.* **2010**, 4945.
- [44] S. Lupart, S. Pagano, O. Oeckler, W. Schnick, *Eur. J. Inorg. Chem.* **2011**, 2118.
- [45] W. H. Baur, *Crystallogr. Rev.* **1987**, *1*, 59.

- [46] P. Wagatha, P. Pust, V. Weiler, A. S. Wochnik, P. J. Schmidt, C. Scheu, W. Schnick, *Chem. Mater.* **2016**, 28, 1220.
- [47] R. Hübenthal, University of Gießen: Germany, **1993**.
- [48] R. Hoppe, *Angew. Chem.* **1966**, 78, 52; *Angew. Chem., Int. Ed. Engl.* **1966**, 5, 95.
- [49] R. Hoppe, *Angew. Chem.* **1970**, 82, 7; *Angew. Chem., Int. Ed. Engl.* **1970**, 9, 25.
- [50] S. Lupart, G. Gregori, J. Maier, W. Schnick, *J. Am. Chem. Soc.* **2012**, 134, 10132.
- [51] S. Lupart, W. Schnick, *Z. Anorg. Allg. Chem.* **2012**, 638, 2015.
- [52] P. Dorenbos, *J. Phys.: Condens. Matter* **2003**, 15, 2645.
- [53] Y.-C. Lin, M. Karlsson, M. Bettinelli, *Top. Curr. Chem.* **2016**, 374, 21.
- [54] C. Braun, M. Seibald, S. L. Börger, O. Oeckler, T. D. Boyko, A. Moewes, G. Miehe, A. Tücks, W. Schnick, *Chem. - Eur. J.* **2010**, 16, 9646.
- [55] P. Dorenbos, *J. Lumin.* **2003**, 104, 239.
- [56] D. Wilhelm, D. Baumann, M. Seibald, K. Wurst, G. Heymann, H. Huppertz, *Chem. Mater.* **2017**, 29, 1204.
- [57] P. M. Jaffe, E. Banks, *J. Electrochem. Soc.* **1955**, 102, 518.
- [58] N. Yamashita, *J. Electrochem. Soc.* **1993**, 140, 840.
- [59] N. Kunkel, H. Kohlmann, A. Sayede, M. Springborg, *Inorg. Chem.* **2011**, 50, 5873.
- [60] P. Strobel, V. Weiler, C. Hecht, P. J. Schmidt, W. Schnick, *Chem. Mater.* **2017**, 29, 1377.
- [61] A. Meijerink, G. Blasse, *J. Lumin.* **1989**, 43, 283.
- [62] P. Pust, P. J. Schmidt, W. Schnick, *Nat. Mater.* **2015**, 14, 454.
- [63] P. M. Pattison, J. Y. Tsao, M. R. Krames, *Acta Hortic.* **2016**, 1134, 413.

4 Conclusion and Outlook

Ga-containing nitrides are intriguing compounds regarding their crystal structures and their application in the emerging area of LED-technology. The ternary alloys InGaN/AlGaN represent the fundamentals of energy-efficient LED lighting for general illumination.^[1] Additionally, as $\text{Mg}_3\text{GaN}_3\text{:Eu}^{2+}$,^[2] $\text{Ba}_3\text{Ga}_3\text{N}_5\text{:Eu}^{2+}$,^[3] and $\text{Ba}[\text{Mg}_2\text{Ga}_2\text{N}_4]\text{:Eu}^{2+}$ ^[4] demonstrate, Eu^{2+} -doped nitridogallates may show red luminescence after irradiation with UV to green light. This behavior makes them promising candidates for an application as luminescent materials in phosphor-converted LEDs as well. Nevertheless, since nitridogallates have not yet been obtained as bulk materials, they are not suitable for a commercial application. Investigations of novel synthetic approaches may help to increase their yield and thus pave the way for practical application. Furthermore, by the employment of alternative synthetic strategies, formation of thermodynamic products may be avoided and novel structures can be obtained.

The common synthesis route for nitridogallates starts from pure metals, NaN_3 as nitrogen source, and Na metal as fluxing agent in weld-shut Ta ampules. It is known as NaN_3 route. Thereby, already known nitridogallates $\text{Ca}_2\text{MgGa}_3\text{N}_5$,^[5] $\text{Sr}_3\text{Ga}_3\text{N}_5$,^[6] $\text{Ba}_3\text{Ga}_2\text{N}_4$,^[7] and several others were obtained in the past. $\text{CaMg}_2\text{GaN}_3$ and $\text{CaMg}_2\text{Ga}_2\text{N}_4$ represent the first quaternary nitridogallates, which were synthesized by employing a solid-state metathesis reaction. The driving force of this reaction is the formation of a metathesis salt, namely, LiF, which contributes to avoiding thermodynamic sinks and the synthesis of already known compounds. $\text{CaMg}_2\text{GaN}_3$ and $\text{CaMg}_2\text{Ga}_2\text{N}_4$ were obtained in high percentages. Since previous investigations of novel nitridogallates are based on single-particle approaches, solid-state metathesis reactions represent a breakthrough in preparative chemistry of nitridogallates. It opens up a completely new approach for novel nitridogallates and paves the way for their application as phosphors in the field of LED lighting.

Regarding syntheses and crystal structures, nitridogermanates are very similar to nitridogallates. Syntheses are also performed by employing the NaN_3 route, even with slight variations, for example, by substituting Ge metal through GeO_2 . Furthermore, and in contrast to nitridogallates, addition of small amounts of Li in order to facilitate crystal growth is reported. DiSalvo et al. described the charge balanced substitutability of 2Ga^{3+} by Mg^{2+} and Ge^{4+} , demonstrated by the example of $\text{Sr}_3\text{MgGeN}_4$ and the homeotypic nitridogallate $\text{Sr}_3\text{Ga}_2\text{N}_4$.^[6,8] A few years later, they

reported on the homeotypic compounds $\text{Sr}[\text{Mg}_3\text{GeN}_4]$ and $\text{Sr}[\text{Mg}_2\text{Ga}_2\text{N}_4]$,^[9] which represent the second example of substitutability and therefore close structural relationship between nitridogallates and nitridogermanates. Within this thesis, several new representatives showing the phenomenon of substitutability of network-building ions were synthesized, characterized, and compared with their isostructural compounds. These include the novel Mg-containing nitridogermanate $\text{Ca}_2\text{Mg}_5\text{GeN}_6$, which is isostructural to $\text{CaMg}_2\text{GaN}_3$. $\text{Ca}_2\text{Mg}_5\text{GeN}_6$ represents the first layered nitridogermanate known in the literature.

Furthermore, the homeotypic nitrides $\text{Ca}_4\text{Mg}_5\text{Ge}_3\text{N}_{10}$ and $\text{Sr}_2\text{Mg}_3\text{GaN}_{4.33}$ were investigated. $\text{Ca}_4\text{Mg}_5\text{Ge}_3\text{N}_{10}$ represents the Ge-containing equivalent to the already known nitridogallate $\text{Ca}_2\text{MgGa}_3\text{N}_5$.^[5] As mentioned above, doubling the sum formula of $\text{Ca}_2\text{MgGa}_3\text{N}_5$ leading to " $\text{Ca}_4\text{Mg}_2\text{Ga}_6\text{N}_{10}$ ", followed by a charge balanced substitution of 6 Ga^{3+} by 3 Mg^{2+} and 3 Ge^{4+} results in $\text{Ca}_4\text{Mg}_5\text{Ge}_3\text{N}_{10}$. Thereby, the number of central atoms (8), their positive charge (+22) and, thus, the degree of condensation κ (i.e. the atomic ratio of network-building ions to the number of N atoms surrounding them) remains unchanged. $\text{Sr}_2\text{Mg}_3\text{GaN}_{4.33}$ exhibits same structural motifs as $\text{Ca}_4\text{Mg}_5\text{Ge}_3\text{N}_{10}$, and $\text{Ca}_2\text{MgGa}_3\text{N}_5$. Differences in their sum formulas arise from an exchange of Ca^{2+} by Sr^{2+} , which entails an expansion of the anionic network. This leads to a destabilization of the anionic framework, which has to be compensated by further changes, here, by inverting the ratio $\text{Mg}^{2+}:\text{Ga}^{3+}$ from 1:3 to 3:1 (ionic radii of fourfold coordinated ions: Mg^{2+} 0.64 Å, Ga^{3+} 0.48 Å).^[10] In order to maintain electroneutrality, this inversion is accompanied by modifications in the anionic network, more precisely, in the occupation factors of N sites. Regarding previously investigated nitridogallates, $\text{Sr}_2\text{Mg}_3\text{GaN}_{4.33}$ is the first existing Sr-analogue of a known Ca-containing nitridogallate. Furthermore, it illustrates the structural versatility of nitridogallates.

$\text{Ca}_4\text{Mg}_5\text{Ge}_3\text{N}_{10}$, $\text{Sr}_2\text{Mg}_3\text{GaN}_{4.33}$, and $\text{Ca}_2\text{MgGa}_3\text{N}_5$ represent higher condensed variants ($\kappa = 0.80$) of thoroughly investigated $M_2\text{Si}_5\text{N}_8$ ($M = \text{Sr}, \text{Ba}$; $\kappa = 0.625$),^[11] which is due to additional edge-sharing of tetrahedra in the Mg-containing nitrides. The higher degree of condensation may possibly be ascribed to the incorporation of Mg atoms, which modifies the charge as well as the covalency of the anionic substructure. Since $(\text{Sr}, \text{Ba})_2\text{Si}_5\text{N}_8:\text{Eu}^{2+}$ (2-5-8-phosphor) shows intense orange to red emission and is currently applied in illumination-grade white pc-LEDs, Eu^{2+} -doping and investigations of luminescence properties of the here presented higher condensed variants are of particular interest for subsequent research. Moreover, substituting Ge^{4+} by Si^{4+} in $\text{Ca}_4\text{Mg}_5\text{Ge}_3\text{N}_{10}$ would lead to " $\text{Ca}_4\text{Mg}_5\text{Si}_3\text{N}_{10}$ ". Based on previous findings in the field of Eu^{2+} -doped nitridosilicates, this "higher condensed 2-5-8-phosphor" is also expected to

show luminescence upon doping with Eu^{2+} . Resulting luminescence properties and comparison with common 2-5-8-phosphors may help to understand structure-property relations in more detail.

This same objective, understanding structure-property relations, was previously pursued by screening compounds crystallizing in the UCr_4C_4 and related structure types, which were discussed to be attractive host lattices for luminescent materials. Therefore, several compounds in the classes of nitridogallates ($\text{Ba}[\text{Mg}_2\text{Ga}_2\text{N}_4]$), nitridoaluminates ($M[\text{Mg}_2\text{Al}_2\text{N}_4]$ with $M = \text{Ca}, \text{Sr}, \text{Ba}$, and $M[\text{LiAl}_3\text{N}_4]$ with $M = \text{Ca}, \text{Sr}$),^[4,12,13] and nitridosilicates ($M[\text{Mg}_3\text{SiN}_4]$)^[14,15] were thoroughly investigated with respect to their luminescence properties upon doping with Eu^{2+} . Nevertheless, there were no studies concerning luminescence properties of Eu^{2+} -doped nitridogermanates known so far, not even in the UCr_4C_4 type of structure. In this thesis, the novel Mg-containing nitridogermanate $\text{Ba}[\text{Mg}_3\text{GeN}_4]:\text{Eu}^{2+}$ was investigated and the absence of luminescence was discussed with the help of theoretical calculations of electronic properties. In summary, studies concerning the band gaps of nitridogallates and nitridogermanates reveal that they are mostly too small for an emission within the range of the visible light, and, therefore, an application in pc-LEDs. However, Mg-containing quaternary nitridogallates and nitridogermanates always show mixed occupation Mg/Ga, or Mg/Ge on tetrahedral center sites. The aforementioned investigations of nitrides crystallizing in UCr_4C_4 and related structure types show that ordering of tetrahedrally coordinated network ions leads to more advantageous luminescence properties compared to those, which exhibit disordered tetrahedral positions. An ordered framework within the classes of nitridogallates and nitridogermanates may be obtained by combination of, for example, Li^+ and $\text{Ga}^{3+}/\text{Ge}^{4+}$ as tetrahedral network ions. The marked differences in the ionic charges will presumably result in an ordered network, as was already illustrated by the example of $\text{Ca}[\text{LiAl}_3\text{N}_4]$. Moreover, a few Li-containing nitridogallates and nitridogermanates are known in the literature, namely, LiMGaN_2 ($M = \text{Ca}, \text{Sr}$),^[16,17] $\text{LiBa}_5\text{GaN}_3\text{F}_5$,^[18] and $\text{Li}_4\text{Sr}_3\text{Ge}_2\text{N}_6$.^[19] Thereby, Li^+ acts as counter ion and helps to balance the charges of the anionic network. Novel compounds containing Li as tetrahedrally coordinated ion would increase both the number of known compounds, as well as the structural variety of nitridogallates and nitridogermanates.

Li in tetrahedral coordination by N is, for example, known from the LED-phosphor $\text{Sr}[\text{LiAl}_3\text{N}_4]:\text{Eu}^{2+}$.^[13] In the course of this work, we came across $\text{Ca}_3\text{Mg}[\text{Li}_2\text{Si}_2\text{N}_6]:\text{Eu}^{2+}$, a nitridosilicate with LiN_4 and SiN_4 tetrahedra as common structural motifs. The compound shows luminescence at wavelengths of >700 nm. Because a significant part of the emitted light is

outside the sensitivity range of the human eye, an application of $\text{Ca}_3\text{Mg}[\text{Li}_2\text{Si}_2\text{N}_6]:\text{Eu}^{2+}$ as luminescent material in illumination-grade white pc-LEDs would not be beneficial. However, luminescent materials are not limited to an application in pc-LEDs for general illumination purposes. The nontypical deep-red luminescence of $\text{Ca}_3\text{Mg}[\text{Li}_2\text{Si}_2\text{N}_6]:\text{Eu}^{2+}$ provides optimal conditions for application in more specialized fields, for example, in lifestyle products like smart bracelets, in the medical field, or, especially, in horticulture.

In this thesis, a novel synthetic approach for nitridogallates could be established and several new compounds in the classes of nitridogallates, nitridogermanates, and nitridosilicates as well as their structural relations could be investigated. Moreover, exceptional luminescence properties of a novel Eu^{2+} -doped nitridolithosilicate were presented. The findings of this thesis raise a further incentive to investigate novel compounds in the classes of nitridogallates, nitridogermanates and nitridosilicates in order to get detailed structural insights that will help in understanding structure-property relations and simultaneously enhance the structural variety of these interesting compound classes.

References

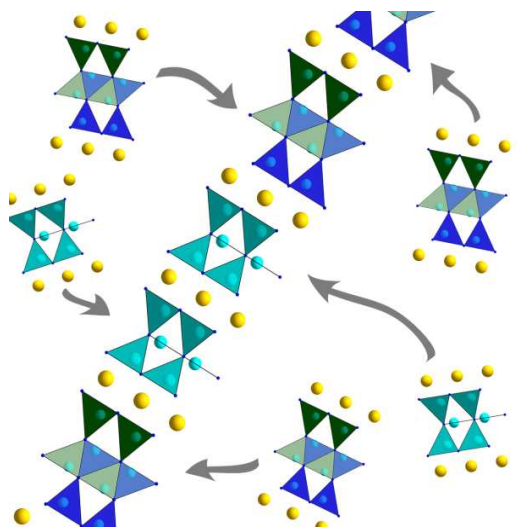
- [1] C. Ronda, *Luminescence - From Theory to Applications*, WILEY-VCH, Weinheim, **2008**.
- [2] F. Hintze, N. W. Johnson, M. Seibald, D. Muir, A. Moewes, W. Schnick, *Chem. Mater.* **2013**, 25, 4044.
- [3] F. Hintze, F. Hummel, P. J. Schmidt, D. Wiechert, W. Schnick, *Chem. Mater.* **2012**, 24, 402.
- [4] P. Pust, F. Hintze, C. Hecht, V. Weiler, A. Locher, D. Zitnanska, S. Harm, D. Wiechert, P. J. Schmidt, W. Schnick, *Chem. Mater.* **2014**, 26, 6113.
- [5] F. Hintze, W. Schnick, *Z. Anorg. Allg. Chem.* **2012**, 638, 2243.
- [6] S. J. Clarke, F. J. DiSalvo, *Inorg. Chem.* **1997**, 36, 1143.
- [7] H. Yamane, F. J. DiSalvo, *Acta Crystallogr., Sect. C: Cryst. Struct. Commun.* **1996**, 52, 760.
- [8] D. G. Park, Z. A. Gál, F. J. DiSalvo, *J. Alloys Compd.* **2003**, 360, 85.
- [9] D. G. Park, Y. Dong, F. J. DiSalvo, *Solid State Sci.* **2008**, 10, 1846.
- [10] W. H. Baur, *Crystallogr. Rev.* **1987**, 1, 59.

- [11] T. Schlieper, W. Milius, W. Schnick, *Z. Anorg. Allg. Chem.* **1995**, 621, 1037.
- [12] P. Pust, A. S. Wochnik, E. Baumann, P. J. Schmidt, D. Wiechert, C. Scheu, W. Schnick, *Chem. Mater.* **2014**, 26, 3544.
- [13] P. Pust, V. Weiler, C. Hecht, A. Tücks, A. S. Wochnik, A.-K. Henß, D. Wiechert, C. Scheu, P. J. Schmidt, W. Schnick, *Nat. Mater.* **2014**, 13, 891.
- [14] S. Schmiechen, H. Schneider, P. Wagatha, C. Hecht, P. J. Schmidt, W. Schnick, *Chem. Mater.* **2014**, 26, 2712.
- [15] S. Schmiechen, P. Strobel, C. Hecht, T. Reith, M. Siegert, P. J. Schmidt, P. Huppertz, D. Wiechert, W. Schnick, *Chem. Mater.* **2015**, 27, 1780.
- [16] M. S. Bailey, F. J. DiSalvo, *J. Alloys Compd.* **2006**, 417, 50.
- [17] D. G. Park, Z. A. Gál, F. J. DiSalvo, *J. Alloys Compd.* **2003**, 353, 107.
- [18] F. Hintze, W. Schnick, *Solid State Sci.* **2010**, 12, 1368.
- [19] D. G. Park, Z. A. Gál, F. J. DiSalvo, *J. Solid State Chem.* **2003**, 172, 166.

5 Summary

5.1 Layered Nitridomagnesogallates $\text{CaMg}_2\text{GaN}_3$ and $\text{CaMg}_2\text{Ga}_2\text{N}_4$

The quaternary nitrides $\text{CaMg}_2\text{GaN}_3$ and $\text{CaMg}_2\text{Ga}_2\text{N}_4$ were synthesized by means of solid-state metathesis reactions. A powder of $\text{CaMg}_2\text{GaN}_3$ was obtained from a mixture of Ca_3N_2 , Mg_3N_2 , GaF_3 , and Li_3N , which was placed in a tungsten crucible and heated in a radio-frequency furnace under a N_2 atmosphere to 850 °C. Block-like single crystals of $\text{CaMg}_2\text{Ga}_2\text{N}_4$ were obtained by reaction of $\text{Ca}(\text{NH}_2)_2$, $\text{Mg}(\text{NH}_2)_2$, GaF_3 , and Li_3N in sealed Ta ampules in a tube

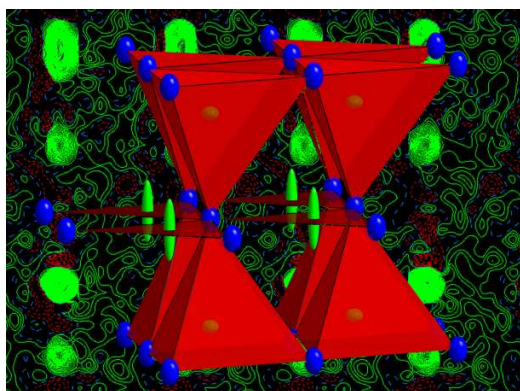


furnace at 1000 °C. Thereby, CsCl was added as flux. The crystal structures were successfully solved and refined using X-ray diffraction on powders [$\text{CaMg}_2\text{GaN}_3$: $P6_3/mmc$ (no. 194), $a = 3.43093(8)$, $c = 17.3989(5)$ Å, $V = 177.368(9)$ Å³, $Z = 2$] and on single-crystals [$\text{CaMg}_2\text{Ga}_2\text{N}_4$: $P\bar{3}m1$ (no. 164), $a = 3.3859(3)$, $c = 11.2378(11)$ Å, $V = 111.57(2)$ Å³, $Z = 1$]. TEM investigations confirmed the metrics of both crystal structures and showed the presence of both compounds as side products within one reaction batch. The crystal structures of $\text{CaMg}_2\text{GaN}_3$ and

$\text{CaMg}_2\text{Ga}_2\text{N}_4$ are closely related to each other and show a marked degree of similarity within the ab plane. They contain layers made up of either tetrahedral MN_4 units ($\text{CaMg}_2\text{Ga}_2\text{N}_4$) or both tetrahedral MN_4 units and planar MN_3 triangles ($\text{CaMg}_2\text{GaN}_3$) with mixed occupation Mg and Ga of tetrahedral central sites. Both structures differ in their composition of anionic layers and their stacking along c . Therefore, and as indicated by TEM studies, which show the presence of another nitridomagnesogallate with trigonal metrics and comparable parameters a and b as a minor side phase, the formation of composite crystals seems likely. In this contribution, we could show that solid-state metathesis reactions represent a promising and new synthetic approach for nitridogallates. It opens up a wide range of novel possible crystal structures and high yields of the obtained products.

5.2 $\text{Ca}_2\text{Mg}_5\text{GeN}_6$ – A Layered Nitridomagnesogermanate

The nitridomagnesogermanate $\text{Ca}_2\text{Mg}_5\text{GeN}_6$ was synthesized from pure elements, NaN_3 , and Na metal as fluxing agent in sealed Ta ampules at 780 °C. It crystallizes in the form of colorless platelet-like crystals, which rapidly undergo hydrolysis when exposed to air and moisture. Structure solution and refinement of $\text{Ca}_2\text{Mg}_5\text{GeN}_6$ was performed on the basis of single-crystal X-ray diffraction data [space group $P6_3/mmc$ (no. 194), $Z = 1$, $a = 3.453(2)$, $c = 17.506(13)$ Å,

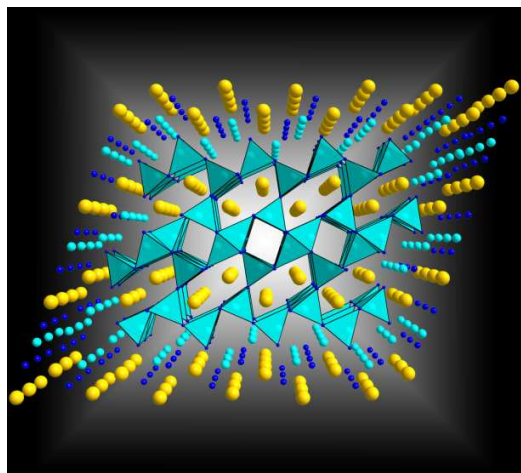


and $V = 180.8(2)$ Å³]. $\text{Ca}_2\text{Mg}_5\text{GeN}_6$ represents the first example of a quaternary nitridogermanate containing Ca^{2+} as counterion and is even the first layered nitridogermanate known to date. Its layers are made up of corner-sharing $(\text{Mg/Ge})\text{N}_4$ tetrahedra and corner-sharing $(\text{Mg/Ge})\text{N}_3$ triangles with mixed occupancy of Mg and Ge. Ca^{2+} ions are located in between the sheets and balance the charges of the anionic network. Despite different charges of center

ions (Al^{3+} and Ga^{3+} compared to Ge^{4+}), the crystal structure of $\text{Ca}_2\text{Mg}_5\text{GeN}_6$ is closely related to that of the nitridomagnesioaluminate $\text{CaMg}_2\text{AlN}_3$, the carbides ScAl_3C_3 and UAl_3C_3 , and thus to $\text{CaMg}_2\text{GaN}_3$. This clearly shows the substitutability of center ions, leading to new compounds in other classes of nitrides while maintaining the same structural motifs. Since Eu^{2+} -doped nitridoaluminates and -silicates are suitable for application in high-performance pc-LEDs, research on novel structures within the class of nitridogermanates is quite promising. These can be transferred to nitridoaluminates and -silicates, and thus pave the way to new host lattices with possible application in pc-LEDs.

5.3 $\text{Ca}_4\text{Mg}_5\text{Ge}_3\text{N}_{10}$ and $\text{Sr}_2\text{Mg}_3\text{GaN}_{4.33}$ – Two Mg-Containing Nitrides and Their Structural Relation to $(\text{Sr},\text{Ba})_2\text{Si}_5\text{N}_8$

The quaternary nitrides $\text{Ca}_4\text{Mg}_5\text{Ge}_3\text{N}_{10}$ and $\text{Sr}_2\text{Mg}_3\text{GaN}_{4.33}$ were synthesized employing the Na azide route in weld-shut Ta ampules at 780 and 760 °C, respectively. Both compounds are homeotypic and crystallize in the monoclinic space group $C2/m$ (no. 12). The crystal structures were solved and refined on the basis of single-crystal X-ray diffraction data [$\text{Ca}_4\text{Mg}_5\text{Ge}_3\text{N}_{10}$: $a = 11.269(3)$, $b = 3.3267(11)$, $c = 8.008(3)$ Å, $\beta = 109.80(2)^\circ$, $V = 282.44(16)$ Å³, $Z = 1$;

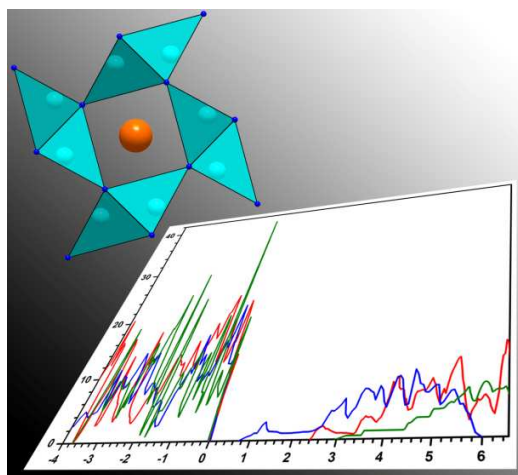


$\text{Sr}_2\text{Mg}_3\text{GaN}_{4.33}$: $a = 11.737(2)$, $b = 3.4610(7)$, $c = 7.8610(16)$ Å, $\beta = 108.03(3)^\circ$, $V = 303.65(12)$ Å³, $Z = 1$). The three-periodic anionic substructures of both nitrides represent more highly condensed variants of the $M^{\text{II}}_2\text{Si}_5\text{N}_8$ ($M^{\text{II}} = \text{Sr}, \text{Ba}$) type of structure and therefore illustrate the strong relationship between nitridogermanates, nitridogallates and nitridosilicates. The crystal structures of $\text{Ca}_4\text{Mg}_5\text{Ge}_3\text{N}_{10}$ and $\text{Sr}_2\text{Mg}_3\text{GaN}_{4.33}$ are made up of MN_4 tetrahedra with mixed occupation of central

atoms Mg/Ge, or Mg/Ga. Corner- and edge-sharing of MN_4 tetrahedra results in *vierer* and *sechser* ring channels along [010]. Alkaline earth metal ions Ca^{2+} and Sr^{2+} are located inside the channels of *sechser* rings, whereas the *vierer* ring channels are not filled. The same structural motifs can be found in the homeotypic nitridogallate $\text{Ca}_2\text{MgGa}_3\text{N}_5$. The inverse ratio of central atoms Mg and Ga in $\text{Ca}_2\text{MgGa}_3\text{N}_5$ (Mg:Ga = 1:3) and $\text{Sr}_2\text{Mg}_3\text{GaN}_{4.33}$ (Mg:Ga = 3:1) may be explained by an expansion of the anionic network, which is due to the exchange of Ca^{2+} through larger Sr^{2+} , and accompanied by slight modifications in the anionic network.

5.4 The Crystal Structure of Nitridomagnesogermanate $\text{Ba}[\text{Mg}_3\text{GeN}_4]:\text{Eu}^{2+}$ and Theoretical Calculations of Its Electronic Properties

$\text{Ba}[\text{Mg}_3\text{GeN}_4]:\text{Eu}^{2+}$ has been synthesized by the NaN_3 route from pure metals Ba, Mg, and Ge, NaN_3 , and Na metal as fluxing agent in weld-shut Ta ampules at 780 °C. The crystal structure was solved and refined on the basis of single-crystal X-ray diffraction data. $\text{Ba}[\text{Mg}_3\text{GeN}_4]:\text{Eu}^{2+}$ crystallizes in the UCr_4C_4 type of structure [space group $I4/m$ (no. 87), $a = 8.3921(12)$, $c = 3.4813(7)$ Å, $Z = 2$] and exhibits a highly condensed anionic network made up of statistically

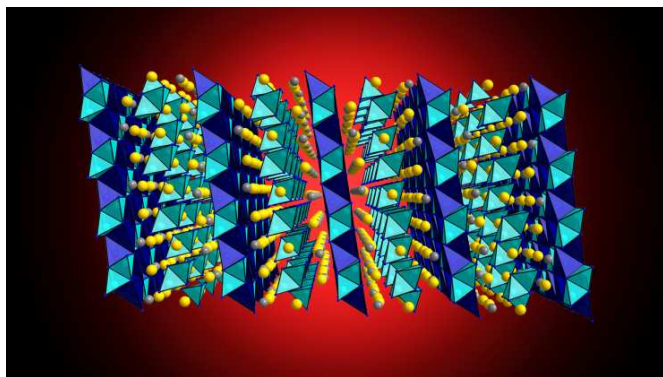


disordered $(\text{Mg}/\text{Ge})\text{N}_4$ tetrahedra. These are connected to each other through common vertices and edges by forming *vierer* ring channels along $[001]$. Ba^{2+} is located within every second channel and has a cube-like coordination by eight N. The same structure can be found in the nitridoaluminates $M[\text{Mg}_2\text{Al}_2\text{N}_4]$ ($M = \text{Ca}, \text{Sr}, \text{Ba}$) and $M[\text{LiAl}_3\text{N}_4]$ ($M = \text{Ca}, \text{Sr}$), the nitridogallate $\text{Ba}[\text{Mg}_2\text{Ga}_2\text{N}_4]$, and the nitridosilicates $M[\text{Mg}_3\text{SiN}_4]$ ($M = \text{Sr}, \text{Ba}$). Upon doping with Eu^{2+} , and after irradiation with UV to green light,

all of these compounds show red luminescence. In contrast, $\text{Ba}[\text{Mg}_3\text{GeN}_4]:\text{Eu}^{2+}$ show no luminescence under UV to green irradiation, neither at room temperature nor under cooling with liquid nitrogen. Theoretical calculations of electronic properties of $\text{Ba}[\text{Mg}_3\text{GeN}_4]:\text{Eu}^{2+}$ were performed to understand the absence of photoluminescence within the visible range as well as to allow for comparison with other luminescent materials, which are structurally related to $\text{Ba}[\text{Mg}_3\text{GeN}_4]:\text{Eu}^{2+}$.

5.5 Crystal Structure and Nontypical Deep-Red Luminescence of $\text{Ca}_3\text{Mg}[\text{Li}_2\text{Si}_2\text{N}_6]:\text{Eu}^{2+}$

A solid-state metathesis reaction in weld-shut Ta ampules yielded an inhomogeneous sample with orange-colored crystals of $\text{Ca}_3\text{Mg}[\text{Li}_2\text{Si}_2\text{N}_6]:\text{Eu}^{2+}$. The crystal structure was solved and refined on the basis of single-crystal X-ray diffraction data. $\text{Ca}_3\text{Mg}[\text{Li}_2\text{Si}_2\text{N}_6]:\text{Eu}^{2+}$ crystallizes in the monoclinic space group $C2/m$ (no. 12) with $a = 5.966(1)$, $b = 9.806(2)$, $c = 11.721(2)$ Å, $\beta = 99.67(3)^\circ$, and $Z = 4$. The layered anionic network of the nitridolithosilicate is made up of



edge- and corner-sharing LiN_4 tetrahedra and $[\text{Si}_2\text{N}_6]^{10-}$ bow-tie units. Layers are separated by further $[\text{Si}_2\text{N}_6]^{10-}$ bow-tie units, and by Ca^{2+} and Mg^{2+} ions, which balance the charges of the anionic framework. The crystal structure of $\text{Ca}_3\text{Mg}[\text{Li}_2\text{Si}_2\text{N}_6]:\text{Eu}^{2+}$ is closely related to that of $\text{Ca}_2\text{Mg}[\text{Li}_4\text{Si}_2\text{N}_6]$. The differences

are the additional bow-tie units in between layers in the crystal structure of $\text{Ca}_3\text{Mg}[\text{Li}_2\text{Si}_2\text{N}_6]:\text{Eu}^{2+}$. However, rare-earth-doped nitridosilicates have been intensively studied for solid-state lighting. Upon irradiation with UV to blue light, red emission of $\text{Ca}_3\text{Mg}[\text{Li}_2\text{Si}_2\text{N}_6]:\text{Eu}^{2+}$ at exceptionally long wavelengths ($\lambda_{\text{em}} = 734$ nm, $\text{fwhm} \approx 2293$ cm^{-1}) is observed. Comparable luminescence properties are not yet known for any Eu^{2+} -doped nitrides. According to emission in the near-infrared, application of $\text{Ca}_3\text{Mg}[\text{Li}_2\text{Si}_2\text{N}_6]:\text{Eu}^{2+}$ as luminescent material in LEDs for specialized fields, for example, in horticultural lighting appears promising.

6 Appendix

6.1 Supporting Information for Chapter 2.2

Christine Poesl, Lukas Neudert, and Wolfgang Schnick, *Eur. J. Inorg. Chem.* **2017**, 1067-1074.

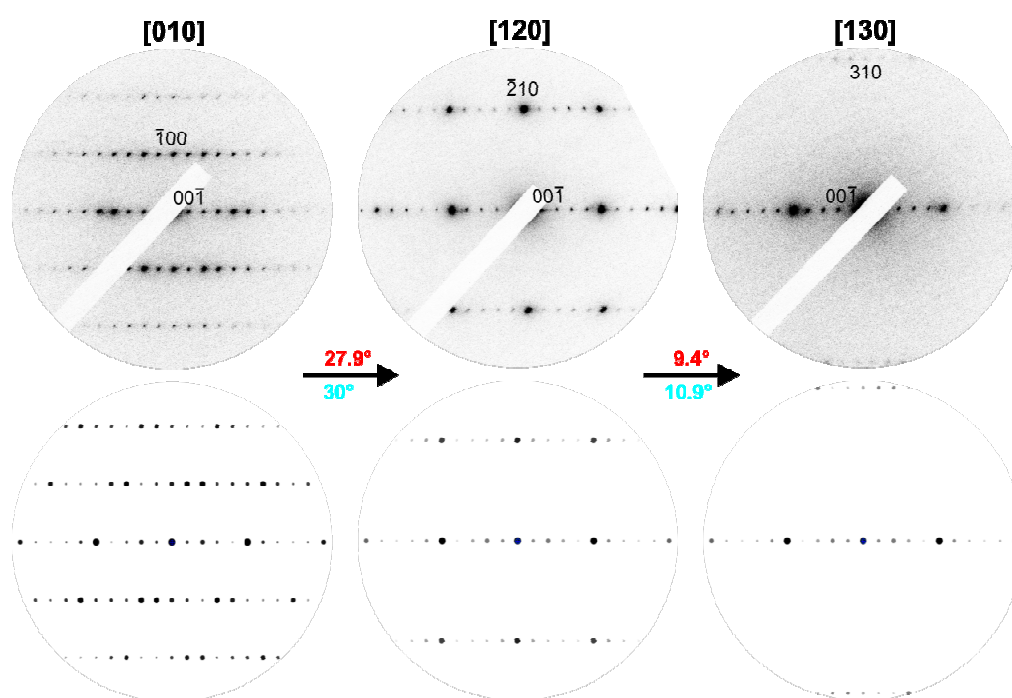


Figure S1. SAED tilt series of thick micro crystals of $\text{CaMg}_2\text{Ga}_2\text{N}_4$. Experimental pattern and tilt angles (top), simulated data based on structure model from X-ray data (bottom).

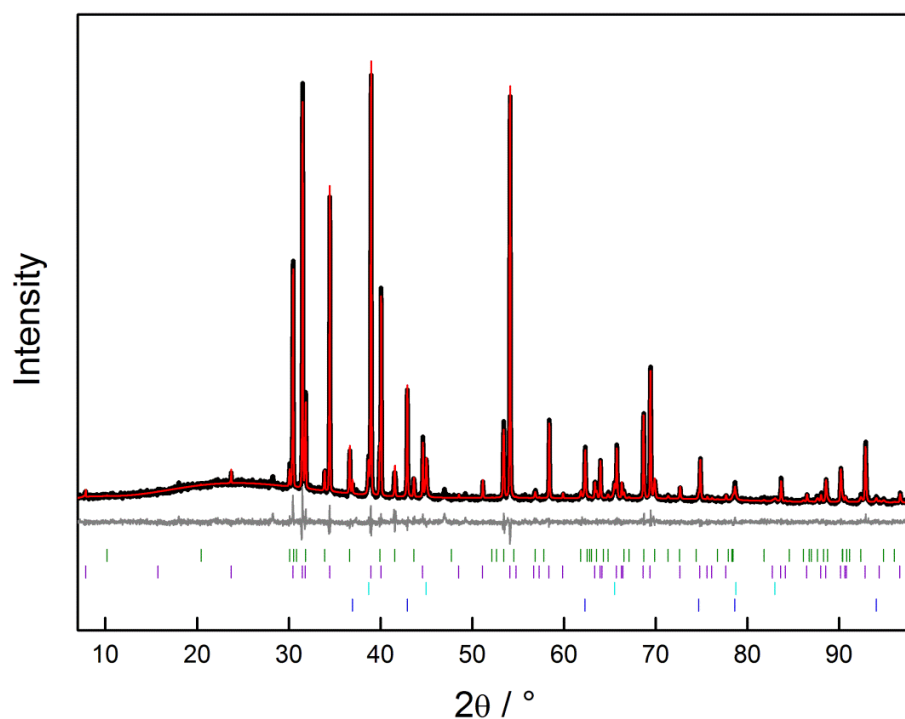


Figure S2. Rietveld refinement of the reaction product containing $\text{CaMg}_2\text{GaN}_3$ and $\text{CaMg}_2\text{Ga}_2\text{N}_4$ as well as secondary phases LiF and MgO. Observed (black line) and calculated (red line) powder diffraction pattern. The theoretical reflection positions of $\text{CaMg}_2\text{GaN}_3$ (green bars), $\text{CaMg}_2\text{Ga}_2\text{N}_4$ (violet bars), LiF (light blue bars) and MgO (dark blue bars) as well as the difference plot (gray line) are displayed below the refinement.

Table S1. Details of the Rietveld refinement.

Formula	CaMg ₂ GaN ₃	CaMg ₂ Ga ₂ N ₄	LiF	MgO
Formula mass / g · mol ⁻¹	200.44	298.19	25.94	40.30
Crystal System	Hexagonal	Trigonal	Cubic	Cubic
Space group	<i>P6₃/mmc</i> (no. 194)	<i>P3m1</i> (no. 164)	<i>Fm3m</i> (no. 225)	<i>Fm3m</i> (no. 225)
Lattice parameters / Å	<i>a</i> = 3.42732(7) <i>c</i> = 17.3706(7)	<i>a</i> = 3.38804(6) <i>c</i> = 11.2478(3)	<i>a</i> = 4.0268(1)	<i>a</i> = 4.21163(8)
Cell Volume / Å ³	176.71(1)	111.814(4)	65.294(7)	74.705(4)
Formula units per unit cell	1	1	4	4
X-ray density / g · cm ⁻³	3.61(4)	4.09(3)	2.6388(3)	3.5835(2)
Linear absorption coefficient / cm ⁻¹	241(2)	256(2)	30.955(3)	103.098(6)
Number of observed reflections	53	67	5	6
Constraints	5	4	0	0
Weight percent of the content / %	19	54	15	12
<i>R</i> _{Bragg}	2.534	2.656	0.995	1.761
<i>R</i> _{wp}			6.690	
<i>R</i> _{exp}			6.051	
<i>R</i> _p			5.101	
Radiation		Cu-K _{α1} (λ = 154.059 pm)		
Monochromator		Ge(111)		
Diffractometer		Stoe StadiP		
Detector		MYTHEN 1K		
2θ-range / °		5-98		
Temperature		298(2)		
Number of parameters / background parameters		70 / 12		
Program used		TOPAS Academic		
Profile function		fundamental parameters model		
Background function		Shifted Chebychev		

6.2 Supporting Information for Chapter 2.3

Christine Poesl and Wolfgang Schnick, *Z. Anorg. Allg. Chem.* **2016**, 642, 882-886.

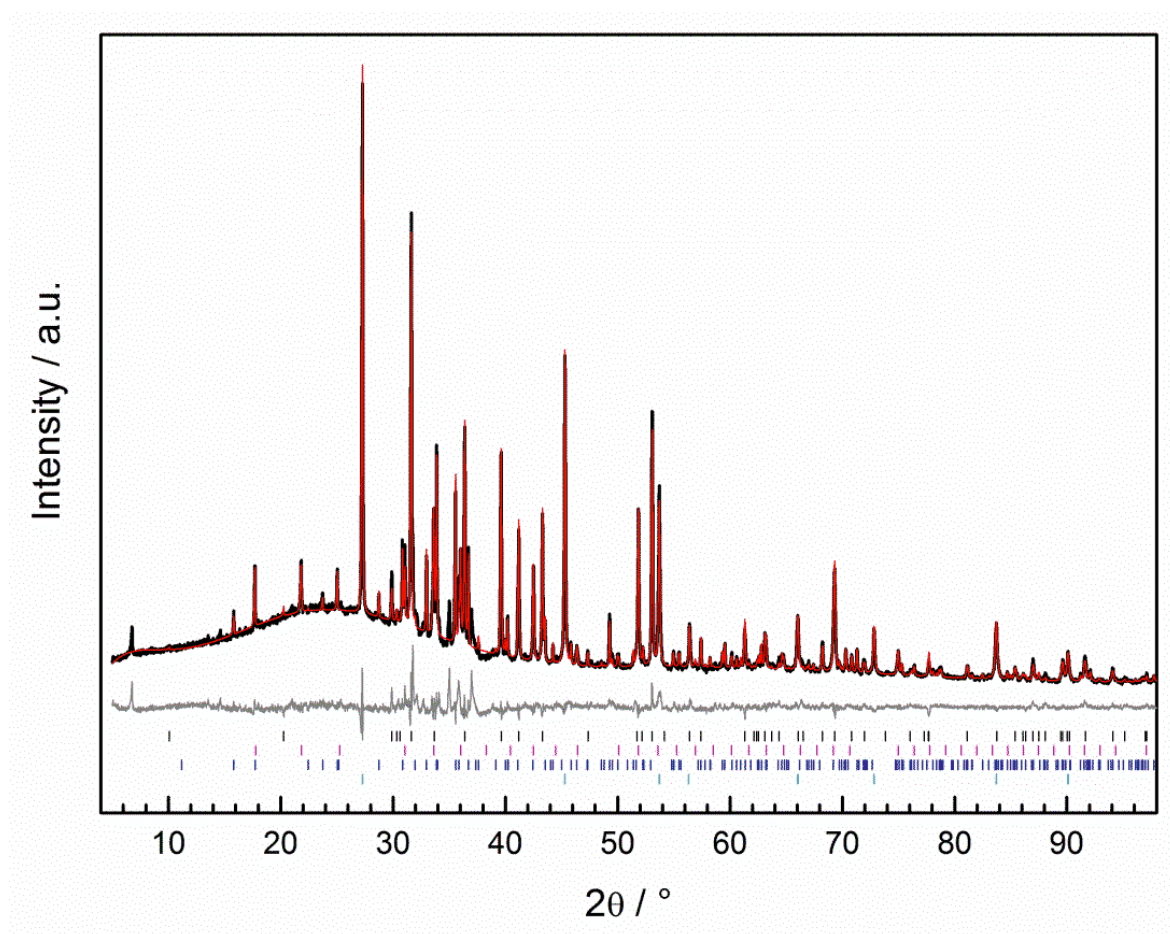


Figure S1. Rietveld refinement of the reaction product. Observed (black line) and calculated (red line) powder diffraction pattern. The theoretical reflection positions of $\text{Ca}_2\text{Mg}_5\text{GeN}_6$ (black vertical bars) and secondary phases Mg_3N_2 (pink vertical bars), Ca_2GeN_2 (blue vertical bars) and Ge (light blue vertical bars) as well as the difference plot (gray line) are displayed below the refinement.

Table S1. Details of the Rietveld refinement.

Formula	Ca ₂ Mg ₅ GeN ₆	Mg ₃ N ₂	Ca ₂ GeN ₂	Ge
Formula mass / g · mol ⁻¹	358.36	100.93	180.81	72.64
Crystal System	Hexagonal	Cubic	Tetragonal	Cubic
Space group	<i>P6₃/mmc</i> (no. 194)	<i>Ia-3</i>	<i>P4₂/mbc</i>	<i>Fd-3m</i>
Lattice parameters / Å	<i>a</i> = 3.44793(5) <i>c</i> = 17.5129(4)	<i>a</i> = 9.9661(2)	<i>a</i> = 11.1872(2) <i>c</i> = 5.0449(1)	<i>a</i> = 5.65609(8)
Cell Volume / Å ³	180.305(6)	989.86(5)	631.38(3)	180.946(7)
Formula units per unit cell	1	16	8	8
X-ray density / g · cm ⁻³	3.09(2)	2.7090(1)	3.8036(2)	5.3307(2)
Linear absorption coefficient / cm ⁻¹	204(1)	84.181(4)	396.41(2)	363.28(1)
Number of observed reflections	53	84	184	9
Constraints	2	0	0	0
Weight percent of the content / %	48	29	13	10
<i>R</i> _{Bragg}	3.389	2.155	2.202	2.212
<i>R</i> _{wp}			5.683	
<i>R</i> _{exp}			2.853	
<i>R</i> _p			3.967	
Radiation		Cu-Kα ₁ (λ = 154.059 pm)		
Monochromator		Ge(111)		
Diffractionmeter		Stoe StadiP		
Detector		MYTHEN 1K		
2θ-range / °		5-98		
Temperature		298(2)		
Number of parameters / background parameters		68 / 12		
Program used		TOPAS Academic		
Profile function		fundamental parameters model		
Background function		Shifted Chebychev		

6.3 Supporting Information for Chapter 2.4

Christine Poesl and Wolfgang Schnick, Eur. J. Inorg. Chem. 2017, 1498-1503.

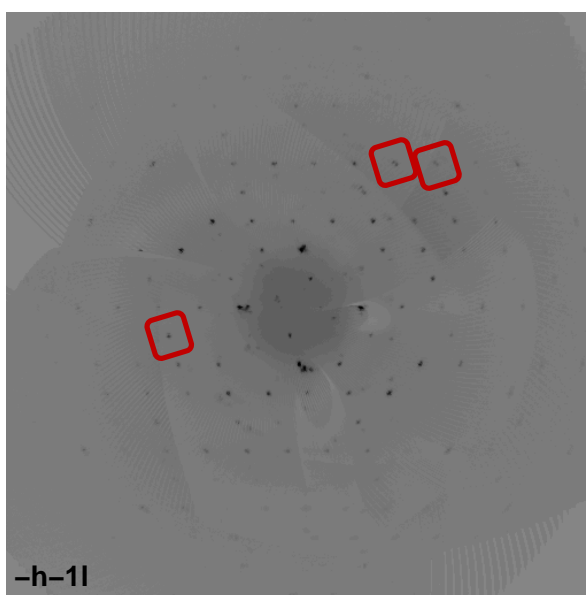
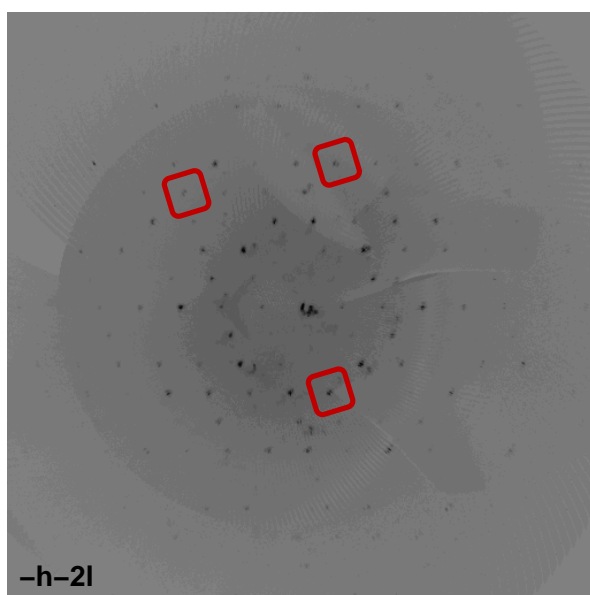
Table S1. Selected bond angles in the crystal structures of $\text{Ca}_4\text{Mg}_5\text{Ge}_3\text{N}_{10}$ and $\text{Sr}_2\text{Mg}_3\text{GaN}_{4.33}$.^[a]

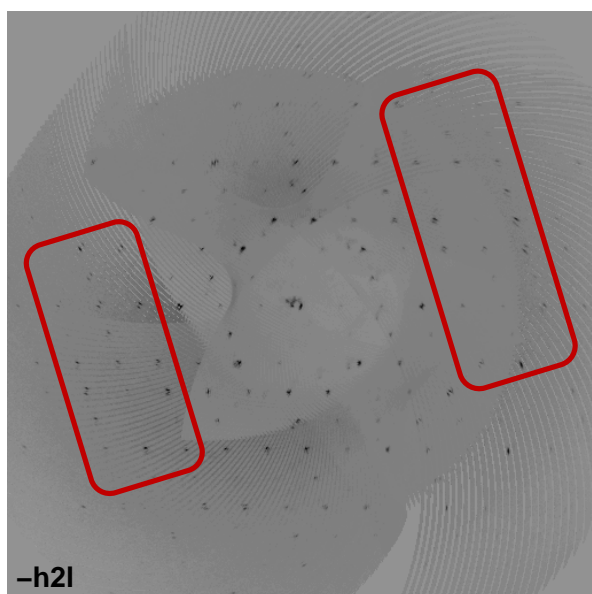
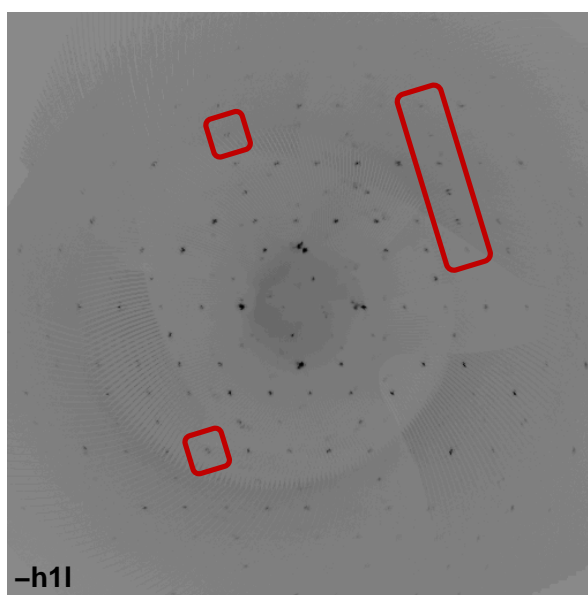
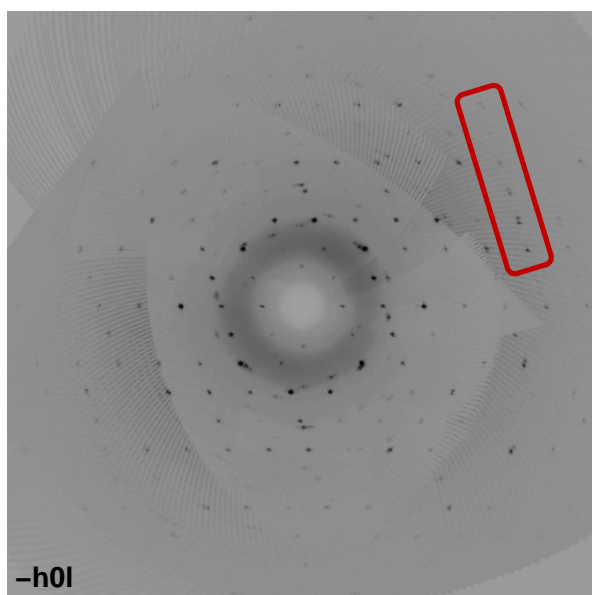
$\text{Ca}_4\text{Mg}_5\text{Ge}_3\text{N}_{10}$			
N1–Ge1–N2	99.4(3)	N1–Ge2–N1	95.7(2)
N1–Ge1–N3	116.6(2)	N1–Ge2–N3	104.1(3)
N2–Ge1–N3	106.5(2)	N1–Ge2–N3	121.1(2)
N3–Ge1–N3	109.6(3)		
$\text{Sr}_2\text{Mg}_3\text{GaN}_{4.33}$			
N1–Mg1/Ga1–N2	109.7(19)	N1–Mg2–N3	123.2(2)
N1–Mg1/Ga1–N3	120.9(10)	N1–Mg2–N4	92.8(2)
N2–Mg1/Ga1–N1	114(2)	N2–Mg2–N4	93(2)
N2–Mg1/Ga1–N2	123(3)	N3–Mg2–N4	85.0(12)
N2–Mg1/Ga1–N2	96.1(7)	N1–Ga2–N1	111.6(4)
N2–Mg1/Ga1–N3	117(2)	N1–Ga2–N2	119.0(7)
N2–Mg1/Ga1–N3	99.5(7)	N1–Ga2–N3	121.3(4)
N2–Mg1/Ga1–N3	93.2(7)	N1–Ga2–N4	101.1(3)
N3–Mg1/Ga1–N3	97.3(5)	N2–Ga2–N4	100(2)
N1–Mg2–N1	113.6(3)	N3–Ga2–N4	92.6(12)
N1–Mg2–N2	122.9(3)		

[a] Standard deviations are given in parantheses.

Reciprocal lattice sections $hn/$ ($-2 \leq n \leq 2$)

The following figures illustrate the reciprocal lattice sections $hn/$ ($-2 \leq n \leq 2$), in which the splitting of reflections is clearly visible. A few of them are highlighted with red boxes. Besides, there are a few reflections at low diffraction angles that cannot be indexed with the metrics of $\text{Sr}_2\text{Mg}_3\text{GaN}_{4.33}$ and probably derive from impurities on the surface of the investigated single crystal.





6.4 Supporting Information for Chapter 2.5

Christine Poesl, Robin Niklaus, and Wolfgang Schnick, *Eur. J. Inorg. Chem.* **2017**, 2422-2427.

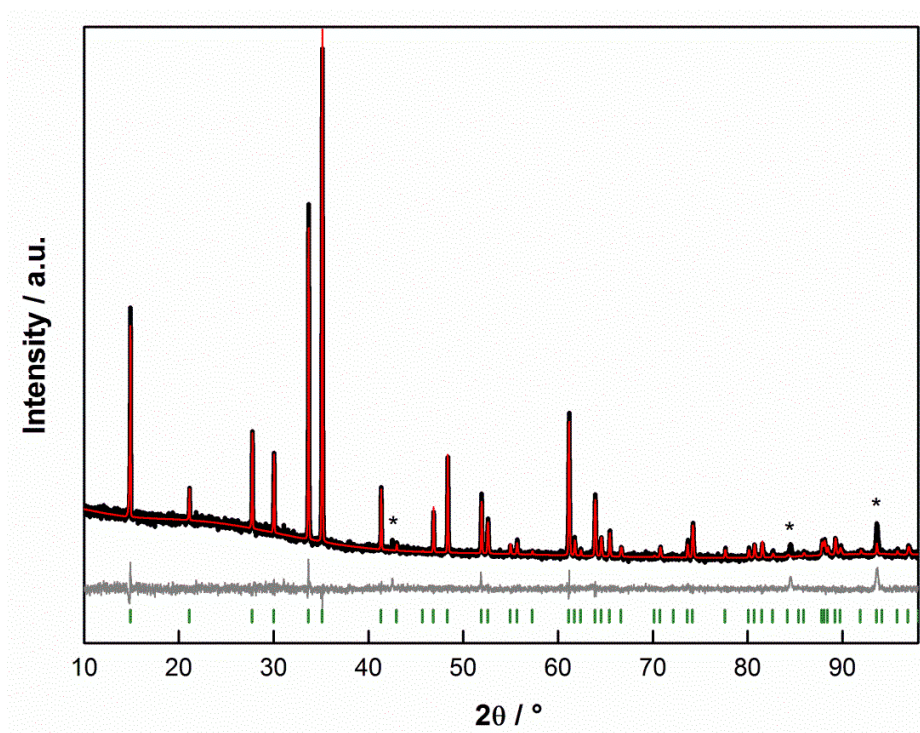


Figure S1. Rietveld refinement of the reaction product containing Ba[Mg₃GeN₄]:Eu²⁺. Observed (black line) and calculated (red line) powder diffraction pattern. The theoretical reflection positions of Ba[Mg₃GeN₄]:Eu²⁺ (green vertical bars) and the difference plot (gray line) are displayed below the refinement. Additional reflections, which are due to small amounts of secondary phases of the reaction product, are marked with asterisks.

Table S1. Details of the Rietveld refinement.

Formula	Ba[Mg ₃ GeN ₄]:Eu ²⁺
Crystal System	Tetragonal
Space group	<i>I</i> 4/ <i>m</i> (no. 87)
Lattice parameters / Å	<i>a</i> = 8.4132(11) <i>c</i> = 3.47836(6)
Cell Volume / Å ³	246.203(8)
Formula units per unit cell	2
X-ray density / g · cm ⁻³	4.54(3)
Linear absorption coefficient / cm ⁻¹	720(5)
Number of observed reflections	75
Constraints	1
Weight percent of the content / %	100
<i>R</i> _{Bragg}	2.932
<i>R</i> _{wp}	8.370
<i>R</i> _{exp}	8.041
<i>R</i> _p	6.005
Radiation	Cu-K _{α1} (λ = 154.059 pm)
Monochromator	Ge(111)
Diffractometer	Stoe StadiP
Detector	MYTHEN 1K
2θ-range / °	5-98
Temperature	298(2)
Number of parameters / background parameters	27 / 12
Program used	TOPAS Academic
Profile function	fundamental parameters model
Background function	Shifted Chebychev

6.5 Supporting Information for Chapter 3.2

Christine Poesl and Wolfgang Schnick, *Chem. Mater.* **2017**, 29, 3778-3784.

Table S1. Selected bond lengths /Å in the crystal structure of $\text{Ca}_3\text{Mg}[\text{Li}_2\text{Si}_2\text{N}_6]\text{:Eu}^{2+}$. Standard deviations are given in parantheses.

Bond	Bond length	Bond	Bond length	Bond	Bond length
Ca1–N1	2.310(4)	Ca2–N1 (2x)	2.437(4)	Si1–N1	1.719(5)
Ca1–N1	2.437(4)	Ca2–N1 (2x)	2.730(5)	Si1–N1	1.720(5)
Ca1–N2	2.516(5)	Ca2–N3 (2x)	2.743(5)	Si1–N3	1.783(6)
Ca1–N2	2.508(5)	Li1–N2	2.091(10)	Si1–N3	1.810(7)
Ca1–N3	2.744(5)	Li1–N2	2.088(11)	Si2–N2 (2x)	1.738(5)
Ca1–N4	2.563(5)	Li1–N2	2.225(11)	Si2–N4	1.805(6)
Mg1–N1 (2x)	2.199(5)	Li1–N4	2.172(12)	Si2–N4	1.843(7)
Mg1–N2 (2x)	2.159(5)				

Table S2. Selected bond angles /° in the crystal structure of $\text{Ca}_3\text{Mg}[\text{Li}_2\text{Si}_2\text{N}_6]\text{:Eu}^{2+}$. Standard deviations are given in parantheses.

N1–Ca1–N1	99.65(16)	N1–Ca2–N1	161.8(2)	N2–Si2–N2	107.9(3)
N1–Ca1–N2	85.77(14)	N1–Ca2–N1 (2x)	88.99(15)	N2–Si2–N4 (2x)	114.17(17)
N1–Ca1–N2	92.52(15)	N1–Ca2–N1 (2x)	102.23(13)	N2–Si2–N4 (2x)	112.89(19)
N1–Ca1–N2	95.88(15)	N1–Ca2–N1	104.1(2)	N4–Si2–N4	94.5(3)
N1–Ca1–N2	163.87(14)	N1–Ca2–N3 (2x)	68.02(16)	N1–Mg1–N1	80.4(2)
N1–Ca1–N3	92.06(14)	N1–Ca2–N3 (2x)	99.60(16)	N1–Mg1–N2 (2x)	168.1(2)
N1–Ca1–N3	68.16(16)	N1–Ca2–N3 (2x)	156.92(16)	N1–Mg1–N2 (2x)	97.94(15)
N1–Ca1–N4	166.19(17)	N1–Ca2–N3 (2x)	83.64(13)	N2–Mg1–N2	81.2(2)
N1–Ca1–N4	92.92(17)	N3–Ca2–N3	97.77(18)	N2–Li1–N2	113.3(5)
N2–Ca1–N2	92.96(16)	N1–Si1–N1	111.2(3)	N2–Li1–N2	113.2(5)
N2–Ca1–N3	159.95(16)	N1–Si1–N3 (2x)	112.28(18)	N2–Li1–N2	115.2(5)
N2–Ca1–N3	107.09(16)	N1–Si1–N3	111.32(18)	N2–Li1–N4	88.5(4)
N2–Ca1–N4	88.02(14)	N1–Si1–N3	111.31(18)	N2–Li1–N4	111.8(5)
N2–Ca1–N4	72.12(17)	N3–Si1–N3	97.8(3)	N2–Li1–N4	112.0(5)
N3–Ca1–N4	97.93(13)				

Table S3. Anisotropic displacement parameters /Å² for $\text{Ca}_3\text{Mg}[\text{Li}_2\text{Si}_2\text{N}_6]\text{:Eu}^{2+}$. Standard deviations are given in parantheses.

Atom	<i>U</i> 11	<i>U</i> 22	<i>U</i> 33	<i>U</i> 23	<i>U</i> 13	<i>U</i> 12
Ca1	0.0061(4)	0.0066(4)	0.0080(4)	0.0024(4)	0.0017(4)	0.0015(4)
Ca2	0.0078(6)	0.0110(7)	0.0076(6)	0	0.0042(5)	0
Si1	0.0036(8)	0.0055(8)	0.0059(8)	0	0.0002(6)	0
Si2	0.0041(8)	0.0050(9)	0.0047(8)	0	–0.0005(6)	0
Mg1	0.0099(12)	0.0054(11)	0.0109(12)	0	–0.0042(9)	0
Li1	0.018(5)	0.014(5)	0.011(4)	–0.004(4)	0.004(4)	–0.004(4)
N1	0.0060(18)	0.006(2)	0.0089(19)	0.0011(15)	0.0004(14)	0.0013(14)
N2	0.0051(18)	0.007(2)	0.0068(19)	0.0002(14)	–0.0006(14)	0.0001(14)
N3	0.004(3)	0.016(3)	0.005(3)	0	0.003(2)	0
N4	0.006(3)	0.011(3)	0.003(2)	0	0.002(2)	0

7 Publications

7.1 List of Publications

1 Layered Nitridomagnesogallates $\text{CaMg}_2\text{GaN}_3$ and $\text{CaMg}_2\text{Ga}_2\text{N}_4$

Christine Poesl, Lukas Neudert, and Wolfgang Schnick

Eur. J. Inorg. Chem. **2017**, 1067-1074

For this contribution, writing the main part of the manuscript, screening of literature, syntheses of the samples, structure determination based on single-crystal and powder X-ray diffraction data, and Rietveld refinement were done by Christine Poesl. Bond valence sum calculations, TOPOS analyses as well as TEM investigations, and interpretation of measured data were performed by Lukas Neudert. Sample preparation for TEM investigations was done by Christine Poesl in close collaboration with Lukas Neudert. Help of Lucien Eisenburger for TEM investigations and interpretations as well as help of Gregor Dahl and Eugenia Elzer for syntheses, and selection of single-crystals under instructions of Lukas Neudert and Christine Poesl is acknowledged. Wolfgang Schnick supervised the work. All authors revised the manuscript.

2 $\text{Ca}_2\text{Mg}_5\text{GeN}_6$ – A Layered Nitridomagnesogermanate

Christine Poesl and Wolfgang Schnick

Z. Anorg. Allg. Chem. **2016**, 642, 882-886

Writing the manuscript, screening of literature, structure determination by using single-crystal X-ray diffraction data, Rietveld refinement, syntheses, and creation of graphical material were performed by Christine Poesl. Wolfgang Schnick supervised the work and revised the manuscript.

3 $\text{Ca}_4\text{Mg}_5\text{Ge}_3\text{N}_{10}$ and $\text{Sr}_2\text{Mg}_3\text{GaN}_{4.33}$ – Two Mg-Containing Nitrides and Their Structural Relation to $(\text{Sr},\text{Ba})_2\text{Si}_5\text{N}_8$

Christine Poesl and Wolfgang Schnick

Eur. J. Inorg. Chem. **2017**, 1498-1503

For this article, writing the manuscript, syntheses of the samples, crystal selection and preparation, single-crystal structure analyses, and evaluation of structure data as well as literature research, and creation of graphical material were done by Christine Poesl. Supervision of the research project was carried out by Wolfgang Schnick.

4 The Crystal Structure of Nitridomagnesogermanate $\text{Ba}[\text{Mg}_3\text{GeN}_4]\text{:Eu}^{2+}$ and Theoretical Calculations of Its Electronic Properties

Christine Poesl, Robin Niklaus, and Wolfgang Schnick

Eur. J. Inorg. Chem. **2017**, 2422-2427

For this contribution, syntheses, crystal selection and preparation, evaluation of single-crystal X-ray diffraction data, Rietveld refinement, and creation of main graphical material as well as main literature research were performed by Christine Poesl. Robin Niklaus did the calculations of electronic properties and its interpretations. Wolfgang Schnick supervised the work. All authors revised the manuscript.

5 Crystal Structure and Nontypical Deep-Red Luminescence of $\text{Ca}_3\text{Mg}[\text{Li}_2\text{Si}_2\text{N}_6]\text{:Eu}^{2+}$

Christine Poesl and Wolfgang Schnick

Chem. Mater. **2017**, 29, 3778-3784

Syntheses of the sample, preparation of single-crystals, elucidation of single-crystal X-ray diffraction data, interpretation of luminescence investigations, literature research, creation of main graphical material, and writing the manuscript was done by Christine Poesl. Luminescence investigations were done at Lumileds in Aachen. Help of Petra Huppertz, Peter J. Schmidt, and Detlef Wiechert for luminescence investigations and interpretations is acknowledged. Wolfgang Schnick supervised the work and revised the manuscript.

7.2 Conference Contributions

Galliumnitrid-Verbindungen (talk)

Christine Poesl, Wolfgang Schnick

Obergurgl-Seminar Festkörperchemie, 2014

Synthetic Approach to Promising Nitride Host Lattices (poster presentation)

Christine Poesl, Dajana Durach, Frauke Hintze, Wolfgang Schnick

11th International Krutyn Summer School, Krutyn, 2012

7.3 Deposited Crystallographic Data

Crystallographic data of investigated nitrides were deposited at the Fachinformationszentrum (FIZ) Karlsruhe, 76344 Eggenstein-Leopoldshafen, Germany (fax: +49-7247-808-666; e-mail: crysdata@fiz-karlsruhe.de) on quoting the corresponding CSD depository numbers.

Compound	CSD number
CaMg ₂ GaN ₃	432100
CaMg ₂ Ga ₂ N ₄	432099
Ca ₂ Mg ₅ GeN ₆	431362
Ca ₄ Mg ₅ Ge ₃ N ₁₀	432308
Sr ₂ GaMg ₃ N _{4.33}	432309
Ba[Mg ₃ GeN ₄]:Eu ²⁺	432528
Ca ₃ Mg[Li ₂ Si ₂ N ₆]:Eu ²⁺	432605

8 Curriculum Vitae

Personal Data

Name	Christine Poesl
Date of birth	15.12.1987
Place of birth	Berlin, Germany
Nationality	German

Academic Career

Since 01/2013	Doctoral thesis / Research assistant in the group of Prof. Dr. W. Schnick <i>Ludwig-Maximilians-Universität München, Germany</i> ■ Title: "Synthetic Strategies and Structural Chemistry of Novel Nitridogallates, Nitridogermanates and Nitridosilicates"
04/2011 – 12/2012	Master of Science (Chemistry) <i>Ludwig-Maximilians-Universität München, Germany</i> ■ Master thesis: "Synthesis and Characterization of $\text{Sr}_2\text{GaMg}_3\text{N}_{4.33}$ and $\text{Sr}_{0.8}\text{Ca}_{0.2}\text{Mg}_2\text{Ga}_2\text{N}_4\text{:Eu}^{2+}$ as well as doping of $\text{Ca}_2\text{Ga}_3\text{MgN}_5$ " (supervisor: Prof. Dr. W. Schnick)
10/2007 – 03/2011	Bachelor of Science (Chemistry and Biochemistry) <i>Ludwig-Maximilians-Universität München, Germany</i> ■ Bachelor thesis: "Untersuchungen zur Nitridierung der Digallide von Strontium und Barium" (supervisor: Prof. Dr. W. Schnick)
06/2007	Allgemeine Hochschulreife
09/1998 – 06/2007	Secondary School <i>Lise-Meitner-Gymnasium Unterhaching, Germany</i>

Advanced Qualification

10/2015	Project management (Methods and techniques, project organization and risk management)
---------	---